Aspects of PT-symmetric quantum mechanics

Millican-Slater, Adam

Aspects Of $\mathcal{PT}$-Symmetric Quantum Mechanics

Adam Millican-Slater

A Thesis presented for the degree of
Doctor of Philosophy

Centre for Particle Theory
Department of Mathematical Sciences
University of Durham
England

September 2004

Dedicated to

Becky

In Loving Memory of

Mrs Mary Millican, Old Granny.

$\mathcal{PT}$-Symmetric Quantum Mechanics

Adam Millican-Slater

Submitted for the degree of Doctor of Philosophy
September 2004

Abstract

$\mathcal{PT}$-symmetric quantum mechanics is an alternative to the usual hermitian quantum mechanics. We will start this thesis by taking an overview of the subject, seeing some of the elementary consequences of this different approach.

The main part of the work will be an depth study of a specific Hamiltonian:

$$\left(-\frac{d^2}{dx^2} - (ix)^{2M} + \frac{l(l+1)}{x^2} \right) \tag{1}$$

This is a generalisation of the well understood harmonic oscillator with angular momentum. By making this generalisation we break the hermiticity of the problem. This leads to some intriguing results. We will be particularly interested in the merging of eigenvalues for $M < 1$.

We study the problem using a number of techniques. First the Hamiltonian is studied at the classical level and the behaviour of a particle moving in the corresponding potential is studied.

Having seen the consequences at the classical level we return to the quantum case. The Hamiltonian is first solved perturbativly. This method is shown to be valid for $\mathcal{PT}$-symmetric quantum mechanics. It is shown that asymptotic limits of the matrix do not capture the full behaviour of the energy levels.

We then move on to study the problem considering techniques arising from the ODE/IM correspondence. Using this approach we are able to give an analytic description of the phenomena and explain the merging of eigenvalues.

Declaration

The work in this thesis is based on research carried out at the the Department of Mathematical Sciences, the University of Durham, England. No part of this thesis has been submitted elsewhere for any other degree or qualification. Chapter 1, 2 and 5 as well as sections 6.1 and 6.2 (except the proof of the second half of property 3 in subsection 6.2.1) all contain necessary background material and no claim of originality is made. The remaining work is believed to be original, unless stated otherwise.

That part of chapter 6 not mentioned above has been done in collaboration with Patrick Dorey and Roberto Tateo [16].

Acknowledgements

Thank you to Patrick Dorey for his support and encouragement over the course of this PhD. Also to Roberto Tateo. I would also like to acknowledge EPSRC for their financial support.

My friends and family who have been there for me. A special mention must go to Dave and Ian. Also Jon, Mick, Simon, Becky, Jess, Anton, Paul, my Mum and my Dad.

Contents

List of Figures

Chapter 1

$\mathcal{PT}$-Symmetry

The subject of $\mathcal{PT}$-symmetry is relatively new. The possibility that non-hermitian Hamiltonians could have a rôle to play was originally brought up, in a private communication, by Bessis and Zinn-Justin. They conjectured that the spectrum of the eigenvalue problem:

$$\Big(-\frac{d^2}{dx^2}+ix^3\Big)\psi(x)=E\psi(x), \qquad \psi(x)\in L^2(\Re) \tag{1.1}$$

is entirely real and positive. In conventional quantum mechanics the Hamiltonian is always hermitian. Assuming conventional boundary conditions, this constrains the energy spectrum to be real (Appendix A). The non-hermiticity of this potential means that the usual arguments for the reality of the spectrum cannot be used. Carl Bender and Stefan Boettcher [6] interpreted the reality of this spectrum as being due to its $\mathcal{PT}$-symmetry. That is, if we simultaneously reflect in space and reverse time, the potential remains unchanged.

The fact that it may be possible to find real eigenvalues in a Hamiltonian which is non-hermitian caused some interest, particularly as the concept of $\mathcal{PT}$-symmetry appears to have a more physical interpretation than the very mathematical concept of hermiticity. The idea of complex Hamiltonians had previously surfaced in a variety of diverse areas, such as conventional quantum mechanical scattering [37], population biology, superconductors and quantum chemistry [22] [23] [31]. Energies of solitons on a complex Toda lattice have also been found to be real [24].

One concern about these $\mathcal{PT}$-symmetric theories is that, although we can show

them to have real energy levels, this does not make them physical theories. One of the necessary requirements for a physical theory is that there is a Hilbert space of vectors, which has a positive norm and for which the time evolution is unitary. There has been a lot of discussion about this in the literature.

One possible way to solve this problem was put forward by Bender, Brody and Jones [8] [9]. Their idea is to create a dynamic inner product, that is one based on the wave-functions themselves. This is done by defining a new operator $\mathcal{C}$.

$$\mathcal{C}(x,y) = \sum_n \phi_n(x)\phi_n(y) \tag{1.2}$$

Where the ϕ_n are the wave-functions of the Hamiltonian.

We now define the inner product:

$$\langle f|g\rangle \equiv \int_C dx[\mathcal{C}(x,x)\mathcal{PT}f(x)]g(x) \tag{1.3}$$

and use this inner product on our Hilbert space. This inner product has both a positive definite signature and leaves the norms of vectors stationary in time. It also reduces to the ordinary inner product from conventional quantum mechanics, when the Hamiltonian is hermitian.

Another idea that has been put forward as an extension of conventional hermitian quantum mechanics, is pseudo-hermiticity [30]. A Hamiltonian is said to be η-pseudo-hermitian if:

$$H^\dagger = \eta H \eta^{-1} \tag{1.4}$$

There are many conflicting ideas and philosophical view points on these issues. In this thesis we shall not be concerning ourselves with this. We shall instead concentrate on some of the mathematical implications of extending conventional quantum mechanics to $\mathcal{PT}$-symmetric quantum mechanics. In particular, we shall be studying how energy eigenvalues behave as $\mathcal{PT}$-symmetry is spontaneously broken in a specific Hamiltonian.

The rest of this chapter will take the following form. First we shall look at the definition of $\mathcal{PT}$-symmetry and look through some elementary consequences of $\mathcal{PT}$-symmetry. We will then go on to look at some concrete examples of $\mathcal{PT}$-symmetric potentials that have been studied and found to have real energy levels.

After we have gained an insight into $\mathcal{PT}$-symmetry, in chapter 2 we will define the potential which we will be studying for the rest of this thesis, a generalisation of the Bessis, Zinn-Justin potential (1.1). In doing so we will see some of the complications involved in this extension of conventional quantum mechanics.

Following the firm definition of the problem in the quantum case, in chapter 3 we will take some time studying the problem in the classical case. There are some interesting consequences even at this level.

In chapter 4 we shall return to the quantum case. We will take a perturbative approach generalising work done by Carl Bender and others. We will show that perturbative techniques work very well in this case. We will also show that an asymptotic method advocated by Bender et al, is in fact not sophisticated enough to understand the merging of eigenvalues.

In chapters 5 and 6, we will be using a different method, relying on the ODE/IM correspondence discovered by Patrick Dorey and Roberto Tateo. In chapter 5 we will review some earlier work and obtain the T-Q relation of integrable model theory, from our Hamiltonian. This will lead us into an already understood proof that the eigenvalues of our problem are real and positive.

In chapter 6 we will build on the results of chapter 5 and gain an analytical understanding of some of the interesting structure exhibited by the Hamiltonian, we have been studying.

1.1 Definition of $\mathcal{PT}$

By $\mathcal{PT}$-symmetry we mean reflection in space, with a simultaneous reversal of time. A Hamiltonian written in the form

$$H = p^2 + V(x) \tag{1.5}$$

will be $\mathcal{PT}$-symmetric if:

$$V^*(-x) = V(x) \tag{1.6}$$

We can now see that the Bessis and Zinn-Justin conjecture satisfies this constraint. In fact any polynomial potential will satisfy this constraint, providing any

even power of x has a real coefficient and odd powers have purely imaginary coefficients.

We can define the $\mathcal{P}$ and $\mathcal{T}$ operators separately.

The $\mathcal{P}$ operator is defined as:

$$\begin{aligned} &\mathcal{P}: \\ &\quad x \rightarrow -x \\ &\quad p \rightarrow -p \end{aligned} \tag{1.7}$$

while the $\mathcal{T}$ operator is defined as:

$$\begin{aligned} &\mathcal{T}: \\ &\quad p \rightarrow -p \\ &\quad i \rightarrow -i \end{aligned} \tag{1.8}$$

the $i \rightarrow -i$ being there to keep the commutator $[x, p] = i$ consistent.

We notice that:

$$\mathcal{P}^2 = \mathcal{T}^2 = (\mathcal{PT})^2 = 1 \tag{1.9}$$

The full $\mathcal{PT}$ transformation can be considered in terms of the real and imaginary parts of x. We can see that under $\mathcal{PT}$ $x = \Re e(x) + i\Im m(x) \rightarrow -\Re e(x) + i\Im m(x) = -x^*$.

We have now defined the operator $\mathcal{PT}$. It appears that Hamiltonians which are symmetric under this operator may have real energies. In fact, it is true that if the eigenvectors of the Hamiltonian are also $\mathcal{PT}$-symmetric, then the eigenvalues are real. Let us now see why this should be so.

1.2 A Limited Reality Proof

We can construct a reality proof, for a $\mathcal{PT}$-symmetric potential, given one other constraint.

We start with the fact that the Hamiltonian, H, is $\mathcal{PT}$-symmetric:

$$[H, \mathcal{PT}] = 0 \tag{1.10}$$

and also assume, for now, that the Hamiltonian and the operator $\mathcal{PT}$ are simultaneously diagonalisable. We work in a basis in which both are simultaneously diagonal.

$$H|\phi>= E|\phi> \Longleftrightarrow \mathcal{PT}|\phi>= a|\phi> \tag{1.11}$$

for some constant a. In conventional, hermitian quantum mechanics, if a linear operator commutes with the Hamiltonian, (that is satisfies (1.10)) it is always possible to find a basis such that (1.11) holds . The operator $\mathcal{PT}$ however, is not linear: it sends $i \rightarrow -i$. For this reason the constraint (1.11) does not automatically hold.

We proceed by first showing that the constant a is a pure phase and can therefore be neglected. Consider:

$$|\phi>= \mathcal{PTPT}|\phi>= \mathcal{PT}a|\phi>= a^*a|\phi> \tag{1.12}$$

so,

$$|a|^2 = 1 \tag{1.13}$$

and a is a pure phase as claimed. Now we make the transformation

$$|\phi> \rightarrow a^{1/2}|\phi> \tag{1.14}$$

so that

$$\mathcal{PT}|\phi>= |\phi> \tag{1.15}$$

we have:

$$H\mathcal{PT}|\phi>= E|\phi> \tag{1.16}$$

$$= \mathcal{PT}H|\phi>= \mathcal{PT}E|\phi>= E^*|\phi> \tag{1.17}$$

so:

$$E = E^* \tag{1.18}$$

This proof shows that if the eigenvectors of H are also eigenvectors of the $\mathcal{PT}$ operator the energy eigenvalues are real. However, whether the eigenvectors are simultaneous for any particular potential is a highly non-trivial problem.

1.3 Eigenvalues When $\mathcal{PT}$-Symmetry Is Broken

As well as cases when H and the $\mathcal{PT}$ operator are simultaneously diagonalisable, we can also have cases where this is not true. In these cases (1.10) still holds

$$[H, \mathcal{PT}] = 0 \tag{1.19}$$

as we are still dealing with a $\mathcal{PT}$-symmetric Hamiltonian. However, as $\mathcal{PT}$ is non-linear, H and $\mathcal{PT}$ do not have to be simultaneously diagonalisable. We write $|\phi_E>$ as the eigenvector with energy E, so that

$$H|\phi_E>= E|\phi_E> \tag{1.20}$$

If $\mathcal{PT}$ and H are not simultaneously diagonalisable, we have the situation

$$\begin{aligned} \mathcal{PT}|\phi_E>&= |\psi_E> \\ |\psi_E>&\neq a|\phi_E> \end{aligned} \tag{1.21}$$

for any constant a. i.e. the eigenvectors, $|\phi>$, of H are not eigenvectors of $\mathcal{PT}$. In this case we describe the Hamiltonian's $\mathcal{PT}$-symmetry as being spontaneously broken. The notation $|\psi_E>$, does not tell us as yet, any information about the energy of $|\psi_E>$, it merely denotes the function derived from acting on the wave-function $|\phi_E>$, with the operator $\mathcal{PT}$. Indeed, so far we do not know if $|\psi_E>$ is an eigenfunction of H at all. Using (1.10) we have

$$[H, \mathcal{PT}]|\phi_E>= H\mathcal{PT}|\phi_E> -\mathcal{PT}H|\phi_E>= 0 \tag{1.22}$$

so

$$H|\psi_E>= E^*|\psi_E> \tag{1.23}$$

This tells us that $|\psi>$ is an eigenvector of H with eigenvalue E^*.

$$|\psi_E>= |\phi_{E^*}> \tag{1.24}$$

Assuming there are no degenerate eigenvalues, this means that when the $\mathcal{PT}$-symmetry is broken, the energy eigenvalues come in complex conjugate pairs. The operator $\mathcal{PT}$ interchanges between the eigenvectors with complex conjugate eigenvalues. We can then say that in a $\mathcal{PT}$-symmetric Hamiltonian, all the energy eigenvalues are either real, or occur in complex conjugate pairs.

1.4 Examples Of Hamiltonians Having $\mathcal{PT}$-Symmetry

Having obtained an understanding of the $\mathcal{PT}$ transformation and taken a look at the historical motivation for its study, let us now study some concrete examples.

1.4.1 Extension Of The Bessis, Zinn-Justin Conjecture

The Hamiltonian in the eigenvalue problem proposed by Bessis and Zinn-Justin above was generalised by Bender et al [6] to:

$$p^2 - (ix)^{2M} \qquad M \in \Re \tag{1.25}$$

and studied in some detail. This potential, as well as being a generalisation of the Bessis and Zinn-Justin conjecture, also contains the usual harmonic oscillator as a special case at $M = 1$ and should, in fact, be thought of as a continuation in M of this well known Hermitian potential. It was found, numerically, that for $M \geq 1$ the spectrum was indeed entirely real and positive. For $\frac{1}{2} < M < 1$ there were some real eigenvalues and an infinite number of complex conjugate pairs of eigenvalues and for $M < \frac{1}{2}$ there were no real eigenvalues. Figure 1.1 shows the real eigenvalues of this Hamiltonian for varying M.

The reality of the spectrum in the $M > 1$ region was interpreted as being due to unbroken $\mathcal{PT}$-symmetry. The complexification of the spectrum in the region below $M = 1$ was taken as a sign of the spontaneous breakdown of $\mathcal{PT}$-symmetry.

A point of note concerns the potential when $M = 2$, the "upside down" quartic potential. This potential is usually understood to have a spectrum which is unbounded below. As we can see from the graph (1.1), in the case given above this is not true. This is due to the way in which the potential is obtained from a continuation of the harmonic oscillator and the unusual boundary conditions that are thus obtained. This will be discussed in more detail later.

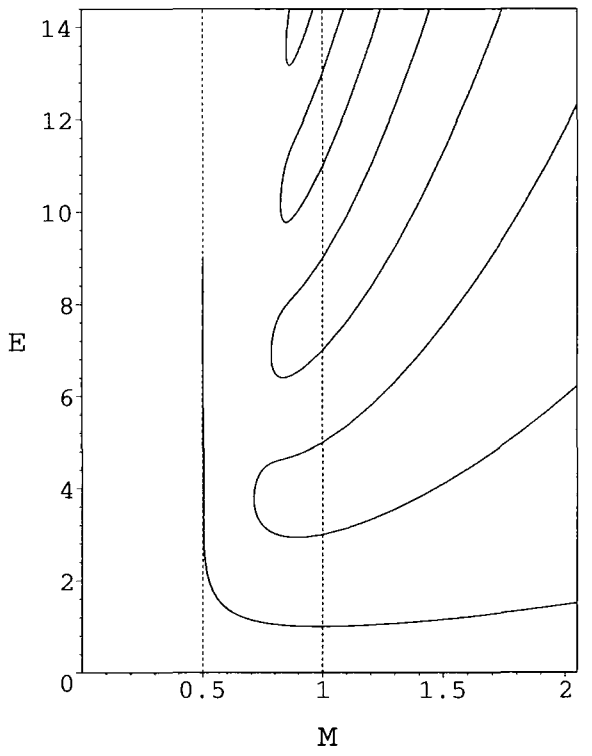

Figure 1.1: The Real Energy Levels For l=0

1.4.2 Angular Momentum

An extension of the original Bender and Boettcher Hamiltonian (1.25) at which we will be looking in detail comes from adding an angular momentum term [18]:

$$H = p^2 - (ix)^{2M} + \frac{l(l+1)}{x^2} \tag{1.26}$$

For $l = 0$, this is clearly the original Bender problem, with eigenvalues real for $M \geq 1$ and a continuing pairing off of eigenvalues into complex conjugate pairs as M tends toward $1/2$ from above. However, if we add a small negative angular momentum term, something interesting happens to the eigenvalues. Compare Figure 1.2 with Figure 1.1. These graphs were constructed from numerical methods based on (6.58). They can be seen in [18].

Although the basic difference either side of the harmonic oscillator point at $M = 1$ is unchanged, the order in which the pairing off in the broken $\mathcal{PT}$ phase, $M < 1$, is changed. We will not dwell on this here, as this Hamiltonian will be studied in more detail later.

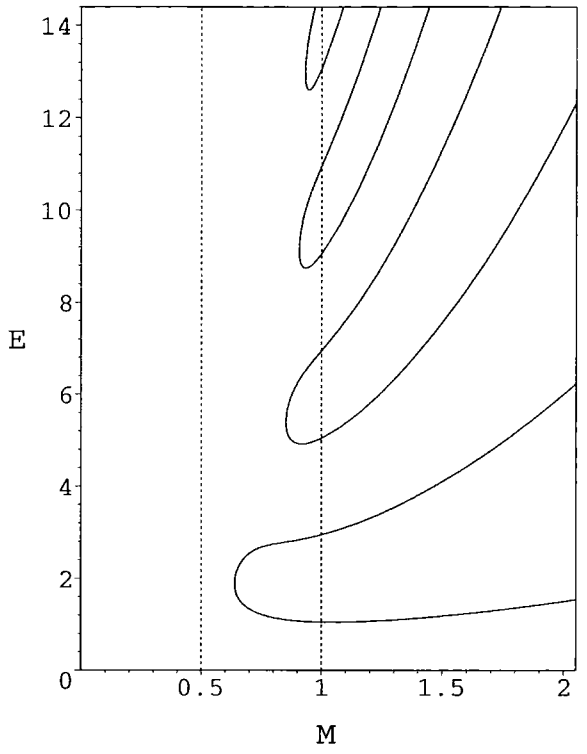

Figure 1.2: The Energy Levels For $l = -0.025$

1.4.3 A Novel Quasi-Exactly Solvable Hamiltonian

Consider the Hamiltonian;

$$H = p^2 - x^4 + 2iax^3 + (a^2 - 2b)x^2 + 2i(ab - J)x \tag{1.27}$$

where a and b are real and J is a positive integer [5].

For each positive integer J, a different potential is formed. A potential is referred to as quasi-exactly solvable if some but not all of the eigenvalues can be found exactly. This potential has J quasi-exactly solvable energy levels. The QES energy levels are the zeros of a polynomial, $Q_J(E)$, which is of order J in E. These polynomials are greatly simplified if we write $E = F + b^2 + Ja$ and $K = 4b + a^2$. The first three polynomials then become:

$$\begin{aligned} Q_1 &= F \\ Q_2 &= F^2 - K \\ Q_3 &= F^3 - 4KF - 16 \end{aligned} \tag{1.28}$$

The energy levels are real if

$$4b + a^2 = K \geq K_{critical} \tag{1.29}$$

where $K_{critical}$ is dependent on J. For $K = K_{critical}$, the lowest two energy levels become degenerate. For $K < K_{critical}$ some of the QES energy levels are complex. In their paper Bender and his collaborators say that, after extensive numerical tests, they have come to the conclusion that the non-QES spectrum is entirely real throughout the (a, b) plane. They also state that for $K > K_{critical}$ the QES levels are the lowest lying. However for $K < K_{critical}$, the remaining real eigenvalues may be in the non-QES spectrum. Fig (1.3), which is taken directly from [5], shows the behaviour of the energy levels as a function of b for $J = 3$ and $a = 0$.

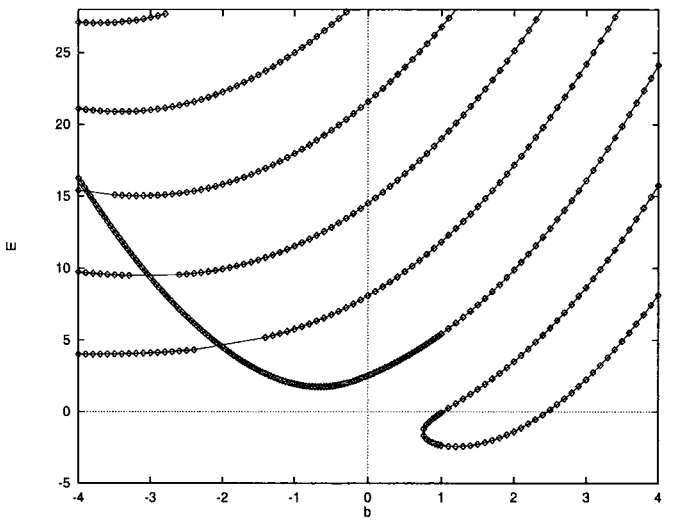

Figure 1.3: The energy levels as a function of b for $J = 3$ and $a = 0$. Taken from [5].

Until the discovery that this class of Hamiltonians admitted the possibility of an entirely real spectrum, which was bounded below, the lowest order quasi-exactly solvable potential was thought to be the sextic. The use of $\mathcal{PT}$-symmetry, instead of hermiticity, has given us a new class of quasi-exactly solvable potentials with real spectra.

1.4.4 A Complex $\mathcal{PT}$-Symmetric Hamiltonian With A Real Spectra

Bagchi and Roychoudhury, [2], have studied complex potentials with a particular relation to a known real potential. They chose to look at potentials of the form:

$$V^{\pm} = U^2 \pm U' \tag{1.30}$$

where U is a complex function of x. They wrote $U \equiv a(x) + ib(x)$, where a and b are both real, continuously differentiable functions. They demanded that V^- be real, thus restricting a:

$$a = \frac{1}{2}\frac{b'}{b} \tag{1.31}$$

Under the condition that V^- must be real we have:

$$V^+ = (a^2 - b^2 + a') + i2b' \tag{1.32}$$

$$V^- = (a^2 - b^2 + a') \tag{1.33}$$

Note that $V^+ = V^- + 2U'$. They studied the particular case:

$$a = -\frac{\mu}{2}\tanh\mu x, \qquad b = \lambda \mathrm{sech}\mu x \tag{1.34}$$

This gives us:

$$V^+ = \tfrac{\mu^2}{4} - \mu^2[\bar{\lambda}(\bar{\lambda}-1)+1]\mathrm{sech}^2\mu x - i2\lambda\mu\mathrm{sech}\mu x\tanh\mu x \tag{1.35}$$

$$V^- = \tfrac{\mu^2}{4} - \mu^2[\bar{\lambda}(\bar{\lambda}-1)+1]\mathrm{sech}^2\mu x \tag{1.36}$$

where $\bar{\lambda}(\bar{\lambda}-1) = \frac{\lambda^2}{\mu^2} - \frac{1}{4}$. The non-zero energy levels for V^- are known, [19], they are:

$$E_n^- = \frac{\mu^2}{4} - (\bar{\lambda} - 1 - n)^2\mu^2, \quad n < \bar{\lambda} - 1 \tag{1.37}$$

with $n = 0, 1, ...$ The corresponding eigenfunctions are:

$$\psi_{even}^-(x) = \cosh^{\bar{\lambda}}\mu x\, {}_2F_1(\tfrac{1}{2}(\bar{\lambda}-1), \tfrac{1}{2}(\bar{\lambda}+1); \tfrac{1}{2}; -\sinh^2\mu x) \tag{1.38}$$

$$\psi_{odd}^-(x) = \cosh^{\bar{\lambda}}\mu x \sinh\mu x\, {}_2F_1(\tfrac{\bar{\lambda}}{2}, \tfrac{\bar{\lambda}}{2}+1; \tfrac{3}{2}; -\sinh^2\mu x) \tag{1.39}$$

where the ${}_2F_1$ are the Gauss functions.

Bagchi and Roychoudhury took the case $\frac{\lambda}{\mu} = -\frac{5}{2}$, for which $\bar{\lambda} = 3$. Using the intertwining relationship, $\psi^+_{n=0,1} = (\frac{d}{dx} + U)\psi^-_{n=0,1}$, they were able to find that in this particular case the eigenvalues for V^+ match those of V^-, for $n = 0$ and 1. That is, the energy levels $\frac{\mu^2}{4} - 4\mu^2$ and $\frac{\mu^2}{4} - \mu^2$ are shared by both potentials. Thus they found a $\mathcal{PT}$-symmetric potential with real energy levels.

1.4.5 Anti-Isospectral Transformations

One way of creating new $\mathcal{PT}$-symmetric potentials, is the anti-isospectral transformation [27]. Consider the situation when $\psi(x)$ is the solution of the Schrödinger equation with real potential $V(x)$ and energy E. Then $\psi(x + i\beta)$ is the solution to the Schrödinger equation with potential $V^{\mathcal{PT}}(x) = -V(ix + \beta)$, with energy $-E$, where β is an arbitrary real constant. If $\psi(x)$ and $\psi(x + i\beta)$ satisfy appropriate boundary conditions then they are eigenfunctions of the relevant potentials. This is known as the anti-isospectral transformation, due to the reversed ordering of the energy levels.

Let us look at a particular example to illustrate the idea. In their paper, [26], Khare and Sukhatme studied a particular Lamé potential:

$$V(x) = a(a+1)m\mathrm{sn}^2(x, m), \quad a = 1, 2, 3, .. \tag{1.40}$$

where a is a non-negative integer and the sn is a Jacobi elliptic function, with elliptic parameter m, $0 < m < 1$. It is doubly periodic with period $[4K(m), i2K'(m)]$, where $K(m) = \int_0^{\pi/2} \frac{d\theta}{(1-m\sin^2\theta)^{1/2}}$ and $K'(m) = \int_0^{\pi/2} \frac{d\theta}{(1-m_1\sin^2\theta)^{1/2}}$, $m_1 = 1 - m$.

This potential is known to have $2a + 1$ eigenstates (band energies) and a band gaps. We let $E_j(m)$ and $\psi_j(x, m)$ with $j = 0, 1, ..., 2a$ denote the band edge energies and wave functions. We make the iso-spectral transformation and obtain the $\mathcal{PT}$-invariant potential:

$$V^{\mathcal{PT}}(x) = -a(a+1)m\mathrm{sn}^2(ix + \beta, m), \quad a = 1, 2, 3, .. \tag{1.41}$$

which has real period $2K'(m)$. The related band energies and eigenfunctions are:

$$E_j^{\mathcal{PT}}(m) = -E_{2a-j}(m), \qquad \psi_j^{\mathcal{PT}}(x, m) \sim \psi_{2a-j}(ix + \beta, m) \tag{1.42}$$

Using their results from [25], they were able, for $a = 3$, write down an explicit form for the ground state energy and wavefunction:

$$E_g = -5 - 5m - 2\delta_3$$
$$\psi_g(x) = \mathrm{sn}(ix + \beta, m)[2 + 2m - \delta_3 - 5m\mathrm{sn}^2(ix + \beta, m)] \tag{1.43}$$

where $\delta_3 \equiv \sqrt{4 - 7m + 4m^2}$. So these ground state energies are real and an example of a $\mathcal{PT}$-symmetric periodic potential with at least one real energy level.

Except for the extensions of the harmonic oscillator, all of the potentials we have seen have had exactly solvable real energy eigenvalues. Later we will see a proof of the reality of the eigenvalues of the extended harmonic oscillator Hamiltonian.

We have now seen what is meant by PT-symmetry and some of its elementary implications. We have also seen some explicit examples of $\mathcal{PT}$-symmetric potentials with real eigenvalues. For the rest of the thesis we shall be focusing on the potential introduced in 1.4.2. We will be principally concerned with the change in the connectivity of eigenvalue merging, for different values of l. In the next chapter, we will take a close look at some of the subtleties involved in the definition of this problem. We will also see in more detail the numerical results, obtained previously, on this potential's eigenvalues.

Chapter 2

A $\mathcal{PT}$-Symmetric Potential Of Particular Interest

2.1 The Model, Its Boundary Conditions and Stokes Sectors

A large part of this thesis will be taken up with the study of one particular model. This model is one we have already seen briefly and is an extension of the Bender-Boettcher potential (1.25). We will be looking at the eigenvalue problem:

$$\left(-\frac{d^2}{dx^2} - (ix)^{2M} + \frac{l(l+1)}{x^2} \right) \psi(x) = E\psi(x) \tag{2.1}$$

This is the same as the potential studied in [6] with the addition of the angular momentum term.

The problem should be viewed as an extension of the well understood problem at $M = 1$, the spherically symmetric harmonic oscillator. Because of the possible non-integer powers of x this eigenvalue problem is defined on the cut Argand plane. We take the cut to be running out from the origin up the positive imaginary axis.

We are interested in the values of E for which $H\psi = E\psi$ has solutions ψ which are square integrable along a specified contour. As we are considering this potential as an extension of the harmonic oscillator, we take for $M = 1$ this contour to be the real axis, with a distortion to avoid the singularity at the origin. For other values of

M the contour needs to be chosen so as to give a consistent analytic continuation of the problem. For this we will need to consider Stokes' sectors.

2.1.1 Stokes Sectors

To illustrate the concept let us consider the case $M = 1$ and $l = 0$, the harmonic oscillator. The asymptotic form of the eigenfunction for this Hamiltonian is:

$$\psi(x) \sim x^{-1/2+E/2} e^{-\frac{1}{2}x^2} \tag{2.2}$$

Usually the wave-function is considered only on the real line and we can see that on the real line $\psi(x) \to 0$ as $|x| \to \infty$, which is the behaviour we require for a solution to the differential equation to be a wavefunction. We, however, will be considering the wave-function on the complex plane.

The WKB approximation for the potential as $|x| \to \infty$ is:

$$\psi^{WKB}(x, E) := AP(x)^{-1/4} e^{\pm \int^x \sqrt{P(t)}dt} \tag{2.3}$$

where A is some normalisation constant and $P(x) = x^2 - E$. If we write $x = re^{i\theta}$, the wavefunction is:

$$\psi(x) \sim r^{-1/2+E/2} e^{i(-1/2+E/2)\theta} e^{\pm \frac{1}{2} r^2 e^{i2\theta}} \tag{2.4}$$

The extra $\pm$ is usually left out as we are only interested in the decaying wavefunctions. Having extended the problem onto the complex plane we can no longer ignore the other solution. We can see that for most values of θ one solution is decaying while the other is growing.

Whether each solution decays as $|r| \to \infty$ is decided by the sign of $\Re e(e^{i2\theta})$. Taking the negative sign in the exponential, for $|\theta| < \pi/4$ and $3\pi/4 < \theta < 5\pi/4$ the wave-function decays exponentially, while for $\pi/4 < \theta < 3\pi/4$ and $5\pi/4 < \theta < 7\pi/4$, the wavefunction grows exponentially. This is reversed, if we take the plus sign in the exponential. At the values $\theta = \pi/4, 3\pi/4, 5\pi/4, 7\pi/4$ the behaviour changes between exponentially growing and decaying; the asymptotic is algebraic. These values of θ we shall call Stokes lines. The values for which the exponential effect is strongest (the real and imaginary axes, in our example) will be called anti-Stokes

lines. The wedges between them are called Stokes sectors. In the diagram (2.1), the Stokes lines are shown as dotted lines and the Stokes sectors are the spaces between them. The anti-Stokes lines are the axes.

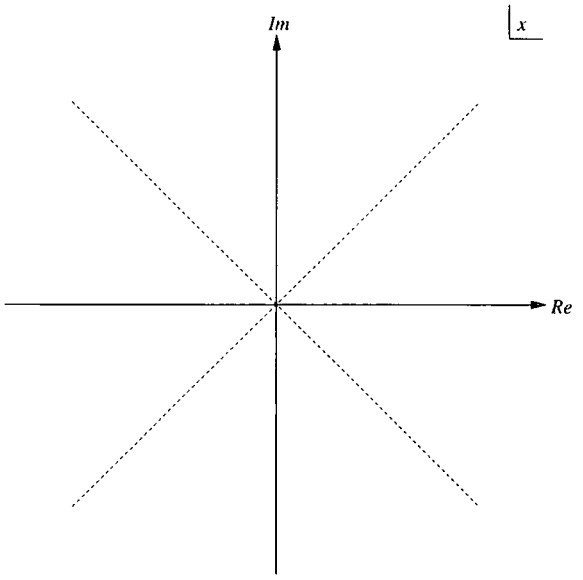

Figure 2.1: Stokes Lines Of The Harmonic Oscillator

The boundary condition then becomes a matter of stating which pair of sectors you wish your wave function to decay in. In the usual harmonic oscillator it is the sectors containing the positive and negative real axes, though we could equally choose any other pair of sectors to give a consistent, but different eigenvalue problem.

A word of warning should be given here: some authors use the terms Stokes' and anti-Stokes line in the opposite manner. The boundary condition $\psi(x) \to 0$ as $|x| \to \infty$ can be seen to hold not just on the real line, but in sectors enclosing the positive and negative real axes.

A piece of terminology we should note is that a solution that grows in a particular sector is referred to as dominant, while one that decays is called subdominant. The subdominant asymptotic is unique. On the other hand the dominant asymptotic is not; we can add terms that are subdominant to a dominant approximation, without changing its asymptotic behaviour.

In the simple harmonic oscillator case we are considering, there are four Stokes sectors, one containing each of the axes. If we label these sectors S_k, with S_0 being

the sector containing the negative imaginary axis, the usual way to approach this problem is to take a wavefunction that decays in the sectors containing the real axes; the sectors S_1 and S_{-1}. In fact the contour taken is the real axis itself. We could however take the solution subdominant in any pair of sectors. This would give us six distinct eigenvalue problems defined by where we demand the eigenfunctions to subdominant. We could choose any from: (S_0, S_1), (S_0, S_1), (S_0, S_2), (S_1, S_2), (S_1, S_1) and (S_1, S_2). The figure 2.2 below show possible integration contours for each of these options.

Having understood Stokes sectors, we can return to our model and a discussion of its boundary conditions.

2.1.2 The Model and Its Boundary Conditions

The Hamiltonian we are interested in is:

$$\left(-\frac{d^2}{dx^2} - (ix)^{2M} + \frac{l(l+1)}{x^2} \right) \psi(x) = E\psi(x) \tag{2.5}$$

with boundary conditions chosen so as to be consistent with the $M = 1$ harmonic oscillator case; the Stokes sectors must be chosen to be smoothly deformed from the $M = 1$ case. For the case $M = 1$ we shall certainly choose the sectors containing the real axes. The question we must now ask is: how do these sectors change as we move M away from the harmonic oscillator point?

Recall the WKB approximation is:

$$\psi^{WKB}(x, E) \sim P(x)^{-1/4} e^{\pm \int^x \sqrt{P(t)} dt} \tag{2.6}$$

as $|x| \to \infty$ with $P(x) = -(ix)^{2M} + l(l+1)x^{-2} - E$. Because the problem is defined on the cut argand plane, we shall label rays by the angle they make with the negative imaginary axis, i.e. we shall set $x = -ire^{i\theta}$.

For the case $M > 1$ the asymptotic behaviour is:

$$\psi_{\pm} \sim x^{-M/2} \exp\left(\pm \frac{1}{M+1} r^{M+1} e^{i(M+1)\theta}\right) \tag{2.7}$$

For $M \leq 1$ the asymptotic of the WKB approximation needs to be modified, in fact each time M passes the point $M = 1/(2m-1)$, for m a positive integer there is

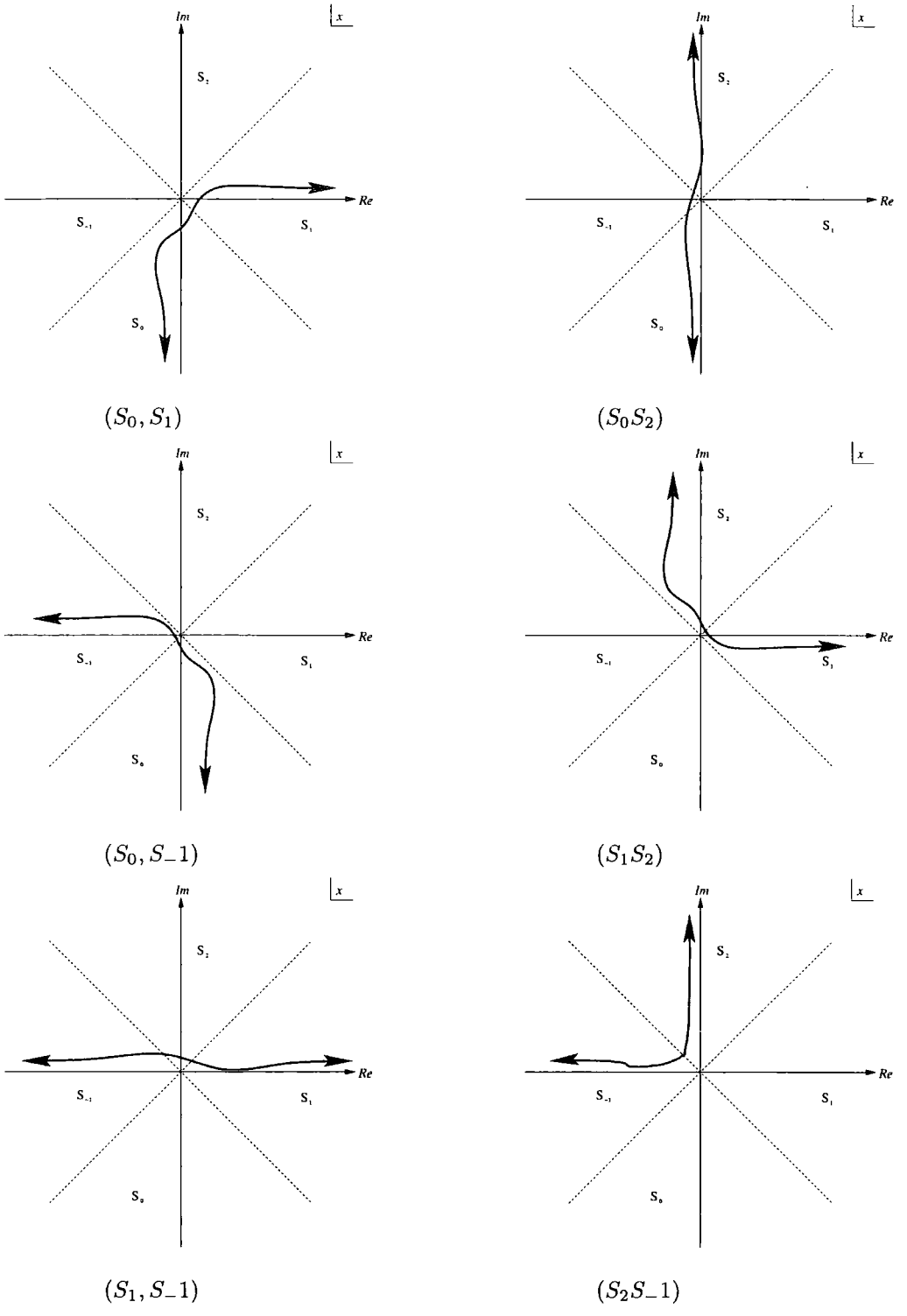

Figure 2.2: The Six Different Eigenvalue Problems Based On $-\frac{d^2x}{dt^2} + x^2 + E$

and additional term in the exponential function. For example for $1/3 < M < 1$ the

asymptotic is:

$$\psi_{\pm} \sim x^{-M/2} \exp\left(\pm\left(\frac{1}{M+1} r^{M+1} e^{i(M+1)\theta} - \frac{E}{2-2M} r^{1-M} e^{i(1-M)\theta}\right)\right) \tag{2.8}$$

This extra term does not effect whether $\psi_{\pm}$ grows or decays for a given θ as $r \to \infty$.

The Stokes lines are then:

$$\theta = \frac{\pm(2n+1)\pi}{2M+2} \tag{2.9}$$

for integer n. We can label the Stokes sectors between as:

$$S_k := \left|\theta - \frac{2\pi k}{2M+2}\right| < \frac{\pi}{2M+2} \tag{2.10}$$

Notice that the sectors which contain the real axes are, for $M < 2$, S_{-1} and S_1.

For $M = 1$, there are four Stokes lines, at $\theta = \pm\frac{\pi}{4}, \pm\frac{3\pi}{4}$. As M grows away from 1, the Stokes lines move down toward the negative imaginary axis and the Stokes sectors get narrower. At the same time new Stokes sectors appear from the branch cut. For $1 < M < 2$ we can still allow our integration contour to tend toward the real axis for large r. A problem occurs at $M = 2$, the upside-down quartic oscillator. The Stokes lines are now:

$$\theta = \frac{\pm\pi}{6}, \frac{\pm\pi}{2}, \frac{\pm 5\pi}{6} \tag{2.11}$$

and we can see that one pair of Stokes lines coincides with the real axis, the sectors S_{-1} and S_1 now lie completely below the real axis. This disallows us from using the real axis as our integration contour. We must instead continue our problem below the real axis. After M has passed 2 we could again use the real axis, however this would not be a continuation of our original $M = 1$ problem, this would be the problem defined in the Stokes sectors S_{-2} and S_2. We should instead use a contour which has been deformed below the real axis to stay within the correct Stokes sectors. Figure 2.3 shows a possible contour for M just larger than 2.

Having gained some understanding of Stokes sectors and boundary conditions on the complex plane we can now make a firm definition of the model we are interested in.

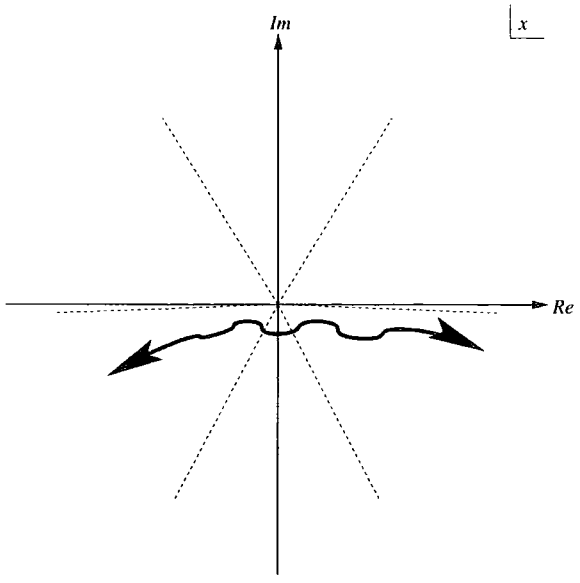

Figure 2.3: The Stokes Sectors For M Just Larger Than 2

2.2 Formal Definition Of The Problem

There are two equivalent definitions of the problem which are useful in different situations.

2.2.1 Definition 1

If we define the Stokes sectors now as:

$$S_k := \left|\theta - \frac{2\pi k}{2M+2}\right| < \frac{\pi}{2M+2} \tag{2.12}$$

with θ defined so that $\theta = 0$ on the negative imaginary axis, or $\theta = \arg(x) - \frac{\pi}{2}$.

The problem we are interested in is:

$$\left(-\frac{d^2}{dx^2} - (ix)^{2M} + \frac{l(l+1)}{x^2}\right)\phi(x) = E\phi(x) \tag{2.13}$$

defined on the complex plane, with a cut running up from the origin to infinity along the positive imaginary axis. We are interested in the values of E for which this problem has solutions that decay in the Stokes sectors S_1 and S_{-1}.

2.2.2 Definition 2

Sometimes it is useful to consider the problem under the transformation $x \to \frac{x}{i}$, $E \to -E$. In this case we define the Stokes sectors as

$$S_k := \left| \theta - \frac{2\pi k}{2M+2} \right| < \frac{\pi}{2M+2} \tag{2.14}$$

where now $\theta = 0$ on the positive real axis, or $\theta = \arg(x)$.

$$\left(-\frac{d^2}{dx^2} + x^{2M} + \frac{l(l+1)}{x^2} \right) \psi(x) = E\psi(x) \tag{2.15}$$

defined on the complex plane, with a cut running up from the origin to infinity along the negative real axis. We are interested in the values of E for which this eigen-problem has eigenfunctions that decay in the Stokes sectors S_1 and S_{-1}. For $M \sim 1$, the sectors S_1 and S_{-1} now, due to the rotation, contain the positive and negative imaginary axes respectively.

These two problems are related by a rotation of $\frac{\pi}{2}$. The energies are the negative of each other.

The first definition should be thought of as the fundamental statement of the problem. The second definition is useful sometimes when studying the problem. We can see that the second definition appears to be hermitian. However the hermiticity of a problem is a property of the Hamiltonian AND its boundary conditions. For this reason the second definition is still non-hermitian as the boundary conditions are complex. We basically have the choice between having the complex part of the problem in either the potential or the boundary conditions.

2.3 Phenomenology of the Energy Spectrum

Using numerical techniques it is possible to graph the first few real energy levels of the spectrum, for particular values of l, as we vary M. Let us look first at $l = 0$ (Figure 2.4).

We can see that for $M = 1$, we get the expected harmonic oscillator. In the region $M > 1$ the energy levels all stay real and grow as M increases. However, for $M < 1$, we get a notably different behaviour. As M decreases the energy levels start

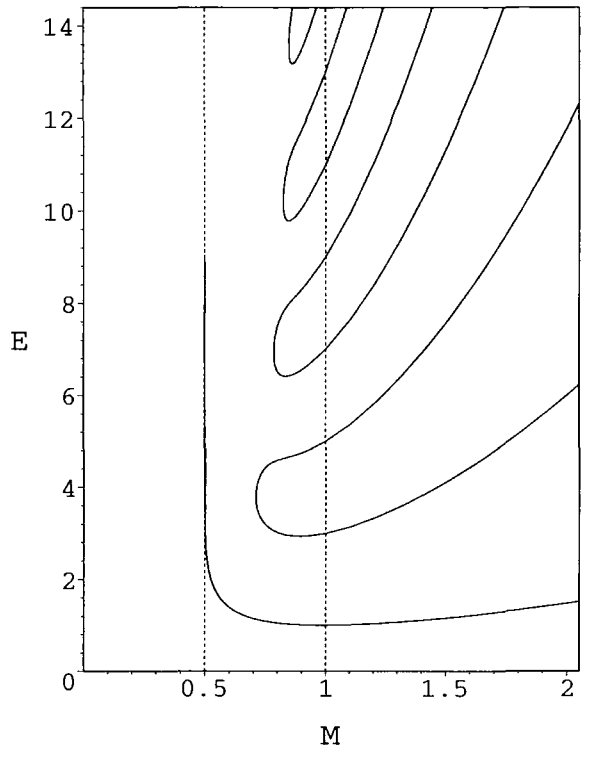

Figure 2.4: The Energy Levels For $l = 0$

pairing off. Where two energy levels meet, they become complex conjugates of each other. As M passes below 1, infinitely many energy levels pair off from the top of the spectrum. As M continues to decrease more and more levels pair off, until there is only one left. This final energy level tends toward infinity as M tends toward $\frac{1}{2}$. There are no real energy levels for $M < \frac{1}{2}$.

We can however also vary l. Let us look at the spectrum with a small value of l (Figure 2.5).

Here we can see there is a marked difference between the two regimes. The case $l = 0.001$ is not greatly different from the $l = 0$ case. The final eigenvalue crosses the line $M = \frac{1}{2}$, but otherwise is qualitatively very similar. Conversely, for $l = -0.025$, the connectivity of the paired off eigenvalues has changed. There is now no final energy level to tend off to infinity. Some idea of how this could happen continuously is given by figure 2.6.

As l increases from -0.025, the lowest pairing moves toward the next highest pairing, until they meet and the pairing changes. Now the lowest and the fourth

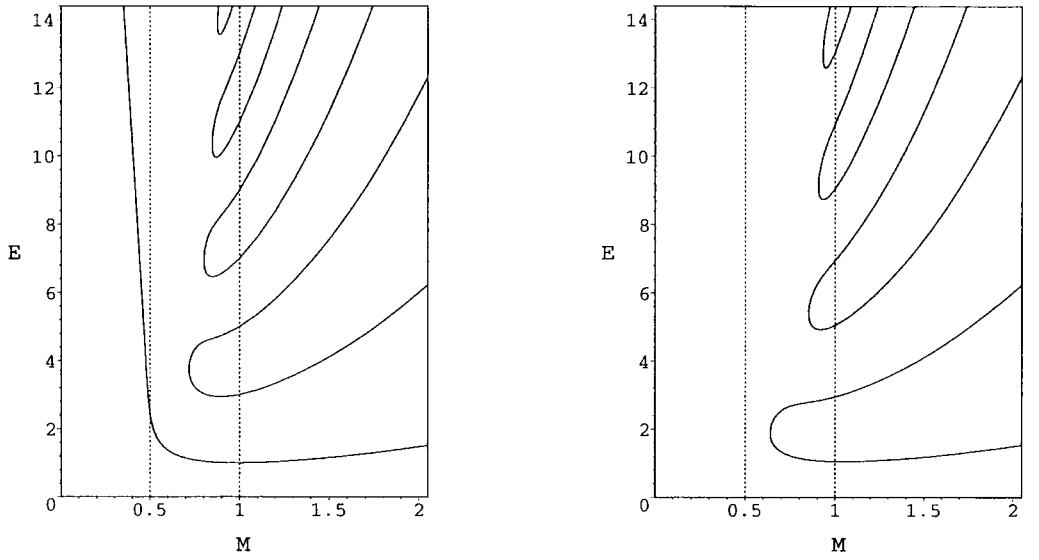

$l = 0.001$ $l = -0.025$

Figure 2.5: The Energy Levels For Two Non-Zero Values of l

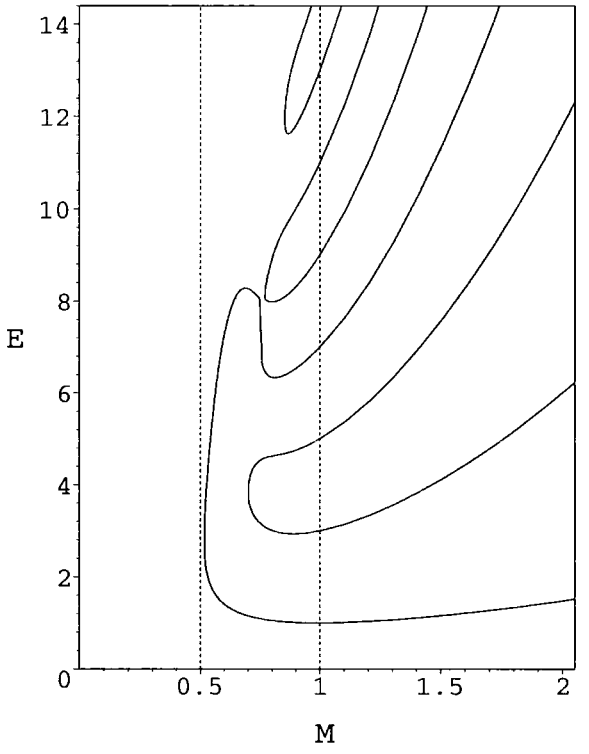

Figure 2.6: The Energy Levels For l=-0.001

lowest merge, as do the second and third lowest. As l continues to increase, the pairing of the lowest energy moves up the spectrum, until we get to the situation at

$l = 0$. From the figure we can see that at $l = -0.001$ the lowest and fourth lowest energy levels are paired and a transition is about to take place. After the transition the lowest and sixth lowest energy levels will be paired.

This, then, is the $\mathcal{PT}$ symmetric problem we shall be studying for the majority of this thesis. The aim will be to understand the numerically observed behaviour, seen above, analytically We shall take a number of approaches. We shall study it at a classical level and see that it exhibits some interesting behaviour as we allow a classical particle to move around the complex plane under the influence of this potential. We will then go on to study the quantum case as defined above from a perturbative approach. Finally we shall use non-perturbative techniques that will take us past the WKB approximation. The main aim is to gain some insight into the merging of eigenvalues for $M < 1$ and in particular the change in connectivity for differing values of l.

First, in the next chapter, we shall see some of the novel behaviour exhibited by this potential in the classical case.

Chapter 3

Classical Trajectories

3.1 Introduction

Before we get into the quantum case, it is an interesting diversion to see the implications at the classical level. This builds on work that has been done by Bender, Boettcher and Meisinger [7]. They studied the classical version of our potential in the case $l = 0$, by extending conventional classical mechanics into the complex plane.

They found some interesting and unexpected results. They allowed a particle to travel in the complex plane under the potential:

$$-(ix)^{2+\epsilon}. \tag{3.1}$$

It was found that, for $\epsilon \geq 0$, the particle would execute closed trajectories. For $\epsilon < 0$ there was a difference in the behaviour; the trajectories were no longer closed and spiralled out to infinity. This was interpreted as a breaking of $\mathcal{PT}$-symmetry and a classical analogue of the eigenvalues becoming complex in the quantum case.

We shall be studying the potential with an angular momentum term:

$$-(ix)^{2+\epsilon} + \frac{l(l+1)}{x^2}, \tag{3.2}$$

focusing on the area around $\epsilon = 0$. We shall reproduce some of the results of [7] and see the difference when the angular momentum term is added. We will demonstrate that it is not only in the region $\epsilon < 0$ that trajectories with broken $\mathcal{PT}$-symmetry can be seen.

3.2 The Method

We shall be exploring the behaviour of a classical particle moving in the potential:

$$-(ix)^{2+\epsilon} + \frac{l(l+1)}{x^2} \tag{3.3}$$

We use Hamilton's equations:

$$\frac{dx}{dt} = \frac{\partial H}{\partial p} = 2p \tag{3.4}$$

$$\frac{dp}{dt} = -\frac{\partial H}{\partial x} = i(2+\epsilon)(ix)^{1+\epsilon} + 2l(l+1)x^{-3} \tag{3.5}$$

So we have:

$$\frac{d^2x}{dt^2} = 2(i(2+\epsilon)(ix)^{1+\epsilon} + 2l(l+1)x^{-3}) \tag{3.6}$$

As t is real and we are interested in the trajectories these particles trace in the complex plane, we can make the transformation $t \rightarrow \frac{t}{2}$

$$\frac{d^2x}{dt^2} = \frac{1}{2}(i(2+\epsilon)(ix)^{1+\epsilon} + 2l(l+1)x^{-3}) \tag{3.7}$$

We integrate once:

$$\frac{dx}{dt} = \pm\sqrt{E + (ix)^{2+\epsilon} - \frac{l(l+1)}{x^2}} \tag{3.8}$$

In Bender et al's paper, not having the x^{-2} term, they were able to rescale the modulus of x and also further rescale t and change the E in their equations to one. We, however, cannot do this so easily. If we try to rescale E out of (3.8), we arrive at the equation:

$$\frac{1}{\sqrt{E}}\frac{dx}{dt} = \pm\sqrt{1 + \frac{(ix)^{2+\epsilon}}{E} - l(l+1)\frac{x^{-2}}{E}} \tag{3.9}$$

If we send $x \rightarrow E^{1/(2+\epsilon)}x$ and $t \rightarrow E^{1/2-1/(2+\epsilon)}$ we still end up with:

$$\frac{dx}{dt} = \pm\sqrt{1 + (ix)^{2+\epsilon} - l(l+1)x^{-2}E^{-\frac{4}{2+\epsilon}}} \tag{3.10}$$

Now if the term $l(l+1)$, were an arbitrary constant we could simply rescale. However, due to this term's symmetry under $l \rightarrow -l-1$, $l(l+1) > -\frac{1}{4}$. Therefore a simple

transform $l(l+1)E^{-\frac{4}{2+\epsilon}} \rightarrow L(L+1)$, loses some of the information in the equations. For $l > 0$, there is no restriction on $l(l+1)$ and this would not be a problem. This is an early sign of the difference between the regions $l \geq 0$ and $l < 0$ at the classical level. Whether this is entirely coincidental, or somehow connected to the way the energy levels behave in the quantum case, is unclear.

As the rescaling is problematical, we shall set $E = 1$, so as to be able to compare with [7]. It is from (3.8) and (3.7) we will be working. Having fixed E, if we then start a particle at an initial point x_0, we determine (up to a sign) the particles velocity. As we know the particles velocity, we can approximate the particles position after a small amount of time, dt, has elapsed. This new position can then be used to calculate the new velocity and so on. We will be using Maple to perform this operation for us repeatedly and studying the resulting paths.

The program with just the velocity term, did not give us the correct closed paths, predicted by Bender and Boethcher in the $l = 0$ case. One possible solution to this problem would have been to decrease the step size. However, a less computationally intensive method is to introduce an acceleration term. This is what was done. It is possible to view the operation as a Taylor expansion around the initial point and if it was necessary, we could add further terms. For instance, the next term to add would be the "jerk". We would write x_{n+1} as:

$$x_{n+1} = x_n + dt\frac{dx}{dt}\bigg|_{x_n} + \frac{1}{2!}dt^2\frac{d^2x}{dt^2}\bigg|_{x_n} + \frac{1}{3!}dt^3\frac{d^3x}{dt^3}\bigg|_{x_n} \tag{3.11}$$

We must take care with the sign in the velocity, as we cross branch cuts associated with the turning points, to ensure a consistent choice. The initial choice of this sign is arbitrary and is a signal that trajectories maybe traversed in either direction. It can also be interpreted as a reversal of time.

For $\epsilon = 0$ our equation is acceptable as a normal classical potential. Let us turn our attention to this case first.

3.3 The Case $\epsilon = 0$

When $\epsilon = 0$, we have:

$$\frac{dx}{dt} = \pm\sqrt{1 - x^2 - \frac{l(l+1)}{x^2}} \tag{3.12}$$

and our system (at least for $l > 0$) is a conventionally allowed classical problem, in that it is possible to find solutions with real energies, momentums and positions. We shall, at first, simplify it even further and set $l = 0$.

3.3.1 $l = 0$

This situation was well covered by Bender et al and so here we are just recapping it, to contrast with the $l \neq 0$ case.

When $l = 0$ and $\epsilon = 0$, we have the *very* well understood quadratic potential. The turning points are at:

$$x_{\text{trn}} = \pm\sqrt{E} \tag{3.13}$$

and the particle executes simple harmonic motion between these two points. In our case this is still true, however, as we are continuing the problem off the real axis, we are not restricted to the real line between our two turning points.

The equation is exactly solvable for x, the solution is:

$$x(t) = \cos[\arccos x(0) \pm t] \tag{3.14}$$

The solutions are nested ellipses, with the two turning points as the foci. Figure (3.1) shows one of these ellipses.

We can see the $\mathcal{PT}$-symmetry explicitly in this figure. Under $\mathcal{PT}$-symmetry $x \rightarrow -x^*$. This is just reflecting the trajectory in the imaginary axis. If we think about the velocity, we can see the direction of travel around the path is reversed. However, to complete the transformation, we also need to send $dt \rightarrow -dt$, equivalent to changing the sign in the velocity. The trajectory, is then mapped onto itself.

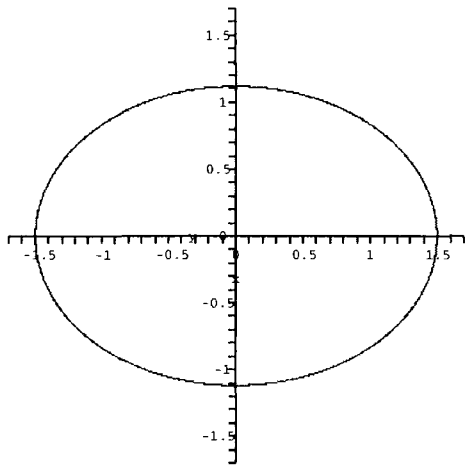

Figure 3.1: Trajectory on the complex plane starting from $x_0 = 1.5$.

3.3.2 $l \neq 0$

The situation is more complicated for $l \neq 0$. There are now four turning points. They are:

$$x^{+}_{\text{trn}} = \pm\sqrt{\frac{1}{2}(1 + \sqrt{1 - 4l(l+1)})} \tag{3.15}$$

and

$$x^{-}_{\text{trn}} = \pm\sqrt{\frac{1}{2}(1 - \sqrt{1 - 4l(l+1)})} \tag{3.16}$$

The x^{+}_{trn} can be thought of as an adjustment of the turning points of the $l = 0$ case. For l positive they drift towards the origin along the real axis. For l negative they drift away from the origin along the real axis.

The x^{-}_{trn} on the other hand are new. They have appeared from the origin and move away from it as we increase l away from zero. Note there is a marked difference depending on the sign of l. If l is positive the x^{-}_{trn} appear from the origin and move out along the real axis. If l is negative the x^{-}_{trn} appear from the origin and move out along the *imaginary* axis.

As $l(l+1)$ is symmetric about $l = -\frac{1}{2}$, we need only consider the case $l > -\frac{1}{2}$. This means that $-4l(l+1) < 1$. When $-\frac{1}{2} < l < 0$ the term $1 - 4l(l+1)$ is always positive, so therefore the turning points are either purely real or purely imaginary.

However, for $l > 0$, there is no limit to how large we can make $l(l+1)$. When $l = \frac{\sqrt{2}-1}{2}$, then $\sqrt{1-4l(l+1)} = 0$. In this case $+x^+_{\text{trn}} = +x^-_{\text{trn}}$ and $-x^+_{\text{trn}} = -x^-_{\text{trn}}$, hence there is only one turning point on each side of the imaginary axis.

For $l > \frac{\sqrt{2}-1}{2}$, there are again four turning points. though now they all lie away from the axes. This is the case in which, conventionally, the particle does not have enough potential energy to reach the bottom of the potential well. This situation is not generally allowed, as it means we need negative velocity squared. However, we are admitting imaginary velocity, so can cope with this situation.

We then have four distinct regimes: 1) $-\frac{1}{2} < l < 0$, 2) $0 < l < \frac{\sqrt{2}-1}{2}$, 3)$l = \frac{\sqrt{2}-1}{2}$ and 4)$l > \frac{\sqrt{2}-1}{2}$.

Far enough away from the origin, we expect the trajectories of the particle to look like those for $l = 0$, as the x^{-2} term will be negligible. We will take a look at each of the regimes closer to the origin, where we expect the x^{-2} to be more influential. As the trajectories cannot cross and there are closed contours further out, we expect to see more closed contours.

$-\frac{1}{2} < l < 0$

This potential has an infinite potential well at the origin. If we start the particle off on either of the axes, on or closer to the origin than the turning points, it accelerates down this well and we never see it again. For this reason it is not conventionally allowed. Let us start off the particle close to the origin, but not on either of the axes. Figure (3.2) shows this.

In the first of these plots we have kept the axes in proportion to make it easier to contrast with the plot further out. We can see that there is some change; the ellipse is deformed slightly. The trajectory comes in closer to the origin, then swings out around the imaginary turning point. For the second of these plots we have started the particle even closer to the origin. We can see that, as expected conventionally, the potential well draws the particle towards it. As it cannot cross the axes inside the turning points, it moves away to pass them on the outside, tracing these rounded crosses. We do have something new here, in the conventional case there is no stable motion. For the complex case, we have periodic orbits.

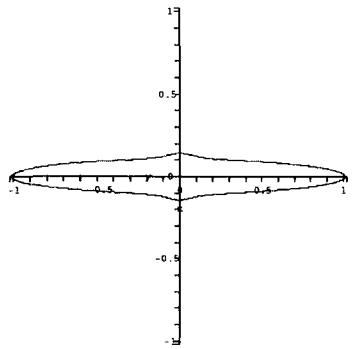

$x_0 = 1.01$

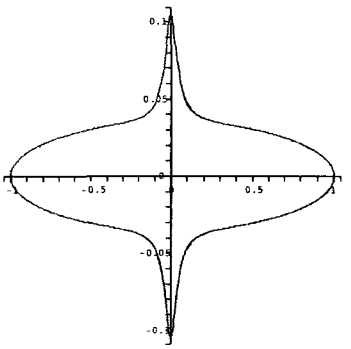

$x_0 = 0.06 + i0.06$

Figure 3.2: Two trajectories on the complex plane for $l = -0.01$

$0 < l < \frac{\sqrt{2}-1}{2}$

This is the only case in which, conventionally, there is a non-trivial periodic solution. In this case (as well as the general $l > 0$ cases), there is still a singularity, but this time it is an infinite peak and the particle will naturally be unable to reach the origin. If we start the particle on the real axis at $-x^+_{\text{trn}} < x < -x^-_{\text{trn}}$ or $+x^-_{\text{trn}} < x < +x^+_{\text{trn}}$, the particle executes a periodic path between the two turning points. These are the conventionally allowed solutions.

Notice we have already seen a notable difference between this and any other case we have seen so far. In all the cases so far, all the paths were $\mathcal{PT}$, that is left-right, symmetric. The conventional solutions to this case do not exhibit this. Each of the two paths takes place entirely on one side of the complex plane. These two paths are the $\mathcal{PT}$-symmetric partners of each other and taken together, we see the entire system does retain $\mathcal{PT}$-symmetry.

Let us search for other trajectories. Figure (3.3) shows one example. We can see we have a $\mathcal{PT}$-symmetric complex path. Compared with the negative l case, it is pinched in as it crosses the imaginary axis, as opposed to peaked.

An interesting question to ask is: what if we start the particle on the real line, but with $x_0 < |x^-_{\text{trn}}|$? Figure (3.4) shows just such an example. We see that again, we have two orbits, one on either side of the complex plane, that are only $\mathcal{PT}$-

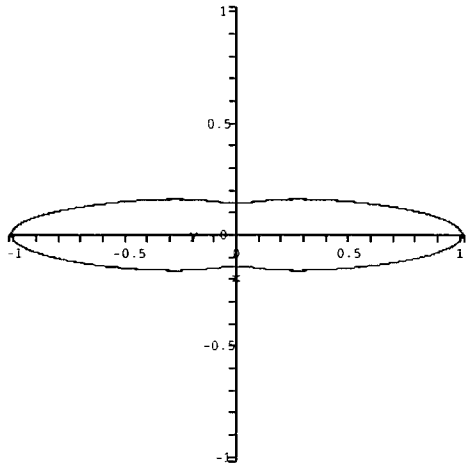

Figure 3.3: Trajectory on the complex plane starting from $x_0 = 1.01$, with $l = 0.01$.

symmetric when taken in partnership. These trajectories encircle the conventional paths.

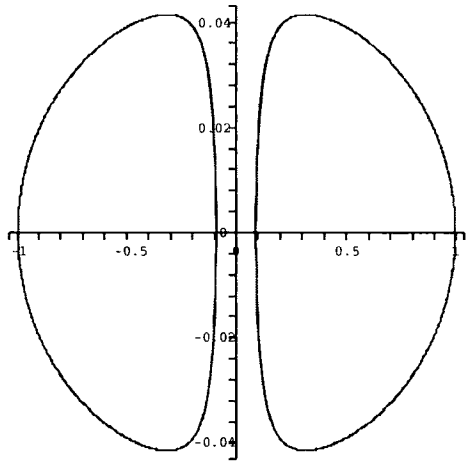

Figure 3.4: Trajectory on the complex plane starting from $x_0 = \pm 0.09$, with $l = 0.01$.

The final piece in our understanding of this case is shown in figure 3.5. This is a graph of four trajectories. The two $\mathcal{PT}$-symmetric partners we have already seen and two others that are $\mathcal{PT}$-symmetric on their own. It should be emphasised that

although these trajectories become very close as they cross the real axis, they do not coincide at any point. We can see that if we start our trajectories just outside x^+_{trn}, we get closed $\mathcal{PT}$-symmetric paths that dip in more and more as we move x_0 towards the origin. Eventually the dipping becomes so severe that the single orbit actually pinches off into two trajectories. This also assists our understanding of the relative directions of the $\mathcal{PT}$ partner trajectories. If the single path encircling all four turning points is travelling in, say, the anti-clockwise direction, then as the split occurs the double paths must keep the same orientation. This means that to have a consistent choice for the sign of the velocity, both the $\mathcal{PT}$ partner paths must travel in the same direction. This conserves the $\mathcal{PT}$-symmetry of the entire plane.

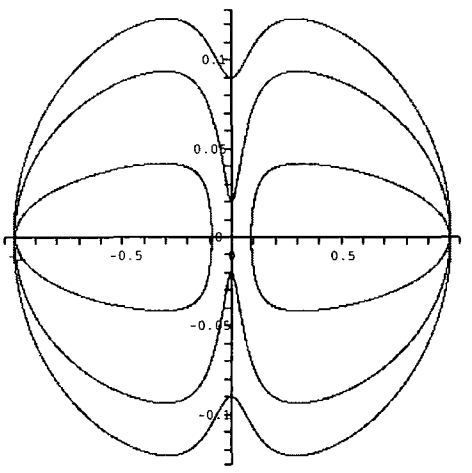

Figure 3.5: Trajectories just outside x^+_{trn}, with $l = 0.01$.

$l = \frac{\sqrt{2}-1}{2}$

In this exceptional case, the x^-_{trn} and x^+_{trn} have met and we have only two distinct turning points. In the conventional case, there is only the trivial solution, where the turning point sits at the bottom of the potential well and does not move. As the potential energy is only defined up to a constant, this would be described as the zero energy state. The turning points are stable stationary points, in that both the velocity and the acceleration are zero. A particle placed here will remain there

for all time. We will again be exploring what happens when the particle is started elsewhere.

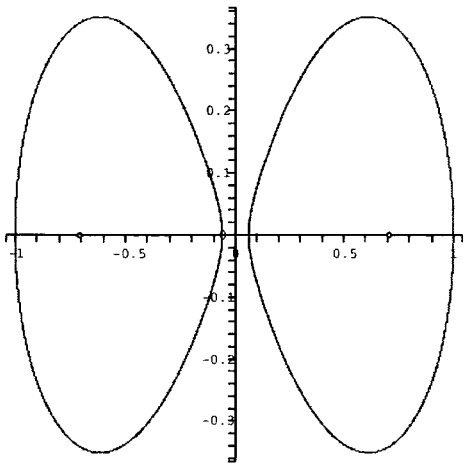

Figure 3.6: Trajectories starting at $x_0 = \pm 0.06$, with $l = \frac{\sqrt{2}-1}{2}$.

Figure (3.6) shows the case when $x_0 = \pm 0.06$. We get two $\mathcal{PT}$-symmetric partner trajectories. These are very similar to those seen for the case $0 < l < \frac{\sqrt{2}-1}{2}$. They again encircle the conventionally allowed solution.

$l > \frac{\sqrt{2}-1}{2}$

Conventionally in this case, there is not enough energy for the particle to even reach the bottom of the potential well. The turning points now lie away from the axes. The x_{trn}^- and x_{trn}^+ are now complex conjugates of each other. Let us see what happens when we release the particle from one of the turning points (figure(3.7)).

As we can see there are two $\mathcal{PT}$ partner paths travelling back and forth between the turning points. Interestingly, for values of l less than the one we chose, but greater than $\frac{\sqrt{2}-1}{2}$, the turning points fall on these paths. We could, therefore draw these lines by plotting the positions of the turning points as l increases from $\frac{\sqrt{2}-1}{2}$, up to our chosen value.

Figure (3.8) shows some other trajectories for this case. Again we have the $\mathcal{PT}$-symmetric trajectories and the $\mathcal{PT}$ partner paths. They are similar to the other

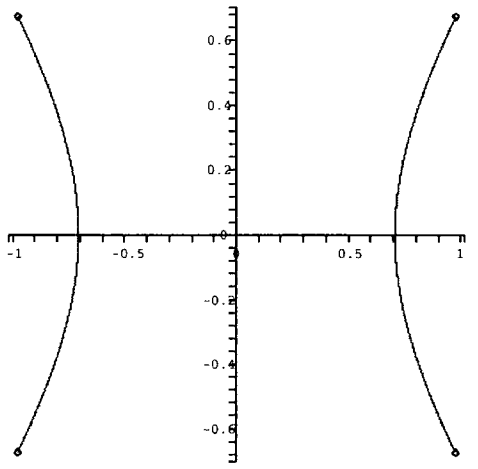

Figure 3.7: Trajectories between turning points, with $l = 1$.

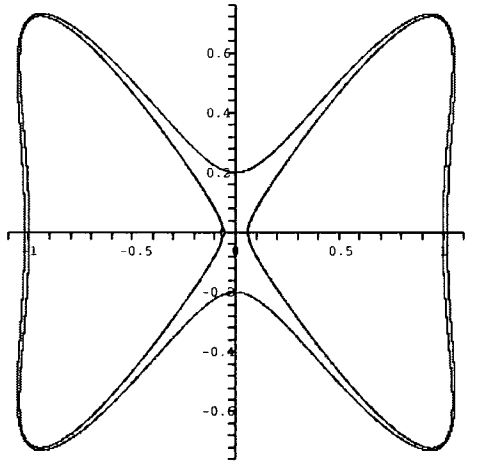

Figure 3.8: Trajectories starting at $x_0 = \pm 0.06$, with $l = 1$.

$l > 0$ examples, but deformed to take account of the turning points.

So, having looked at the what we thought were five different regimes, it turns out there are only really three qualitatively different cases.

- Case $l = 0$. In this situation, we have nested ellipses around the two turning points. All of the complex trajectories can be shrunk onto the conventional so-

lution without passing any turning points. Each trajectory is $\mathcal{PT}$-symmetric.

- Case $-\frac{1}{2} < l < 0$. We have deformed ellipses around the four turning points. The conventional solution is unstable and cannot be obtained from shrinking the complex solutions. The branch cut trajectories all meet at the origin. The orbits cannot be shrunk onto the branch cut paths due to the singularity at the origin. Except for the branch cut solutions, each trajectory is $\mathcal{PT}$-symmetric.

- Case $l > 0$. In this situation we have trajectories that encircle all the turning points and also trajectories that only encircle the branch cut trajectories. Only those that encircle the branch cut paths can be deformed onto them. Only those that encircle all the turning points are $\mathcal{PT}$-symmetric, the others have a $\mathcal{PT}$ partner which maintains the symmetry of the complex plane.

This can be further summarised by the question: Can the complex contours be deformed onto the branch cut paths? The answer being: yes, no, or sometimes for the cases $l = 0$, $-\frac{1}{2} < l < 0$ and $l > 0$ respectively.

We will now look at what happens when $\epsilon \neq 0$. Carl Bender and his collaborators studied the $l = 0$ case, for various values of ϵ. We will focus our attention on $\epsilon \pm 0.1$ and $l = 0$, or $l = \pm 0.01$. Let us first look at the case $\epsilon = 0.1$.

3.4 The Case $\epsilon = 0.1$

We are now dealing with an unashamedly complex potential, there are now no solutions on the real axis. There is also a complication whenever we set ϵ non-integer. We now must introduce a branch cut to take into account the fractional power of x. This means we are no longer working on the standard complex plane, but instead on a multi-sheeted Riemann surface. We put the branch cut running up the imaginary axis to maintain $\mathcal{PT}$-symmetry.

3.4.1 $l = 0$

Figure 3.9, shows us a trajectory in this case. The different colours are parts of the trajectory on different sheets of the Riemann surface, the red part is on the

fundamental sheet. The path now moves onto a new sheet every time the particle crosses the branch cut. As we can see the particle's trajectory moves onto three different sheets, before returning to its initial position. Note, that although the path has become significantly more complicated, $\mathcal{PT}$-symmetry is retained.

Let us see how varying l affects the result.

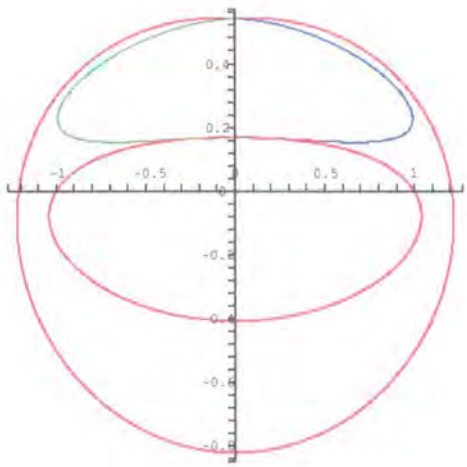

Figure 3.9: Trajectories starting at $x_0 = 1$, with $l = 0$. The red part of the trajectory takes place on the principal sheet.

3.4.2 $l \neq 0$

Let us see what happens if we now add a small positive l term. As in the $\epsilon = 0$ case, it is close to the origin we expect to see the greatest differences. In the ϵ case we could guarantee that closer to the origin we must have closed trajectories, because further out we had closed paths that could not be crossed. This no longer true, due to the multi-sheetedness of the Riemann surface.

Let us start the particle off on the branch cut close to the origin and see how it behaves fig. 3.10. Again the different coloured lines are on different Riemann sheets.

We can see that as before, we have a closed orbit that goes on to three sheets of the Riemann surface. We notice there is a dip in the contour towards the origin. In

Figure 3.10: Trajectories starting at $x_0 = i0.06$, with $l = 0.01$.

the $\epsilon = 0$ case, close enough to the origin, this dipping became a splitting into two $\mathcal{PT}$ partner trajectories. Maybe we can see this behaviour in the $\epsilon = 0.1$ case.

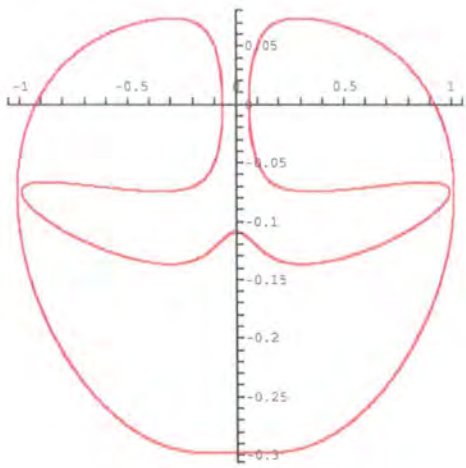

Figure 3.11: Trajectories starting at $x_0 = 0.06$, with $l = 0.01$.

We do not actually see a separation into two trajectories, fig 3.11, but we do see some new behaviour. The pinching off only happens above the real axis. We are left with a $\mathcal{PT}$-symmetric path that only travels on the principal sheet of our

Riemann surface. So we have found that by adding a small positive l term we can create qualitatively different trajectories from the $l = 0$ case.

There is also a third possible class of trajectory, figure 3.12. This is a path that takes place within the inner loop of fig. 3.11. This trajectory contains inside it different turning points that the previous two examples. It is clear now, that fig 3.11, is a deformation of fig. 3.10, the difference being that fig. 3.10 travels onto sheets other than the principal one. The breaking of $\mathcal{PT}$-symmetry of trajectories for $\epsilon = 0$ appears to be related to the way in which the branch cuts link the turning points.

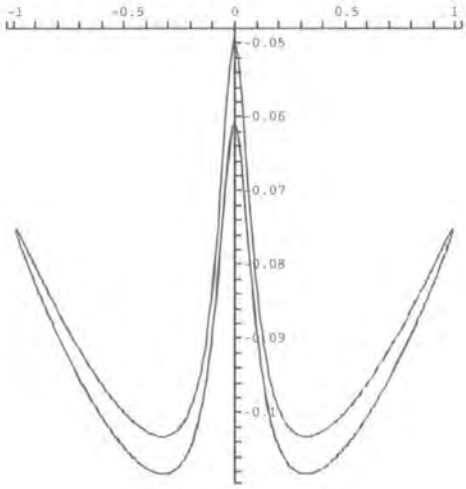

Figure 3.12: Trajectories at $x_0 = 0.5 - i0.1$, with $l = 0.01$.

Let us next study the $l = -0.01$ case. Fig 3.13, shows an example of a trajectory for $l = -0.01$. We can see that, as in the $\epsilon = 0$ case, it is a deformation of the $l = 0$ case. We have only the one class of trajectory, when $l < 0$. As the trajectory passes above the origin, it is deformed upwards, compared to the $l = 0$ case. This is the opposite to the situation when $l > 0$.

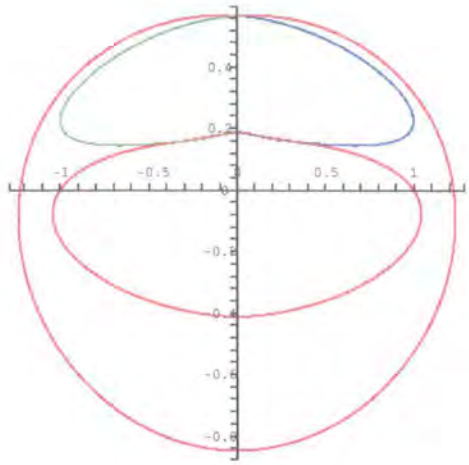

Figure 3.13: Trajectories starting at $x_0 = 1$, with $l = -0.01$.

3.5 The Case $\epsilon = -0.1$

3.5.1 $l = 0$

Bender et al studied this case, for $l = 0$. A particular difference was found between the regions $\epsilon < 0$ and $\epsilon \geq 0$. As we have seen, when $\epsilon \geq 0$, we find closed trajectories. However, for $\epsilon < 0$, this behaviour was not seen. Instead the trajectories spiral out towards infinity.

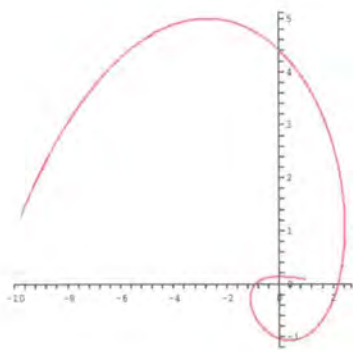

$x_0 = e^{i\pi/38}$

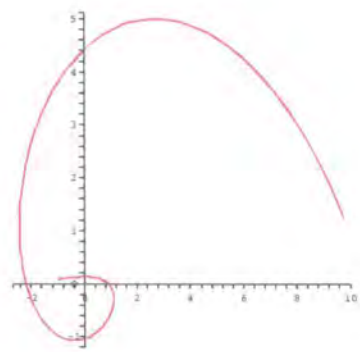

$x_0 = e^{-i\pi/38}$

Figure 3.14: Two trajectories for $l = 01$

We can see two open trajectories in fig 3.14. Bender et al interpreted this lack of closed trajectories as a break down in $\mathcal{PT}$-symmetry and an analogue of the complexification of the energy levels in the quantum case. However, we have already seen non-$\mathcal{PT}$-symmetric paths which were closed. In these cases the symmetry of the plane as a whole was not lost as our paths had $\mathcal{PT}$ partner trajectories. This is similar to what we are seeing here, the difference being that now we see open trajectories.

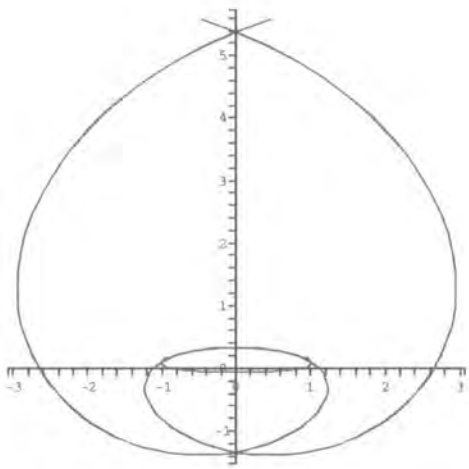

Figure 3.15: Trajectory not starting at a turning point, with $l = 0$.

In fact, we can find $\mathcal{PT}$-symmetric paths by not starting our particle at a turning point. Fig 3.15 shows us an example of this. The particle spirals in from infinity, passes around the turning points and spirals back out to infinity. We can see then that there is no real $\mathcal{PT}$-symmetry breaking, what we lose is the boundedness of the trajectories. From this plot it is difficult to see the behaviour near the origin. Fig 3.16 shows us a closer look at this. If we take the particle to be coming in from the bottom right of the picture, the trajectory loops twice, clockwise, around the origin before going out to infinity again.

Is it possible that we may find a difference for non-zero values of l? Let us take a look at this.

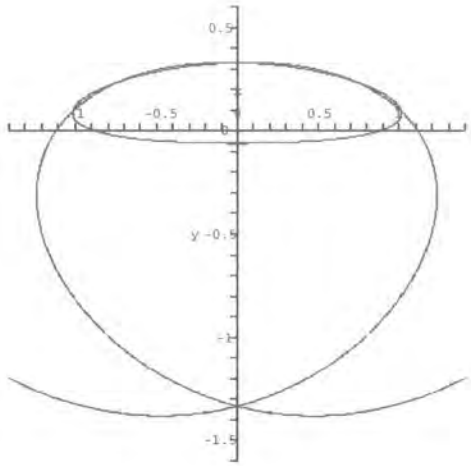

Figure 3.16: A closer look at fig. 3.15.

3.5.2 $l \neq 0$

The difference we have seen so far between the $l > 0$ and $l \leq 0$ regions has been the existence of trajectories that individually do not conserve $\mathcal{PT}$-symmetry. When $\epsilon < 0$ there are, for $l = 0$, already paths that have broken $\mathcal{PT}$-symmetry. They are the paths originating from the turning points. The others are infinite open paths. Let us see what changes occur when we add a small positive l term. Figure 3.17 shows an example of this, as before it is difficult to see the behaviour near the origin so we show in figure 3.18 a closer look at this region.

What we see near the origin is something similar to the $l = 0$ plot. The main difference is the pull towards the origin as we cross the negative imaginary axis, which is also seen for other values of ϵ. As in cases where $\epsilon \geq 0$, we have trajectories displaying a qualitative difference, it is reasonable we might find some sign of them for $\epsilon = -0.1$. Certainly it would make the change from the two regions smoother. Figure 3.19 shows exactly this. What we see here is a trajectory showing broken $\mathcal{PT}$-symmetry.

Let us now study the case for $l < 0$. As in the cases $\epsilon \geq 0$, when $l < 0$ we have a deformation of the $l = 0$ case. Figs. 3.20 and 3.21 show this.

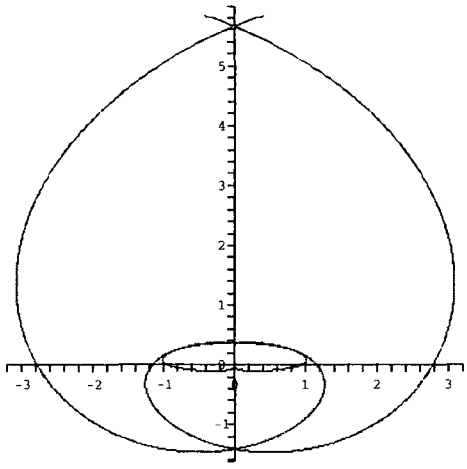

Figure 3.17: The trajectory starting at $x_0 = -i0.06$, with $l = 0.01$.

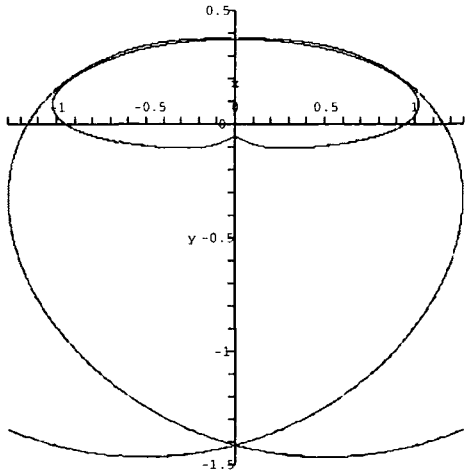

Figure 3.18: A closer look at fig.3.17.

3.6 Conclusion

We have studied the potential:

$$-(ix)^{2+\epsilon} + \frac{l(l+1)}{x^2} \tag{3.17}$$

for differing values of l, around $\epsilon = 0$, where in the quantum case there is a phase change. We were interested if there was any way of seeing, at the classical level, a

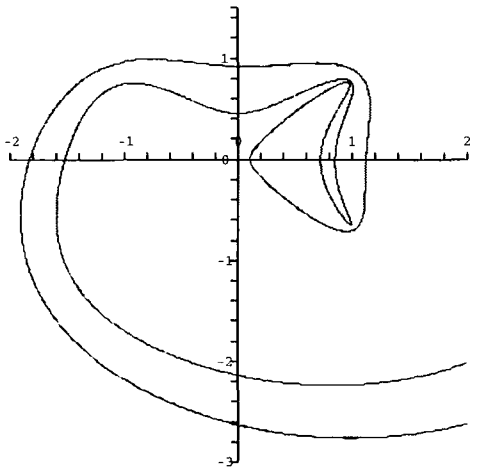

Figure 3.19: The trajectory starting at $x_0 = 0.1$, with $l = 1$.

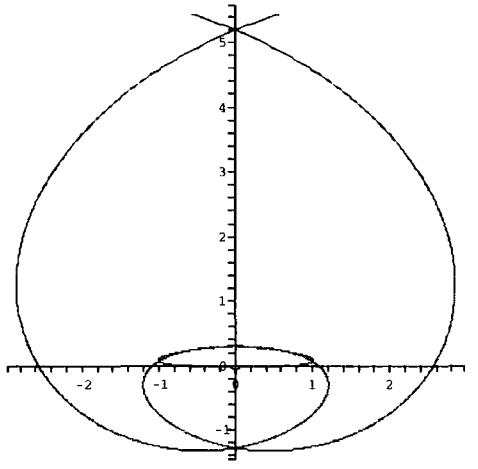

Figure 3.20: The trajectory starting at $x_0 = -i0.1$, with $l = -0.01$.

sign of this change. We knew this was the case for $l = 0$ and wished to see if it continued for other values of l.

It turns out there is. For $\epsilon \geq 0$, we can always find periodic trajectories. In fact in this region the only non-periodic trajectories are those for $\epsilon = 0$ and $l < 0$, along the branch cuts. For $\epsilon < 0$, we find no periodic trajectories. The region in which we can always find closed trajectories matches with the region where the energy

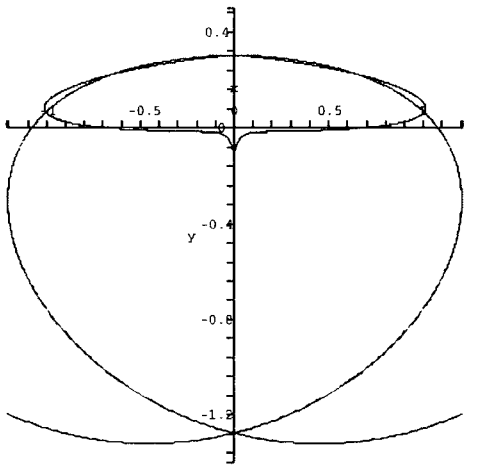

Figure 3.21: A closer look at fig. 3.20

spectrum is entirely real in the quantum case. The region in which we cannot find closed paths, is the same as that in the quantum case where the energy spectrum has complex eigenvalues.

This is a different interpretation, from that offered in [7]. The authors of that paper claimed the difference was due to the breaking of $\mathcal{PT}$-symmetry of the trajectories. However, we have found non-$\mathcal{PT}$-symmetric paths in the region where we know the spectrum to be real in the quantum case, so this can be ruled out.

Some avenues for further study follow naturally from what we have seen. We have not considered the possibility of complex energy. It may be possible to find closed trajectories in the region $\epsilon < 0$, for complex values of E. This would be a confirmation of the link between the classical and quantum behaviour. Any rescaling of E is complicated in this situation, as rescaling is only possible in real values without rotating the plane. Allowing complex E introduces a new parameter, $\arg(E)$. A complex value of E also means that a trajectory crossing the negative imaginary axis on the principal sheet will not be parallel to the real axis, i.e. the velocity will not be real. Hence, the $\mathcal{PT}$-symmetry of the entire plane is broken in this case.

This leads us onto the next idea. The rescaling in our case (with E real), shows a distinct split between $l < 0$ and $l \geq 0$. It would be interesting to know if this was

significant.

Another possible direction concerns the number of sheets of the Riemann surface the particle travels to, when $\epsilon > 0$ and non-integer. In discussion with Carl Bender, it was learnt that when he and his collaborators studied this, they were unable to find trajectories which used more than three sheets of the surface. We have also seen only trajectories that used three or less sheets. There is no obvious reason why this should be so. We also see, for $l > 0$, a breaking of $\mathcal{PT}$-symmetry when $\epsilon = 0$, but not when $\epsilon = 0.1$. This seems to be connected with the behaviour of the branch cuts linking the turning points. It would be interesting to gain some insight into how this change occurred.

Having studied the classical case, we will now return to the quantum. We shall next consider the perturbative method.

Chapter 4

Perturbative Approach

4.1 Introduction

In this chapter we are going to attempt to gain some information about the area $M < 1$ and the change of connectivity as we vary l.

We will be using the unrotated problem 2.2.1.

We are particularly interested in the area around $M = 1$, the harmonic oscillator, which is a well understood potential. We shall, following the method advocated by Bender et al [7], consider our potential as a perturbation about this point. We consider:

$$H_M = H_0 + V_1 \tag{4.1}$$

where

$$H_0 = -\frac{d^2}{dx^2} + x^2 + \frac{l(l+1)}{x^2} \tag{4.2}$$

is the harmonic oscillator Hamiltonian and

$$V_1 = -x^2 - (ix)^{2M} \tag{4.3}$$

As the unperturbed Hamiltonian, H_0 and the perturbed Hamiltonian H_M are very similar, we expect the wave functions of H_M, to be very similar to those of H_0. We will then expand H_M using the wavefunctions of H_0 as a basis. This means calculating the matrix $H_{mn} =< \psi_m|H_M|\psi_n >$. As the major contributions are in the diagonal entries and the entries become smaller as we move out away from the diagonal, it will be fair to truncate the matrix without losing too much of the

information encoded within it. We will then diagonalise the truncated matrix to obtain the approximate eigenvalues of H_M. For the method to be valid, we need $|V_{mn}| = | < \psi_m|V_1|\psi_n > | \ll |E_n^{(0)} - E_m^{(0)}|$, where the $E_n^{(0)}$ are the unperturbed energy levels. We consider the region around $M = 1$ where V_1 is small. To see that V_1 is indeed small, we take a Taylor series expansion, writing $2M = 2 + \epsilon$ we get

$$V_1 \sim \epsilon x^2 \ln(ix) = \epsilon x^2 (i(\frac{\pi}{2} + \arg(x)) + \ln(|x|)) \tag{4.4}$$

which we can see will be suitably small for ϵ small enough.

The Hamiltonian is symmetric under $l \longrightarrow -l-1$ so without loss of generality we can set $l > -1/2$

We need to calculate the matrix elements

$$< \phi_n(x)|H_M|\phi_m(x) > \tag{4.5}$$

where the $\phi_n(x)$ are the wavefunctions of the unperturbed Hamiltonian H_0. We will split this into the sum of three separate matrices:

$$\begin{aligned} < \phi_n(x)|H_M|\phi_m(x) > &=< \phi_n(x)|H_0|\phi_m(x) > \\ - < \phi_n(x)|x^2|\phi_m(x) > &- < \phi_n(x)|(ix)^{2M}|\phi_m(x) > \end{aligned} \tag{4.6}$$

The matrix $< \phi_n(x)|H_0|\phi_m(x) >$ is well known. It is a diagonal matrix with elements that are the energy eigenvalues of the simple harmonic oscillator. Note also that

$$\lim_{M \to 1} < \phi_n(x)|(ix)^{2M}|\phi_m(x) > = - < \phi_n(x)|x^2|\phi_m(x) > \tag{4.7}$$

This means if we can calculate the matrix elements $< \phi_n(x)|(ix)^{2M}|\phi_m(x) >$, we should have the necessary results to calculate the whole matrix $< \phi_n(x)|H_M|\phi_m(x) >$.

Before we calculate the matrix elements we shall need some knowledge of generalised hypergeometric functions and for this reason we will spend a short while reviewing them. Then in later sections we go on to use these functions to calculate the matrix elements described above.

4.2 Generalised Hypergeometric Functions

In the following discussion we will be making use of the generalised hypergeometric functions. It will therefore be instructive to spend some time looking at their basic

properties. The majority of this discussion is derived from that found in [1] [36] [40].

4.2.1 The Γ Function

The Gamma function, $\Gamma(z)$, is an analytic extension of the factorial function related as

$$\Gamma(z+1) = z! \tag{4.8}$$

It has the property

$$\Gamma(z+1) = z\Gamma(z) \tag{4.9}$$

It has poles at zero and negative integers.

Written as an integral it is

$$\Gamma(z) = p^z \int_0^\infty e^{-pt} t^{z-1} dt, \qquad \Re e(p) > 0, \quad \Re e(z) > 0. \tag{4.10}$$

4.2.2 The Pockhammer Symbol

We write

$$(a)_n \equiv a(a+1)(a+2)(a+3)...(a+n-1) \tag{4.11}$$

in particular $(a)_0 \equiv 1$. The $(a)_n$ is known as the Pockhammer symbol. We shall state some of its properties.

$$(1)_n = n! \tag{4.12}$$

If a is not a negative integer or zero then

$$(a)_n = \frac{\Gamma(a+n)}{\Gamma(a)} \tag{4.13}$$

If a is a negative integer, $-m$, we get

$$(a)_n = (-m)_n \qquad \text{if} \quad m \geq n \tag{4.14}$$

$$(a)_n = 0 \qquad \text{if} \quad m < n \tag{4.15}$$

We also note

$$(a)_{n-r} = \frac{(-1)^r (a)_n}{(1-a-n)_r} \tag{4.16}$$

and

$$(y-k)_n = \frac{(1-y)_k (y)_n}{(1-y-n)_k} \tag{4.17}$$

for integer n and k.

4.2.3 The Generalised Hypergeometric Function

The generalised hypergeometric function or generalised Gauss function is defined as

$$\begin{aligned} 1 \; + \; & \frac{a_1 a_2 ... a_A}{b_1 b_2 ... b_B} \frac{z}{1!} + \frac{a_1(a_1+1)a_2(a_2+1)...a_A(a_A+1)}{b_1(b_1+1)b_2(b_2+1)...b_B(b_B+1)} \frac{z^2}{2!} + ... \\ = \; & \sum_{k=0}^{\infty} \frac{(a_1)_k (a_2)_k ... (a_A)_k}{(b_1)_k (b_2)_k ... (b_B)_k} \frac{z^k}{k!} \end{aligned} \tag{4.18}$$

The function has A numerator parameters $a_1, a_2, ..., a_A$, B denominator parameters $b_1, b_2, ..., b_B$ and one variable z. The denominator parameters cannot, in general, be negative integers or zero as the function is undefined. Apart from this restriction the parameters and variable may take any value, real or complex. The sum of this series, if it exists, is denoted as

$${}_A F_B(a_1, a_2, ..., a_A; b_1, b_2, ..., b_B; z) \tag{4.19}$$

The generalised hypergeometric functions are immensely powerful, containing as they do many of the commonly used functions of analysis as special cases. For example the Laguerre polynomials are [36]

$$L_n^{\alpha}(x) = \frac{(\alpha+1)_n}{n!} {}_1F_1(-n; \alpha+1; x) \tag{4.20}$$

Another example is the function ${}_0F_0(;;z)$, the exponential function [36].

$${}_0F_0(;;z) = 1 + z + \frac{z^2}{2!} + ... + \frac{z^k}{k!} + ... = e^z \tag{4.21}$$

Other commonly used functions which can be written in terms of generalised hypergeometric functions are the Bessel functions, the Hermite polynomials, the Airy functions and the Coulomb Wave functions. In fact the above are special cases of either the ${}_2F_1$, otherwise known as the Gauss function, or the ${}_1F_1$ function, which sometimes goes by the name of the Confluent Hypergeometric or Kummer's function.

We will look at some of the properties of hypergeometric functions. In no way does this claim to be an exhaustive list, as this would fill a book and instead we will just state the ones which will be of interest to us.

The series converges if $A \leq B$. If $A = B + 1$ the series converges for $|z| < 1$. Also in this case the series converges if $z = 1$ and

$$Re\left(\sum_{\nu}^{B} b_\nu - \sum_{\nu}^{A} a_\nu\right) > 0, \tag{4.22}$$

and also when $z = -1$ and

$$Re\left(\sum_{\nu}^{B} b_\nu - \sum_{\nu}^{A} a_\nu\right) > -1. \tag{4.23}$$

If $A > B + 1$, the series converges only for $z = 0$.

If one of the numerator parameters is a negative integer, e.g. $a_1 = -m$, we get a terminating series

$${}_AF_B(-m, a_2, ..., a_A; b_1, b_2, ..., b_B; z) = \sum_{k=0}^{m} \frac{(-m)_k (a_2)_k ... (a_A)_k}{(b_1)_k (b_2)_k ... (b_B)_k} \frac{z^k}{k!} \tag{4.24}$$

In this case it is possible for the denominator parameters to take negative integer values, $-n$, provided $n > m$.

An important result known as Gauss's theorem is

$${}_2F_1(a_1, a_2; c; 1) = \frac{\Gamma(c)\Gamma(c - a_1 - a_2)}{\Gamma(c - a_1)\Gamma(c - a_2)} \tag{4.25}$$

When a_2 is a negative integer $-m$ we have the Chu-Vandermonde (sometimes known as Vandermonde) theorem

$${}_2F_1(a, -m; c; 1) = \frac{(c - a)_m}{(c)_m} \tag{4.26}$$

This holds true for all values of a and c when c is not a negative integer less than m; in these cases the series is undefined.

Contiguous Hypergeometric Functions

Two Hypergeometric functions are said to be contiguous if all but one of their parameters are equal, the unequal parameters differing by unity. For example

$${}_AF_B(a_1, ..., a_A; b_1, ..., b_B; 1) \tag{4.27}$$

$${}_AF_B(a_1 + 1, ..., a_A; b_1, ..., b_B; 1) \tag{4.28}$$

are contiguous. There are $(2A + 2B)$ functions contiguous to any hypergeometric function ${}_AF_B$. For ease of notation we shall write

$$F = {}_AF_B(a_1, ..., a_A; b_1, ..., b_B; 1) \tag{4.29}$$

$$F(a_i+) = {}_AF_B(a_1, ..., a_i + 1, ..., a_A; b_1, ..., b_B; 1) \tag{4.30}$$

$$F(b_i-) = {}_AF_B(a_1, ..., a_A; b_1, ..., b_i - 1, ..., b_B; 1) \tag{4.31}$$

Rainville [33] gives us $(A + B - 1)$ relations between a hypergeometric function $F(a_1+)$ and two contiguous functions.

$$(a_1 - a_k)F = a_1F(a_1+) - a_kF(a_k+) \tag{4.32}$$
$$k = 2, ..., A$$

$$(a_1 - b_k + 1)F = a_1F(a_1+) - (b_k - 1)F(b_k-) \tag{4.33}$$
$$k = 1, ..., B$$

Of course, as the order of the upper parameters is unimportant, these relations can be extended to any of the a_i.

Now we have the technology, we can return to the problem of calculating the matrix elements.

4.3 Calculating the Matrix Elements

We are studying the problem (2.2.1)

$$H_M = H^{(0)} + (-x^2 - (ix)^{2M}) \tag{4.34}$$

where $H^{(0)} = -\frac{d^2}{dx^2} + x^2 + \frac{l(l+1)}{x^2}$ is the harmonic oscillator Hamiltonian.

The eigenvalues of the unperturbed Hamiltonian H_0 are well known to be [42]:

$$E^{(0)}_{m,l} = 2m - (-1)^m 2l + 1 \tag{4.35}$$

with m a non-negative integer.

The unperturbed (unnormalised) eigenfunctions are:

$$\phi^+_n(x) = x^{l+1}e^{-\frac{x^2}{2}}L_n^{l+\frac{1}{2}}(x^2) \tag{4.36}$$

$$\phi_n^-(x) = x^{-l} e^{-\frac{x^2}{2}} L_n^{-l-\frac{1}{2}}(x^2) \tag{4.37}$$

where n is a non-negative integer, related to m as $m = 2n$ for the $\phi_n^-(x)$ and $m = 2n+1$ for the $\phi_n^+(x)$.

The L_n^α are the Laguerre polynomials, with the expansion given [1] as:

$$L_n^\alpha = \sum_{k=0}^{n} (-1)^k \frac{\Gamma(n+\alpha+1)}{\Gamma(\alpha+k+1)\Gamma(n-k+1)\Gamma(k+1)} x^k \tag{4.38}$$

The wavefunctions then become

$$\phi_n^+(x) = e^{-\frac{x^2}{2}} \sum_{k=0}^{n} (-1)^k \frac{\Gamma(n+l+\frac{3}{2})}{\Gamma(l+\frac{3}{2}+k)(n-k)!k!} x^{2k+l+1} \tag{4.39}$$

$$\phi_n^-(x) = e^{-\frac{x^2}{2}} \sum_{k=0}^{n} (-1)^k \frac{\Gamma(n-l+\frac{1}{2})}{\Gamma(-l+\frac{1}{2}+k)(n-k)!k!} x^{2k-l} \tag{4.40}$$

Notice that if we send $l \to -l-1$ in $\phi_n^\pm(x)$, we obtain $\phi_n^\mp(x)$.

4.3.1 Normalisation of Wavefunctions

We need to calculate the normalisation constants. Abramowitz and Stegun [1] gives us the normalisation of the orthogonal Laguerre polynomials as

$$\int_0^\infty e^{-x} x^\alpha L_n^\alpha(x) L_m^\alpha(x) dx = \frac{\Gamma(\alpha+n+1)}{n!} \delta_{nm} \tag{4.41}$$

The normalisation integral is:

$$\langle \phi_n^+ \mid \phi_m^+ \rangle = \int_{-\infty}^{\infty} x^{2l+2} e^{-x^2} L_n^{(l+\frac{1}{2})}(x^2) L_m^{(l+\frac{1}{2})}(x^2) dx \tag{4.42}$$

We split the real line into two parts and rotate the negative half line onto the positive half line, picking up a factor of $e^{-i2\pi l}$. The total integral over the full line is then just the integral over the positive half line, multiplied by $(1 + e^{-i2\pi l})$

$$(1 + e^{-i2\pi l}) \int_0^\infty x^{2l+2} e^{-x^2} L_n^{(l+\frac{1}{2})}(x^2) L_m^{(l+\frac{1}{2})}(x^2) dx \tag{4.43}$$

We substitute $t = x^2$

$$\frac{1}{2}(1 + e^{-i2\pi l}) \int_0^\infty t^{l+\frac{1}{2}} e^{-t} L_n^{(l+\frac{1}{2})}(t) L_m^{(l+\frac{1}{2})}(t) dt \tag{4.44}$$

This matches (apart from the prefactor) the integral given in (4.41) and is therefore equal to

$$\frac{1}{2}(1+e^{-2\pi il})\frac{\Gamma(l+n+\frac{3}{2})}{n!}\delta_{nm} \tag{4.45}$$

The normalised wave function $\hat{\phi}_n^+$ is therefore

$$\hat{\phi}_n^+(x) = \sqrt{\frac{n!2}{(1+e^{-2\pi il})\Gamma(l+n+\frac{3}{2})}}\phi_n^+(x) \tag{4.46}$$

and by sending $l \longrightarrow -l-1$ we can see that

$$\hat{\phi}_n^-(x) = \sqrt{\frac{n!2}{(1+e^{2\pi il})\Gamma(-l+n+\frac{1}{2})}}\phi_n^-(x) \tag{4.47}$$

Notice that the normalisation could be problematical for $l = \frac{2k+1}{2}$, k an integer.

We should not let this problem with the normalisation worry us unduly, it is not unexpected. The Frobenius Method, [10], tells us that around a regular singular point of a homogeneous linear differential equation we can find solutions of the form:

$$y(x) = (x-x_0)^\alpha \sum_{n=0}^{\infty} a_n (x-x_0)^n \tag{4.48}$$

where x_0 is the singular point (in our case $x_0 = 0$) and the α are the roots of the indicial equation. In our case the indicial equation is $P(\alpha) = \alpha^2 - \alpha + l(l+1)$, with roots $\alpha = l+1, -l$. The method breaks down for $a_n \neq 0$ and $P(\alpha+n) = 0$. In the case we are considering this is when $l = \frac{2k+1}{2}$, i.e. l is a half integer. In particular, for the case $l = -\frac{1}{2}$, the two wavefunctions become identical. Since we are interested in the area around $l \sim 0$, we can restrict $|l| < \frac{1}{2}$, thus avoiding the problematical values of l.

Having convinced ourselves that the problem for $l = \frac{2k+1}{2}$ is nugatory, let us return to calculating the matrix elements. We are interested in the matrix elements

$$\langle \hat{\phi}_n^\pm(x) | H_M | \hat{\phi}_m^\pm(x) \rangle \tag{4.49}$$

and

$$\langle \hat{\phi}_n^\pm(x) | H_M | \hat{\phi}_m^\mp(x) \rangle \tag{4.50}$$

4.3.2 The Matrix Elements $\langle\hat{\phi}^{\pm}_{\mathbf{n}}(\mathbf{x})|(\mathbf{ix})^{\mathbf{2M}}|\hat{\phi}^{\pm}_{\mathbf{m}}(\mathbf{x})\rangle$

As mentioned above, the Laguerre polynomials can be written in terms of generalised hyper-geometric functions [1]:

$$L_n^{l+\frac{1}{2}}(x^2) = \frac{(l+\frac{3}{2})_n}{n!}{}_1F_1(-n; l+\frac{3}{2}; x^2) \tag{4.51}$$

so our (unnormalised) wavefunctions become:

$$\phi_n^+(x) = x^{l+1}e^{-\frac{x^2}{2}}\frac{(l+\frac{3}{2})_n}{n!}{}_1F_1(-n; l+\frac{3}{2}; x^2) \tag{4.52}$$

$$\phi_n^-(x) = x^{-l}e^{-\frac{x^2}{2}}\frac{(-l+\frac{1}{2})_n}{n!}{}_1F_1(-n; -l+\frac{1}{2}; x^2). \tag{4.53}$$

This means we are interested in the integration

$$\begin{gathered}\langle\phi_n^+(x)|(ix)^{2M}|\phi_m^+(x)\rangle = \\ \int_{-\infty}^{\infty}(ix)^{2M}x^{2(l+1)}e^{-x^2}\frac{(l+\frac{3}{2})_n}{n!}\frac{(l+\frac{3}{2})_m}{m!}\times \\ {}_1F_1(-n; l+\frac{3}{2}; x^2){}_1F_1(-m; l+\frac{3}{2}, x^2)dx\end{gathered} \tag{4.54}$$

We split the integral into two, one from $-\infty$ to zero and one from zero to ∞. In the former we set $x = re^{-i\pi}$, in the latter we set $x = r$. The integral can then be written as:

$$\begin{gathered}\left(e^{iM\pi} + e^{-iM\pi}e^{-i2l\pi}\right)\frac{(l+\frac{3}{2})_n}{n!}\frac{(l+\frac{3}{2})_m}{m!}\times \\ \left(\int_0^{\infty} r^{2(l+1)+2M}e^{-r^2}{}_1F_1(-n; l+\frac{3}{2}, r^2){}_1F_1(-m; l+\frac{3}{2}; r^2)dr\right)\end{gathered} \tag{4.55}$$

To perform the integral we make use of a result from Hall et al [21]. We will state the result without proof here, as we will need to make a generalisation of it when we calculate $\langle\hat{\phi}^{\pm}_n(x)|(ix)^{2M}|\hat{\phi}^{\mp}_m(x)\rangle$. They state that if $2\gamma - \alpha > 0$, then for all pairs of non-negative integers m and n we have:

$$\begin{gathered}\int_0^{\infty} x^{2\gamma-\alpha-1}e^{-\beta x^2}{}_1F_1(-n; \gamma; \beta x^2){}_1F_1(-m; \gamma; \beta x^2)dx = \\ \frac{\beta^{\frac{\alpha}{2}-\gamma}}{2}\frac{(\frac{\alpha}{2})_n\Gamma(\gamma-\frac{\alpha}{2})}{(\gamma)_n}{}_3F_2(-m, \gamma-\frac{\alpha}{2}, 1-\frac{\alpha}{2}; \gamma, 1-\frac{\alpha}{2}-n; 1)\end{gathered} \tag{4.56}$$

If we set $\beta = 1$, $\gamma = l + \frac{3}{2}$ and $\alpha = -2M$, we have $2\gamma - \alpha = 2l + 3 + 2M > 0$, so we can use their result.

$$\langle \phi_n^+(x)|(ix)^{2M}|\phi_m^+(x)\rangle = e^{-il\pi}\left(e^{iM\pi+il\pi} + e^{-iM\pi-il\pi}\right)\frac{(l+\frac{3}{2})_m}{m!n!}(-M)_n\Gamma(l+\tfrac{3}{2}+M)\times {}_3F_2(-m, l+\tfrac{3}{2}+M, 1+M; l+\tfrac{3}{2}, 1+M-n; 1) \quad (4.57)$$

As

$$\langle \hat{\phi}_n^+(x)|(ix)^{2M}|\hat{\phi}_m^+(x)\rangle = 2\sqrt{\frac{n!m!}{\Gamma(l+m+\frac{3}{2})\Gamma(l+n+\frac{3}{2})}}\frac{\langle \phi_n^+(x)|(ix)^{2M}|\phi_m^+(x)\rangle}{1+e^{-2\pi il}} \quad (4.58)$$

we can write

$$\langle \phi_n^+(x)|(ix)^{2M}|\phi_m^+(x)\rangle = \frac{e^{iM\pi+il\pi}+e^{-iM\pi-il\pi}}{e^{il\pi}+e^{-il\pi}}\frac{(l+\frac{3}{2})_m(-M)_n\Gamma(l+\frac{3}{2}+M)}{\sqrt{m!n!\Gamma(l+\frac{3}{2}+m)\Gamma(l+\frac{3}{2}+n)}}\times {}_3F_2(-m, l+\tfrac{3}{2}+M, 1+M; l+\tfrac{3}{2}, 1+M-n; 1) \quad (4.59)$$

Using a bit of trigonometry we arrive at our final answer.

$$\langle \hat{\phi}_n^+(x)|(ix)^{2M}|\hat{\phi}_m^+(x)\rangle = \Big(\cos(M\pi) - \sin(M\pi)\tan(l\pi)\Big)\frac{(-M)_n(l+\frac{3}{2})_m}{\sqrt{n!m!\Gamma(l+m+\frac{3}{2})\Gamma(l+n+\frac{3}{2})}}\times \Gamma(l+\tfrac{3}{2}+M){}_3F_2(-m, l+\tfrac{3}{2}+M, 1+M; l+\tfrac{3}{2}, 1+M-n; 1) \quad (4.60)$$

Notice this may be undefined for $M = 1$. By sending $l \to -l-1$ in (4.59) we can obtain the the matrix elements for $\hat{\phi}^-$.

$$\langle \hat{\phi}_n^-(x)|(ix)^{2M}|\hat{\phi}_m^-(x)\rangle = \Big(\cos(M\pi) + \sin(M\pi)\tan(l\pi)\Big)\frac{(-M)_n(-l+\frac{1}{2})_m}{\sqrt{n!m!\Gamma(-l+m+\frac{1}{2})\Gamma(-l+n+\frac{1}{2})}}\Gamma(-l+\tfrac{1}{2}+M)\times {}_3F_2(-m, -l+\tfrac{1}{2}+M, 1+M; -l+\tfrac{1}{2}, 1+M-n; 1) \quad (4.61)$$

The Case $M = 1$

The hypergeometric functions in the above matrix elements are not defined for $M = 1$ and $n - 2 < m$, due to the negative integer in one of the lower entries of

the function. However, for $n - m \geq 2$ this problem can be easily avoided. As the inner product is symmetric i.e. $\langle\hat{\phi}_n^{\pm}(x)|(ix)^{2M}|\hat{\phi}_m^{\pm}(x)\rangle = \langle\hat{\phi}_m^{\pm}(x)|(ix)^{2M}|\hat{\phi}_n^{\pm}(x)\rangle$ we can reverse the positions of m and n. For $n - m \geq 2$, this will give us a well defined hypergeometric function. In the cases when we have a well defined hypergeometric function, that is $n \geq m + 2$, when $M = 1$ the matrix element is zero, because of the factor $(-M)_n = (-1)_n = 0$.

This still leaves us with a problem when $n = m$ or $n = m \pm 1$. We need to think carefully about the matrix elements in these cases. Using some facts about hyper-geometric functions, we can find the limit as $M \to 1$ of our inner product. We start with $\langle\hat{\phi}_n^{+}(x)|(ix)^{2M}|\hat{\phi}_m^{-}(x)\rangle$:

$$\begin{aligned}&\langle\hat{\phi}_n^{-}(x)|(ix)^{2M}|\hat{\phi}_m^{-}(x)\rangle = \\ &\left(\cos(M\pi) + \sin(M\pi)\tan(l\pi)\right)\frac{(-M)_n(-l+\frac{1}{2})_m}{\sqrt{n!m!\Gamma(-l+m+\frac{1}{2})\Gamma(-l+n+\frac{1}{2})}}\Gamma(-l+\tfrac{1}{2}+M)\times \\ &{}_3F_2(-m,-l+\tfrac{1}{2}+M,1+M;-l+\tfrac{1}{2},1+M-n;1)\end{aligned} \tag{4.62}$$

We will consider the prefactor first. In the term $(-M)_n$, we shall set $M = 1 + \epsilon$ and consider $\epsilon \to 0$. In all the other terms we set $M = 1$. Our prefactor becomes:

$$-(-1-\epsilon)_n(\frac{1}{2}-l)\sqrt{\frac{\Gamma(m-l+\frac{1}{2})}{\Gamma(n+1)\Gamma(m+1)\Gamma(-l+n+\frac{1}{2})}} \tag{4.63}$$

Next we turn to the hypergeometric function. This time we set $M = 1+\epsilon$ in the problematical denominator parameter and $M = 1$ else where:

$${}_3F_2(-m,-l+\frac{1}{2}+1,2;-l+\frac{1}{2},2+\epsilon-n;1) \tag{4.64}$$

Now recall Rainville's formula for contiguous hypergeometric functions (4.32), using this formula we arrive at:

$$\begin{aligned}&{}_3F_2(-m,-l+\tfrac{1}{2}+1,2;-l+\tfrac{1}{2},2+\epsilon-n;1) \\ = \;&\frac{1}{\frac{1}{2}-l}\Big(\tfrac{-3}{2}-l){}_3F_2(-m,-l+\tfrac{1}{2},2;-l+\tfrac{1}{2},2+\epsilon-n;1) \\ &+2{}_3F_2(-m,-l+\tfrac{1}{2},3;-l+\tfrac{1}{2},2+\epsilon-n;1)\Big)\end{aligned} \tag{4.65}$$

Both of the hypergeometric functions on the right hand side have a denominator and numerator parameter that are equal and never zero for $|l| < \frac{1}{2}$. We can cancel

these to give Gauss functions, upon which we use the Chu-Vandermonde theorem (4.26).

$$\begin{aligned} & {}_3F_2(-m,-l+\tfrac{1}{2}+1,2;-l+\tfrac{1}{2},2+\epsilon-n;1) \\ = & \quad \tfrac{1}{\frac{1}{2}-l}\left((-\tfrac{3}{2}-l)\tfrac{(\epsilon-n)_m}{(2+\epsilon-n)_m}+2\tfrac{(\epsilon-1-n)_m}{(2+\epsilon-n)_m}\right) \end{aligned} \tag{4.66}$$

Now we put our two terms together:

$$\begin{aligned} & \lim_{M\to 1}\langle\hat{\phi}_n^-(x)|(ix)^{2M}|\hat{\phi}_m^-(x)\rangle = \\ & \lim_{\epsilon\to 0}\tfrac{(-1-\epsilon)_n}{(2+\epsilon-n)_m}\sqrt{\tfrac{\Gamma(m-l+\frac{1}{2})}{\Gamma(n+1)\Gamma(m+1)\Gamma(-l+n+\frac{1}{2})}} \\ & \times\left((\tfrac{3}{2}-l)(\epsilon-n)_m-2(\epsilon-1-n)_m\right) \end{aligned} \tag{4.67}$$

We can use (4.16) to deduce $\frac{(-1-\epsilon)_n}{(2+\epsilon-n)_m} = (-1)^m(-1-\epsilon)_{n-m}$. Note that the Pockhammer function is only defined for $n-m \geq 0$. We shall then demand this restriction. This is not a problem, as the inner product is symmetric.

$$\begin{aligned} & \lim_{M\to 1}\langle\hat{\phi}_n^-(x)|(ix)^{2M}|\hat{\phi}_m^-(x)\rangle = \\ & \lim_{\epsilon\to 0}(-1)^m(-1-\epsilon)_{n-m}\sqrt{\tfrac{\Gamma(m-l+\frac{1}{2})}{\Gamma(n+1)\Gamma(m+1)\Gamma(-l+n+\frac{1}{2})}} \\ & \times\left((\tfrac{3}{2}-l)(\epsilon-n)_m-2(\epsilon-1-n)_m\right) \end{aligned} \tag{4.68}$$

Now there is no barrier to us setting $\epsilon = 0$, which we do:

$$\begin{aligned} & -\langle\hat{\phi}_n^-(x)|x^2|\hat{\phi}_m^-(x)\rangle = \\ & (-1)^m(-1)_{n-m}\sqrt{\tfrac{\Gamma(m-l+\frac{1}{2})}{\Gamma(n+1)\Gamma(m+1)\Gamma(-l+n+\frac{1}{2})}} \\ & \times\left((\tfrac{3}{2}-l)(-n)_m-2(-1-n)_m\right) \end{aligned} \tag{4.69}$$

By sending $l \to -l-1$ we get

$$\begin{aligned} & -\langle\hat{\phi}_n^+(x)|x^2|\hat{\phi}_m^+(x)\rangle = \\ & (-1)^m(-1)_{n-m}\sqrt{\tfrac{\Gamma(m+l+\frac{3}{2})}{\Gamma(n+1)\Gamma(m+1)\Gamma(l+n+\frac{3}{2})}} \\ & \times\left((\tfrac{5}{2}+l)(-n)_m-2(-1-n)_m\right) \end{aligned} \tag{4.70}$$

Note in both of these formulae, if $n \geq m+2$, the $(-1)_{n-m}$ term is identically zero. This matches with the full expression. We can write this out explicitly and

say:

$$-\langle\hat{\phi}_n^+(x)|x^2|\hat{\phi}_n^+(x)\rangle = \tfrac{1}{2} + l - 2n, \tag{4.71}$$

$$\begin{aligned}-\langle\hat{\phi}_{n+1}^+(x)|x^2|\hat{\phi}_n^+(x)\rangle &= -\langle\hat{\phi}_n^+(x)|x^2|\hat{\phi}_{n+1}^+(x)\rangle \\ &\quad -\sqrt{\frac{n+1}{n+l+\frac{3}{2}}}(\frac{1}{2}+l-n)\end{aligned} \tag{4.72}$$

and

$$-\langle\hat{\phi}_n^+(x)|x^2|\hat{\phi}_m^+(x)\rangle = -\langle\hat{\phi}_m^+(x)|x^2|\hat{\phi}_n^+(x)\rangle = 0 \qquad \text{if} \quad m \neq n, n+1. \tag{4.73}$$

We next need to calculate $\langle\hat{\phi}_n^{\pm}(x)|(ix)^{2M}|\hat{\phi}_m^{\mp}(x)\rangle$.

4.3.3 The Matrix Elements $\langle\hat{\phi}_{\mathbf{n}}^{\pm}(\mathbf{x})|(\mathbf{ix})^{\mathbf{2M}}|\hat{\phi}_{\mathbf{m}}^{\mp}(\mathbf{x})\rangle$

Having calculated the matrix elements $\langle\hat{\phi}_n^{\pm}(x)|(ix)^{2M}|\hat{\phi}_m^{\pm}(x)\rangle$, we must now calculate $\langle\hat{\phi}_n^{\pm}(x)|(ix)^{2M}|\hat{\phi}_m^{\mp}(x)\rangle$. Recall the wave functions in terms of hypergeometric functions are

$$\phi_n^+(x) = x^{l+1}e^{-\frac{x^2}{2}}\frac{(l+\frac{3}{2})_n}{n!}{}_1F_1(-n; l+\frac{3}{2}; x^2) \tag{4.74}$$

$$\phi_n^-(x) = x^{-l}e^{-\frac{x^2}{2}}\frac{(-l+\frac{1}{2})_n}{n!}{}_1F_1(-n; -l+\frac{1}{2}; x^2) \tag{4.75}$$

Consequently we should study

$$\begin{aligned}&\langle\phi_n^+(x)|(ix)^{2M}|\phi_m^-(x)\rangle = \tfrac{(l+\frac{3}{2})_n}{n!}\tfrac{(-l+\frac{1}{2})_m}{m!}e^{iM\pi} \times \\ &\int_{-\infty}^{\infty} x^{2M+1}e^{-x^2}{}_1F_1(-n; l+\tfrac{3}{2}; x^2){}_1F_1(-m; -l+\tfrac{1}{2}; x^2)dx\end{aligned} \tag{4.76}$$

We, as before, rotate the negative real axis onto the positive real axis using $x = re^{-i\pi}$

$$\begin{aligned}&\langle\phi_n^+(x)|(ix)^{2M}|\phi_m^-(x)\rangle = 2i\sin(M\pi)\tfrac{(l+\frac{3}{2})_n}{n!}\tfrac{(-l+\frac{1}{2})_m}{m!} \times \\ &\int_0^{\infty} r^{2M+1}e^{-r^2}{}_1F_1(-n; l+\tfrac{3}{2}; r^2){}_1F_1(-m; -l+\tfrac{1}{2}; r^2)dx\end{aligned} \tag{4.77}$$

We are looking to be able to use the Hall result (4.56) again. However, the second parameters in the confluent hypergeometric functions are different ($l+\frac{3}{2}$ and $-l+\frac{1}{2}$), so we cannot use this result. We need a generalised version of it.

Generalisation of the Hall Result

We will generalise the result (4.56) to one that is suitable for the calculation of $\langle\hat{\phi}_n^{\pm}(x)|(ix)^{2M}|\hat{\phi}_m^{\mp}(x)\rangle$. We will show that if $\gamma+\rho-\alpha>0$, then for all pairs of non-negative integers m and n we have:

$$\int_0^\infty x^{\gamma+\rho-\alpha-1}e^{-\beta x^2}{}_1F_1(-n;\gamma;\beta x^2){}_1F_1(-m;\rho;\beta x^2)dx = \frac{\beta^{\frac{\alpha}{2}-\frac{\gamma+\rho}{2}}}{2}\frac{(\frac{\alpha+\gamma-\rho}{2})_n\Gamma(\frac{\gamma+\rho}{2}-\frac{\alpha}{2})}{(\gamma)_n}$$
$$\times{}_3F_2(-m,\tfrac{\gamma+\rho}{2}-\tfrac{\alpha}{2},1-\tfrac{\gamma-\rho}{2}-\tfrac{\alpha}{2};\rho,1-\tfrac{\gamma-\rho}{2}-\tfrac{\alpha}{2}-n;1) \qquad (4.78)$$

from which the original Hall result (4.56) can be recovered by setting $\rho=\gamma$.

We set the left hand side of (4.78) to be I_{mn} and write the confluent hypergeometric functions in their series representations (4.24).

$$I_{mn}=\sum_{a=0}^{n}\sum_{b=0}^{m}\frac{(-n)_a(-m)_b\beta^{a+b}}{(\gamma)_a(\rho)_b a!b!}\int_0^\infty x^{\gamma+\rho-\alpha-1+2a+2b}e^{-\beta x^2}dx \qquad (4.79)$$

if we set $t=x^2$, the integral is now $\frac{1}{2}\int_0^\infty t^{\frac{\gamma+\rho}{2}-\frac{\alpha}{2}-1+a+b}e^{-\beta t}dt$ which is familiar as the Gamma function integral (4.10) provided $\frac{\gamma+\rho}{2}-\frac{\alpha}{2}+a+b>0$. As we are summing from $a,b=0$, this means we need $\gamma+\rho-\alpha>0$, which gives us the restriction to our formula.

$$I_{mn}=\frac{1}{2}\sum_{a=0}^{n}\sum_{b=0}^{m}\frac{(-n)_a(-m)_b\beta^{\frac{\alpha}{2}-\frac{\gamma+\rho}{2}}}{(\gamma)_a(\rho)_b a!b!}\Gamma\Big(\frac{\gamma+\rho}{2}-\frac{\alpha}{2}+a+b\Big) \qquad (4.80)$$

This can be rewritten as

$$\frac{1}{2}\beta^{\frac{\alpha}{2}-\frac{\gamma+\rho}{2}}\sum_{b=0}^{m}\left[\sum_{a=0}^{n}\frac{(-n)_a}{(\gamma)_a a!}\Gamma\Big(\frac{\gamma+\rho}{2}-\frac{\alpha}{2}+a+b\Big)\right]\frac{(-m)_b}{(\rho)_b b!} \qquad (4.81)$$

We will now consider the part in square brackets and eliminate the summation sign. We write the Gamma function in terms of Pockenhammer symbols (4.13).

$$\sum_{a=0}^{n}\frac{(-n)_a}{(\gamma)_a a!}\Gamma\Big(\frac{\gamma+\rho}{2}-\frac{\alpha}{2}+a+b\Big)=$$
$$\sum_{a=0}^{n}\frac{(-n)_a}{(\gamma)_a a!}\Big(\frac{\gamma+\rho}{2}-\frac{\alpha}{2}+b\Big)_a\Gamma\Big(\frac{\gamma+\rho}{2}-\frac{\alpha}{2}+b\Big) \qquad (4.82)$$

Apart from the Gamma function this is a Gauss function:

$${}_2F_1(-n,\frac{\gamma+\rho}{2}-\frac{\alpha}{2}+b;\gamma;1)\Gamma\Big(\frac{\gamma+\rho}{2}-\frac{\alpha}{2}+b\Big) \qquad (4.83)$$

We invoke Chu-Vandermonde's theorem (4.26) to obtain:

$$\sum_{a=0}^{n} \frac{(-n)_a}{(\gamma)_a a!}\Gamma\Big(\frac{\gamma+\rho}{2}-\frac{\alpha}{2}+a+b\Big) = \Gamma\Big(\frac{\gamma+\rho}{2}-\frac{\alpha}{2}+b\Big)\frac{(\frac{\alpha}{2}+\frac{\gamma-\rho}{2}-b)_n}{(\gamma)_n} \tag{4.84}$$

We put this back into (4.81)

$$I_{mn} = \frac{1}{2}\frac{\beta^{\frac{\alpha}{2}-\frac{\gamma+\rho}{2}}}{(\gamma)_n}\sum_{b=0}^{m}\Gamma\Big(\frac{\gamma+\rho}{2}-\frac{\alpha}{2}+b\Big)\Big(\frac{\alpha}{2}+\frac{\gamma-\rho}{2}-b\Big)_n\frac{(-m)_b}{(\rho)_b b!} \tag{4.85}$$

We write $\Gamma\Big(\frac{\gamma+\rho}{2}-\frac{\alpha}{2}+b\Big) = (\frac{\gamma+\rho}{2}-\frac{\alpha}{2})_b\Gamma\Big(\frac{\gamma+\rho}{2}-\frac{\alpha}{2}\Big)$. For the term $\Big(\frac{\alpha}{2}+\frac{\gamma-\rho}{2}-b\Big)_n$ we use the identity (4.17)

$$(y-k)_n = \frac{(1-y)_k(y)_n}{(1-y-n)_k} \tag{4.86}$$

for integer n and k, to obtain

$$\Big(\frac{\alpha}{2}+\frac{\gamma-\rho}{2}-b\Big)_n = \frac{(1-\frac{\alpha}{2}-\frac{\gamma-\rho}{2})_b(\frac{\alpha}{2}+\frac{\gamma-\rho}{2})_n}{(1-\frac{\alpha}{2}-\frac{\gamma-\rho}{2}-n)_b} \tag{4.87}$$

We put both of these results back into our expression (4.85

$$I_{mn} = \tfrac{1}{2}\tfrac{\beta^{\frac{\alpha}{2}-\frac{\gamma+\rho}{2}}}{(\gamma)_n}\Gamma\Big(\tfrac{\gamma+\rho}{2}-\tfrac{\alpha}{2}\Big)\Big(\tfrac{\alpha}{2}+\tfrac{\gamma-\rho}{2}\Big)_n \times \sum_{b=0}^{m}\Big(\tfrac{\gamma+\rho}{2}-\tfrac{\alpha}{2}\Big)_b\tfrac{(1-\frac{\alpha}{2}-\frac{\gamma-\rho}{2})_b}{(1-\frac{\alpha}{2}-\frac{\gamma-\rho}{2}-n)_b}\tfrac{(-m)_b}{(\rho)_b b!} \tag{4.88}$$

We have now arranged the pieces inside the summation into the form of a generalised hypergeometric function (4.24).

$$I_{mn} = \frac{\beta^{\frac{\alpha}{2}-\frac{\gamma+\rho}{2}}}{2}\frac{(\frac{\alpha+\gamma-\rho}{2})_n\Gamma(\frac{\gamma+\rho}{2}-\frac{\alpha}{2})}{(\gamma)_n} \times {}_3F_2(-m, \tfrac{\gamma+\rho}{2}-\tfrac{\alpha}{2}, 1-\tfrac{\gamma-\rho}{2}-\tfrac{\alpha}{2}; \rho, 1-\tfrac{\gamma-\rho}{2}-\tfrac{\alpha}{2}-n; 1) \tag{4.89}$$

This is the required result.

The Matrix Elements

We are attempting to calculate

$$\langle\phi_n^+(x)|(ix)^{2M}|\phi_m^-(x)\rangle = 2i\sin(M\pi)\tfrac{(l+\frac{3}{2})_n}{n!}\tfrac{(-l+\frac{1}{2})_m}{m!} \times \int_0^\infty r^{2M+1}e^{-r^2}{}_1F_1(-n; l+\tfrac{3}{2}; r^2){}_1F_1(-m; -l+\tfrac{1}{2}; r^2)dx \tag{4.90}$$

We can now use our generalisation of the Hall result (4.78) if we set $\gamma = l + \frac{3}{2}$, $\rho = -l + \frac{1}{2}$, $\beta = 1$ and $\alpha = -2M$.

$$\langle \phi_n^+(x)|(ix)^{2M}|\phi_m^-(x)\rangle = i\sin(M\pi)\frac{(-l+\frac{1}{2})_m}{m!n!}(l - M + \tfrac{1}{2})_n\Gamma(M+1)\times$$
$${}_3F_2(-m, 1+M, 1+M-l-\tfrac{1}{2}; \tfrac{1}{2}-l, 1+M-l-\tfrac{1}{2}-n; 1) \qquad (4.91)$$

The normalisation constant is

$$\sqrt{\frac{n!2}{(1+e^{-2\pi il})\Gamma(l+n+\frac{3}{2})}}\sqrt{\frac{m!2}{(1+e^{2\pi il})\Gamma(-l+m+\frac{1}{2})}} = \frac{1}{\cos(\pi l)}\sqrt{\frac{n!m!}{\Gamma(-l+m+\frac{1}{2})\Gamma(l+n+\frac{3}{2})}} \qquad (4.92)$$

Therefore

$$\langle \hat{\phi}_n^+(x)|(ix)^{2M}|\hat{\phi}_m^-(x)\rangle = i\frac{\sin(M\pi)(-l+\frac{1}{2})_m}{\cos(\pi l)\sqrt{\Gamma(-l+m+\frac{1}{2})\Gamma(l+n+\frac{3}{2})m!n!}}(l - M + \tfrac{1}{2})_n\Gamma(M+1)\times$$
$${}_3F_2(-m, 1+M, M-l+\tfrac{1}{2}; \tfrac{1}{2}-l, M-l+\tfrac{1}{2}-n; 1) \qquad (4.93)$$

Notice that we do not have the problem at $M = 1$, we had with the $\langle \hat{\phi}_n^{\pm}(x)|(ix)^{2M}|\hat{\phi}_m^{\pm}(x)\rangle$ case. Also as $\langle \hat{\phi}_m^-(x)|(ix)^{2M}|\hat{\phi}_n^+(x)\rangle = \langle \hat{\phi}_n^+(x)|(ix)^{2M}|\hat{\phi}_m^-(x)\rangle$ it is not necessary to calculate $\langle \hat{\phi}_n^{\mp}(x)|(ix)^{2M}|\hat{\phi}_m^{\pm}(x)\rangle$.

4.3.4 Summary Of Results

In this section we have calculated $\langle \hat{\phi}_n^{\pm}(x)|(ix)^{2M}|\hat{\phi}_m^{\pm}(x)\rangle$ and $\langle \hat{\phi}_n^{\pm}(x)|(ix)^{2M}|\hat{\phi}_m^{\mp}(x)\rangle$ we collect the results here for ease of reference.

$\langle \hat{\phi}_{\mathbf{n}}^{\pm}(\mathbf{x})|(\mathbf{ix})^{\mathbf{2M}}|\hat{\phi}_{\mathbf{m}}^{\pm}(\mathbf{x})\rangle$ for $\mathbf{M \neq 1}$

$$\langle \hat{\phi}_n^+(x)|(ix)^{2M}|\hat{\phi}_m^+(x)\rangle =$$
$$\Big(\cos(M\pi) - \sin(M\pi)\tan(l\pi)\Big)\frac{(-M)_n(l+\frac{3}{2})_m}{\sqrt{n!m!\Gamma(l+m+\frac{3}{2})\Gamma(l+n+\frac{3}{2})}}\times$$
$$\Gamma(l+\tfrac{3}{2}+M){}_3F_2(-m, l+\tfrac{3}{2}+M, 1+M; l+\tfrac{3}{2}, 1+M-n; 1) \qquad (4.94)$$

$$\langle \hat{\phi}_n^-(x)|(ix)^{2M}|\hat{\phi}_m^-(x)\rangle =$$
$$\Big(\cos(M\pi) + \sin(M\pi)\tan(l\pi)\Big)\frac{(-M)_n(-l+\frac{1}{2})_m}{\sqrt{n!m!\Gamma(-l+m+\frac{1}{2})\Gamma(-l+n+\frac{1}{2})}}\Gamma(-l+\tfrac{1}{2}+M)\times$$
$${}_3F_2(-m, -l+\tfrac{1}{2}+M, 1+M; -l+\tfrac{1}{2}, 1+M-n; 1) \qquad (4.95)$$

$\langle\hat{\phi}^{\pm}_{\mathbf{n}}(\mathbf{x})|(\mathbf{ix})^{\mathbf{2M}}|\hat{\phi}^{\pm}_{\mathbf{m}}(\mathbf{x})\rangle$ **for** $\mathbf{M = 1}$

$$-\langle\hat{\phi}^{+}_{n}(x)|x^2|\hat{\phi}^{+}_{n}(x)\rangle = \tfrac{1}{2} + l - 2n, \tag{4.96}$$

$$\begin{aligned}-\langle\hat{\phi}^{+}_{n+1}(x)|x^2|\hat{\phi}^{+}_{n}(x)\rangle &= -\langle\hat{\phi}^{+}_{n}(x)|x^2|\hat{\phi}^{+}_{n+1}(x)\rangle \\ &= -\sqrt{\frac{n+1}{n+l+\frac{3}{2}}}(\frac{1}{2} + l - n)\end{aligned} \tag{4.97}$$

$$-\langle\hat{\phi}^{+}_{n}(x)|x^2|\hat{\phi}^{+}_{m}(x)\rangle = -\langle\hat{\phi}^{+}_{m}(x)|x^2|\hat{\phi}^{+}_{n}(x)\rangle = 0 \qquad \text{if} \quad m \neq n, n+1. \tag{4.98}$$

$$-\langle\hat{\phi}^{-}_{n}(x)|x^2|\hat{\phi}^{-}_{n}(x)\rangle = -\tfrac{1}{2} - l - 2n, \tag{4.99}$$

$$\begin{aligned}-\langle\hat{\phi}^{-}_{n+1}(x)|x^2|\hat{\phi}^{-}_{n}(x)\rangle &= -\langle\hat{\phi}^{-}_{n}(x)|x^2|\hat{\phi}^{-}_{n+1}(x)\rangle \\ &= -\sqrt{\frac{n+1}{n-l+\frac{1}{2}}}(-\frac{1}{2} - l - n)\end{aligned} \tag{4.100}$$

$$-\langle\hat{\phi}^{-}_{n}(x)|x^2|\hat{\phi}^{-}_{m}(x)\rangle = -\langle\hat{\phi}^{-}_{m}(x)|x^2|\hat{\phi}^{-}_{n}(x)\rangle = 0 \qquad \text{if} \quad m \neq n, n+1. \tag{4.101}$$

$\langle\hat{\phi}^{\pm}_{\mathbf{n}}(\mathbf{x})|(\mathbf{ix})^{\mathbf{2M}}|\hat{\phi}^{\mp}_{\mathbf{m}}(\mathbf{x})\rangle$

$$\begin{aligned}\langle\hat{\phi}^{+}_{n}(x)|(ix)^{2M}|\hat{\phi}^{-}_{m}(x)\rangle = i\frac{\sin(M\pi)(-l+\frac{1}{2})_m}{\cos(\pi l)\sqrt{\Gamma(-l+m+\frac{1}{2})\Gamma(l+n+\frac{3}{2})m!n!}}(l - M + \tfrac{1}{2})_n\Gamma(M+1)\times \\ {}_3F_2(-m, 1+M, M-l+\tfrac{1}{2}; \tfrac{1}{2}-l, M-l+\tfrac{1}{2}-n; 1)\end{aligned} \tag{4.102}$$

4.4 The Matrix

Recall the problem we are considering is

$$H_M = H^{(0)} + (-x^2 - (ix)^{2M}) \tag{4.103}$$

where $H^{(0)} = -\frac{d^2}{dx^2} + x^2 + \frac{l(l+1)}{x^2}$. The matrix we are interested in is

$$H_{nm} = \langle\Psi_n(x)|H|\Psi_m(x)\rangle =$$
$$\langle\Psi_n(x)|H^{(0)}|\Psi_m(x)\rangle - \langle\Psi_n(x)|x^2|\Psi_m(x)\rangle - \langle\Psi_n(x)|(ix)^{2M}|\Psi_m(x)\rangle \quad (4.104)$$

where

$$\Psi_n(x) = \hat{\phi}^-_{\frac{n}{2}}(x) \qquad \text{for } n \text{ even} \quad (4.105)$$
$$\Psi_n(x) = \hat{\phi}^+_{\frac{n-1}{2}}(x) \qquad \text{for } n \text{ odd} \quad (4.106)$$

so the ϕ^+ and ϕ^-, refer to odd and even values of n respectively. There is then a noticeable difference between the matrix elements $\langle\Psi_{2n}(x)|H|\Psi_{2m}(x)\rangle$ and $\langle\Psi_{2n}(x)|H|\Psi_{2m+1}(x)\rangle$.

We write

$$A^{\pm}_{kk'}(M,l) = \langle\hat{\phi}^{\pm}_k(x)|(ix)^{2M}|\hat{\phi}^{\pm}_{k'}(x)\rangle \quad (4.107)$$

and

$$B^{\pm}_{kk'}(M,l) = \langle\hat{\phi}^{\pm}_k(x)|(ix)^{2M}|\hat{\phi}^{\mp}_{k'}(x)\rangle \quad (4.108)$$

The unperturbed energy, $\langle\Psi_n(x)|H^{(0)}|\Psi_n(x)\rangle$, we write as

$$E^{(0)}_n = \langle\Psi_n(x)|H^{(0)}|\Psi_n(x)\rangle = 2n + 1 - (-1)^n 2l \quad (4.109)$$

This means the unperturbed matrix is

$$\langle\Psi_n(x)|H^{(0)}|\Psi_m(x)\rangle = E^{(0)}_n\delta_{nm} \quad (4.110)$$

If we write $a = n \bmod 2$ and $b = m \bmod 2$, the matrix $-\langle\Psi_n(x)|x^2|\Psi_m(x)\rangle$ can be written as

$$-\langle\Psi_n(x)|x^2|\Psi_m(x)\rangle = A^-_{\frac{n}{2}\frac{m}{2}}(1,l)\delta_{0a}\delta_{0b} + A^+_{\frac{n-1}{2}\frac{m-1}{2}}(1,l)\delta_{1a}\delta_{1b}$$
$$+B^+_{\frac{n-1}{2}\frac{m}{2}}(1,l)\delta_{1a}\delta_{0b} + B^-_{\frac{n}{2}\frac{m-1}{2}}(1,l)\delta_{0a}\delta_{1b} \quad (4.111)$$

However, we know from our calculations that $B^{\pm}_{nm}(1,l) = 0$, so these terms can be neglected:

$$-\langle\Psi_n(x)|x^2|\Psi_m(x)\rangle = A^-_{\frac{n}{2}\frac{m}{2}}(1,l)\delta_{0a}\delta_{0b} + A^+_{\frac{n-1}{2}\frac{m-1}{2}}(1,l)\delta_{1a}\delta_{1b} \quad (4.112)$$

Written in matrix form this is

$$\begin{pmatrix} A^-_{00}(1,l) & 0 & A^-_{01(1,l)} & 0 & 0 & \dots \\ 0 & A^+_{00}(1,l) & 0 & A^+_{01}(1,l) & 0 & \dots \\ A^-_{10}(1,l) & 0 & A^-_{11}(1,l) & 0 & A^-_{12}(1,l) & \dots \\ 0 & A^+_{10}(1,l) & 0 & A^+_{11}(1,l) & 0 & \dots \\ 0 & 0 & A^-_{21}(1,l) & 0 & A^-_{22}(1,l) & \dots \\ \vdots & \vdots & \vdots & \vdots & \vdots & \ddots \end{pmatrix} \tag{4.113}$$

As $A^{\pm}_{nm}(1,l) = 0$, except where $n = m$ or $n = m \pm 1$, nearly all the entries are zero. The only non-zero entries are those on either the main diagonal or the next-to-next-to-main diagonal.

We know that $A^{\pm}_{nm}(M,l) = A^{\pm}_{mn}(M,l)$ i.e. the A matrices are symmetric, we make this explicit in our matrix

$$\begin{pmatrix} A^-_{00}(1,l) & 0 & A^-_{10}(1,l) & 0 & 0 & \dots \\ 0 & A^+_{00}(1,l) & 0 & A^+_{10}(1,l) & 0 & \dots \\ A^-_{10}(1,l) & 0 & A^-_{11}(1,l) & 0 & A^-_{21}(1,l) & \dots \\ 0 & A^+_{10}(1,l) & 0 & A^+_{11}(1,l) & 0 & \dots \\ 0 & 0 & A^-_{21}(1,l) & 0 & A^-_{22}(1,l) & \dots \\ \vdots & \vdots & \vdots & \vdots & \vdots & \ddots \end{pmatrix} \tag{4.114}$$

The final part we need to consider is the matrix $-\langle\Psi_n(x)|(ix)^{2M}|\Psi_m(x)\rangle$

$$\begin{aligned} -\langle\Psi_n(x)|(ix)^{2M}|\Psi_m(x)\rangle = &-A^-_{\frac{n}{2}\frac{m}{2}}(M,l)\delta_{0a}\delta_{0b} - A^+_{\frac{n-1}{2}\frac{m-1}{2}}(M,l)\delta_{1a}\delta_{1b} \\ &-B^+_{\frac{n-1}{2}\frac{m}{2}}(M,l)\delta_{1a}\delta_{0b} - B^-_{\frac{n}{2}\frac{m-1}{2}}(M,l)\delta_{0a}\delta_{1b} \end{aligned} \tag{4.115}$$

We can rewrite

$$B^{+}_{\frac{n-1}{2}\frac{m}{2}}(M,l) \equiv B_{\frac{n-1}{2}\frac{m}{2}}(M,l) \qquad \text{for } n \text{ odd} \tag{4.116}$$

$$B^{-}_{\frac{n}{2}\frac{m-1}{2}}(M,l) \equiv B_{\frac{m-1}{2}\frac{n}{2}}(M,l) \qquad \text{for } n \text{ even} \tag{4.117}$$

because $B^{\pm}_{nm} = B^{\mp}_{mn}$. We then get

$$\begin{aligned} X_{nm}(M,l) &= -\langle \Psi_n(x)|(ix)^2|\Psi_m(x)\rangle = \\ &-A^{-}_{\frac{n}{2}\frac{m}{2}}(M,l)\delta_{0a}\delta_{0b} - A^{+}_{\frac{n-1}{2}\frac{m-1}{2}}(M,l)\delta_{1a}\delta_{1b} \\ &-B_{\frac{n-1}{2}\frac{m}{2}}(M,l)\delta_{1a}\delta_{0b} - B_{\frac{m-1}{2}\frac{n}{2}}(M,l)\delta_{0a}\delta_{1b} \end{aligned} \tag{4.118}$$

Written out as a matrix this is

$$X_{nm}(M,l) = \begin{pmatrix} -A^{-}_{00}(M,l) & -B_{00}(M,l) & -A^{-}_{10}(M,l) & -B_{10}(M,l) & -A^{-}_{20}(M,l) & \dots \\ -B_{00}(M,l) & -A^{+}_{00}(M,l) & -B_{01}(M,l) & -A^{+}_{10}(M,l) & -B_{02}(M,l) & \dots \\ -A^{-}_{10}(M,l) & -B_{01}(M,l) & -A^{-}_{11}(M,l) & -B_{11}(M,l) & -A^{-}_{21}(M,l) & \dots \\ -B_{10}(M,l) & -A^{+}_{10}(M,l) & -B_{11}(M,l) & -A^{+}_{11}(M,l) & -B_{12}(M,l) & \dots \\ -A^{-}_{20}(M,l) & -B_{02}(M,l) & -A^{-}_{21}(M,l) & -B_{12}(M,l) & -A^{-}_{22}(M,l) & \dots \\ \vdots & \vdots & \vdots & \vdots & \vdots & \ddots \end{pmatrix} \tag{4.119}$$

which is explicitly symmetric.

We can put together all of these, (4.110),(4.112),(4.118), to get

$$\begin{aligned} H_{nm} &= H^{(0)}_{nm}(l) - X_{nm}(1,l) + X_{nm}(M,l) = \\ &E^{(0)}_{n}\delta_{nm} + (A^{-}_{\frac{n}{2}\frac{m}{2}}(1,l) - A^{-}_{\frac{n}{2}\frac{m}{2}}(M,l))\delta_{0a}\delta_{0b} + (A^{+}_{\frac{n-1}{2}\frac{m-1}{2}}(1,l) - A^{+}_{\frac{n-1}{2}\frac{m-1}{2}}(M,l))\delta_{1a}\delta_{1b} \\ &-B_{\frac{n-1}{2}\frac{m}{2}}(M,l)\delta_{1a}\delta_{0b} - B_{\frac{m-1}{2}\frac{n}{2}}(M,l)\delta_{0a}\delta_{1b} \end{aligned} \tag{4.120}$$

or

$$\begin{pmatrix}
E_0^{(0)} + A_{00}^-(1,l) - A_{00}^-(M,l) & -B_{00}(M,l) & A_{10}^-(1,l) - A_{10}^-(M,l) & -B_{10}(M,l) & -A_{20}^-(M,l) & \dots \\
-B_{00}(M,l) & E_1^{(0)} + A_{00}^+(1,l) - A_{00}^+(M,l) & -B_{01}(M,l) & A_{10}^+(1,l) - A_{10}^+(M,l) & -B_{02}(M,l) & \dots \\
A_{10}^-(1,l) - A_{10}^-(M,l) & -B_{01}(M,l) & E_2^{(0)} + A_{11}^-(1,l) - A_{11}^-(M,l) & -B_{11}(M,l) & A_{21}^-(1,l) - A_{21}^-(M,l) & \dots \\
-B_{10}(M,l) & A_{10}^+(1,l) - A_{10}^+(M,l) & -B_{11}(M,l) & E_3^{(0)} + A_{11}^+(1,l) - A_{11}^+(M,l) & -B_{12}(M,l) & \dots \\
-A_{20}^-(M,l) & -B_{02}(M,l) & A_{21}^-(1,l) - A_{21}^-(M,l) & -B_{12}(M,l) & E_4^{(0)} + A_{22}^-(1,l) - A_{22}^-(M,l) & \dots \\
\vdots & \vdots & \vdots & \vdots & \vdots & \ddots
\end{pmatrix} \tag{4.121}$$

4.5 Diagonalising The Matrix Using Maple

In the previous sections have obtained a matrix expression for our Hamiltonian. The next thing we should consider is truncating our (infinite) matrix to smaller sizes and diagonalising it. There are, basically, two ways of doing this.

The first of these is truncating the top of our matrix, so that the lowest energy level in our truncated matrix, is the actual lowest energy level of the system. Using this method we should be able to reproduce the numerical results we have already seen, such as fig.2.4. The second of these is to truncate from both the top and the bottom.

When we graph our results we expect a loss of accuracy based on the numerical prediction. The inaccuracy comes from two sources. One is the inherent approxima-

tion in the perturbative method. This will be most evident away from $M = 1$, the point we are perturbing about. We also expect a loss in accuracy from truncating the matrix. This is expected to be worse for energy levels closest to the truncated levels. The perturbation of each energy level, from the $M = 1$ unperturbed energy level, is most affected by the energy levels closest to it. For this reason, truncating from the top only, is a good idea as there is only one "truncated edge."

We will first study the matrix truncated from the top only.

4.5.1 Truncating The Matrix From The Top

For the interested reader the MAPLE programme used to diagonalise the matrix is in Appendix B.1.

Truncation To Five Energy Levels

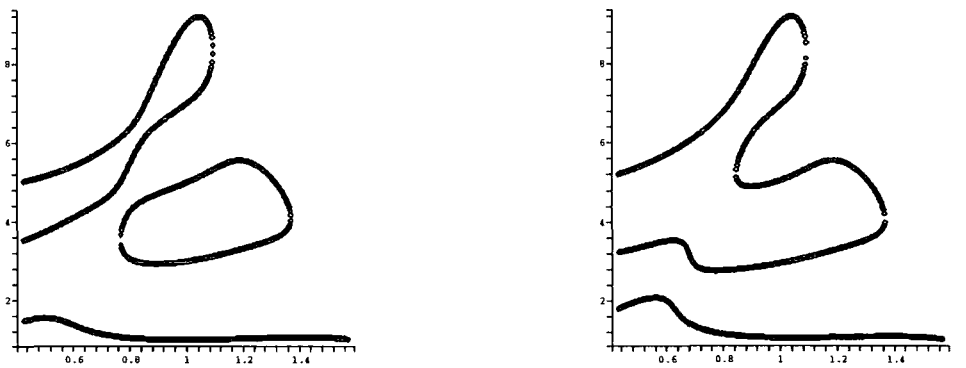

$l = 0$ $\qquad$ $l = -0.025$

Figure 4.1: The Spectrum For The Matrix Truncated To The First Five Energy Levels.

Fig.4.1 shows the energy levels of the matrix truncated to just five energy levels, for $l = 0$ and $l = -0.025$. As you can see, we are far away from the numerical results we expect. There is some qualitative agreement, such as, in the $l = 0$ case the second and third energy levels pair off as expected, but not in the $l = -0.025$ case. However we are seeing the pairing off for both $M < 1$ and $M > 1$ and further,

the lowest two energy levels do not pair off for $l = -0.025$. We can say then, that a truncation to the first five energy levels, is too extreme to give us any accurate information. Let us try truncating to ten energy levels.

Truncation To Ten Energy Levels

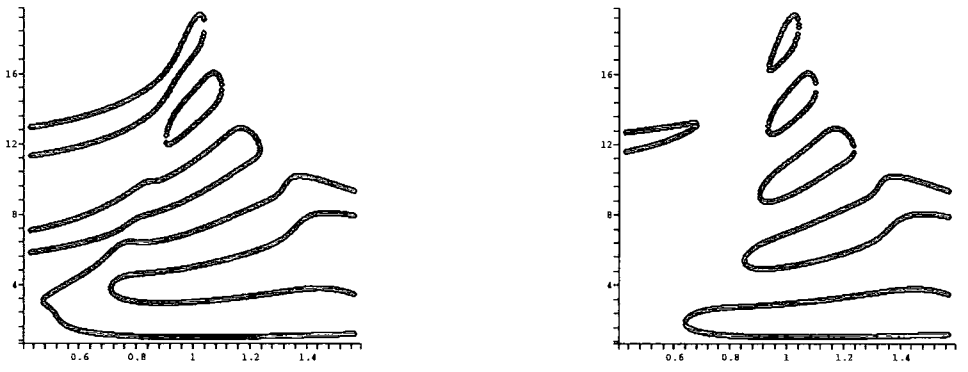

$l = 0$ $l = -0.025$

Figure 4.2: The Spectrum For The Matrix Truncated To The First Ten Energy Levels.

Fig.4.2 shows the energy levels of the matrix truncated to ten energy levels, for $l = 0$ and $l = -0.025$ respectively.

Again, the match with numerical results is not particularly satisfying. In the $l = 0$ case we still have the second and third energy levels pairing off, but other than that, there is little to make us think we have a match. The $l = -0.025$ case is somehow more intriguing. There is a definite sense as to in which direction the energy levels are pairing off. We still run into the problem of pairing off on both sides of the harmonic oscillator point $M = 1$, but it is beginning to suggest the result we are looking for.

Truncation To Fifteen Energy Levels

The obvious next step to take is to study an even larger truncation of the matrix. Fig.4.3 shows the energy levels of the matrix truncated to fifteen energy levels, for

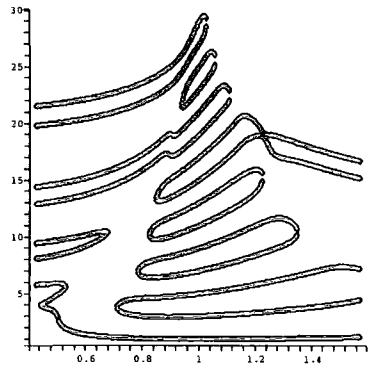

$l = 0$

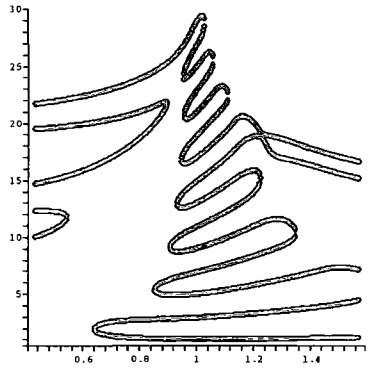

$l = -0.025$

Figure 4.3: The Spectrum For The Matrix Truncated To The First Fifteen Energy Levels.

$l = 0$ and $l = -0.025$ respectively.

In the $l = 0$ case we see a definite improvement over the truncation to only ten energy levels. There is a clear direction in which the pairing off takes place, leaving the lowest energy level to not be paired off at all. In both cases we have we continue to see the problem of pairing off of energy levels for $M > 1$ and $M < 1$.

It is interesting to note, that if we compare the plots for $l = 0$ and $l = -0.025$, there is a far greater difference between the regions $M < 1$, than there is between the regions for $M > 1$, where they are almost identical. This is also true for the previous two pairs of plots and the exact numerical data, from chapter 1, we are attempting to recreate. The line that separates these two regions is also the line that separates the $\mathcal{PT}$-symmetric region from the non-$\mathcal{PT}$-symmetric region.

Truncation To Twenty Energy Levels

Fig.4.4 shows the energy levels of the matrix truncated to twenty energy levels, for $l = 0$ and $l = -0.025$ respectively. We can see that there is a continuing improvement of our approximation for the lower energy levels.

So far, we have been looking at the plot of all energy levels, within our truncation range. We can see that the approximation appears to be improving with larger

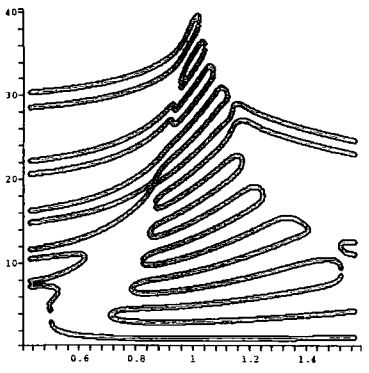

$l = 0$

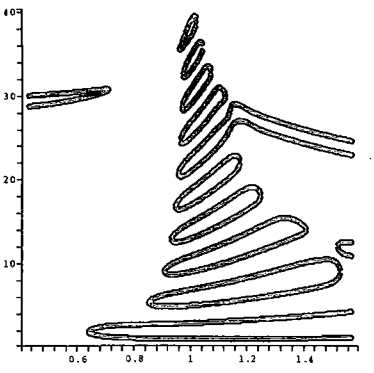

$l = -0.025$

Figure 4.4: The Spectrum For The Matrix Truncated To The First Twenty Energy Levels.

truncations. Also, the lower lying energy levels seem to be a better match with our numerical data. This is not unexpected, as the lower energy levels are further from the truncation and so effected less by the truncation. We are however, unlikely to learn more from continuing to enlarge the truncation and studying the entire range. For this reason it may be beneficial to focus now on only the lowest lying energy levels. We know that the higher energy levels will not behave as expected numerically, but might be able to see a good match in the lower lying energy levels. We will look at the lowest nine energy levels when they are below $E = 14.2$. Figs 4.5 shows this.

We can see that we get the required pairing off, for both values of l. Unfortunately we have the energy levels pairing off on both sides. In the $l = 0$ case, we do not see the final energy level behave quite as expected, as well as seeing eigenvalues reappearing for low M. We expect these problems to improve with increased truncation level.

Larger Truncations

As our results are converging towards the expected results, we will take a slightly different approach for the truncations to twenty-five and thirty levels. Now the graphs will be collected by the value of l, to aid the comparison between the different

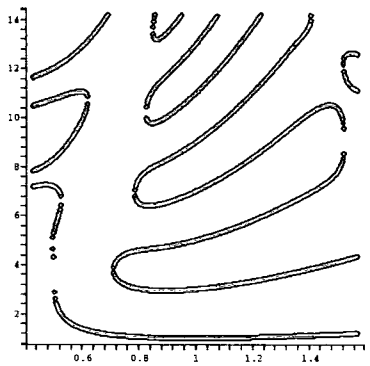

$l = 0$

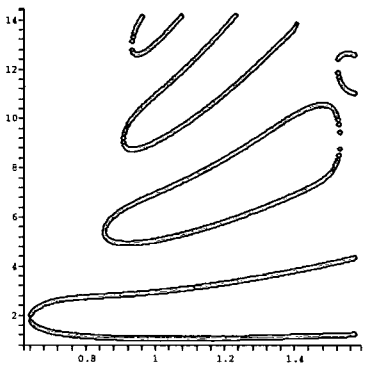

$l = -0.025$

Figure 4.5: The Spectrum For The Matrix Truncated To The First Twenty Energy Levels, Showing Only The Lowest Nine Levels Below 14.2.

truncation levels.

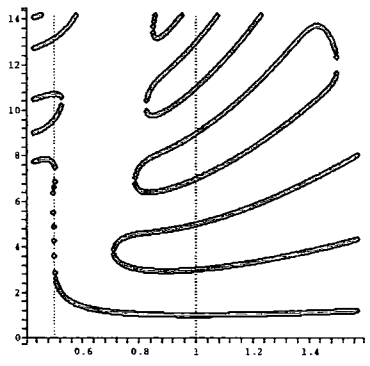

Truncation at twenty-five

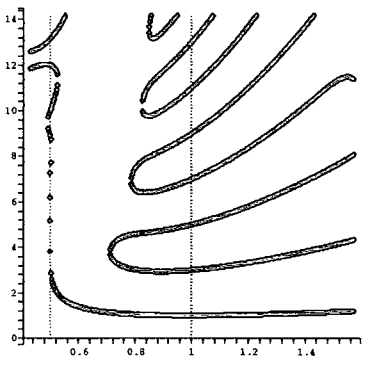

Truncation at thirty

Figure 4.6: The Spectrum For The Matrix Truncated To The First Twenty-Five And Thirty Energy Levels, For $l = 0$.

We are able then to see in each instance the improvement that takes place for the increase to a truncation level of thirty, compared to the truncation at twenty levels. The differences are most evident further away from $M = 1$ and higher up the spectrum, as we would expect. Of all the graphs the most notable improvement is in the behaviour of the final energy level in the $l = 0$ case.

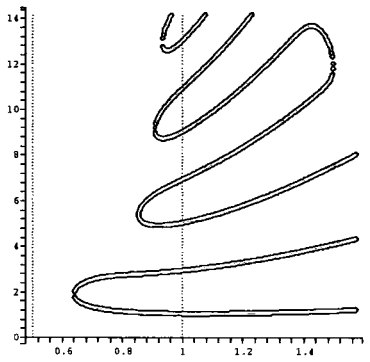

Truncation at twenty-five

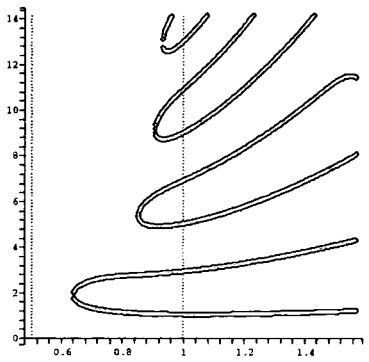

Truncation at thirty

Figure 4.7: The Spectrum For The Matrix Truncated To The First Twenty-Five And Thirty Energy Levels, For $l = -0.025$.

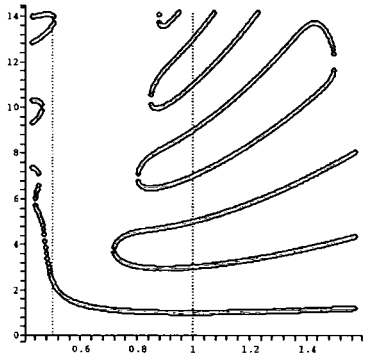

Truncation at twenty-five

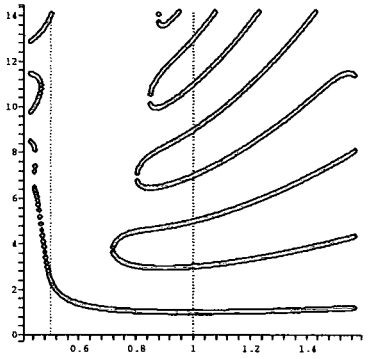

Truncation at thirty

Figure 4.8: The Spectrum For The Matrix Truncated To The First Twenty-Five And Thirty Energy Levels, For $l = 0.001$.

Finally figs 4.10 and 4.11 show our perturbative data graphed against the numerical data so we can see the match that takes place.

Smaller Truncations

So far we have been studying successively larger truncations of the matrix. We have seen that as we increase the truncation level, we get a steadily improving approx-

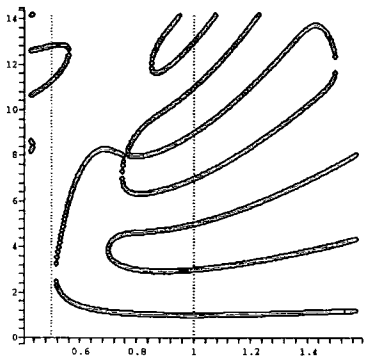

Truncation at twenty-five

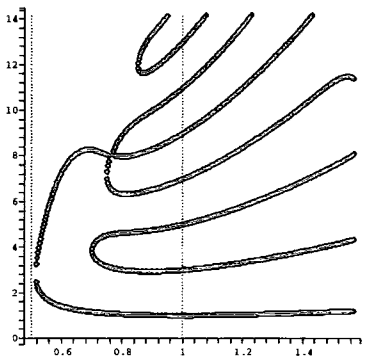

Truncation at thirty

Figure 4.9: The Spectrum For The Matrix Truncated To The First Twenty-Five And Thirty Energy Levels, For $l = -0.001$.

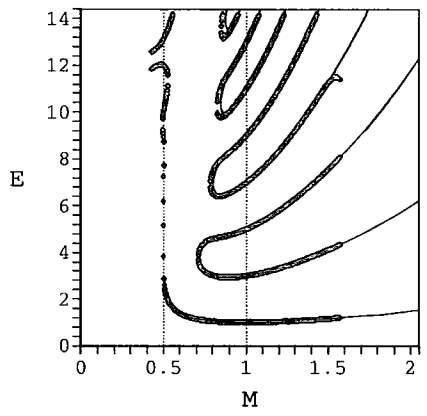

$l = 0$

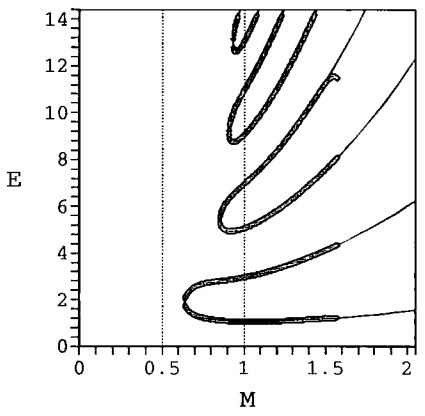

$l = -0.025$

Figure 4.10: Comparison of perturbative data against numerical, truncation level is thirty.

imation of our numerical results. However, even for the truncation to five energy levels, we can see the some hint of the expected pairing off. Smaller truncations are somehow preferable, as we are closer to an analytical understanding of the problem. The larger truncations, conversely, are close to a numerical result. It would be interesting to see how small we can make our truncations and see still something we could describe as a qualitative match with our expectations. Let us look at a

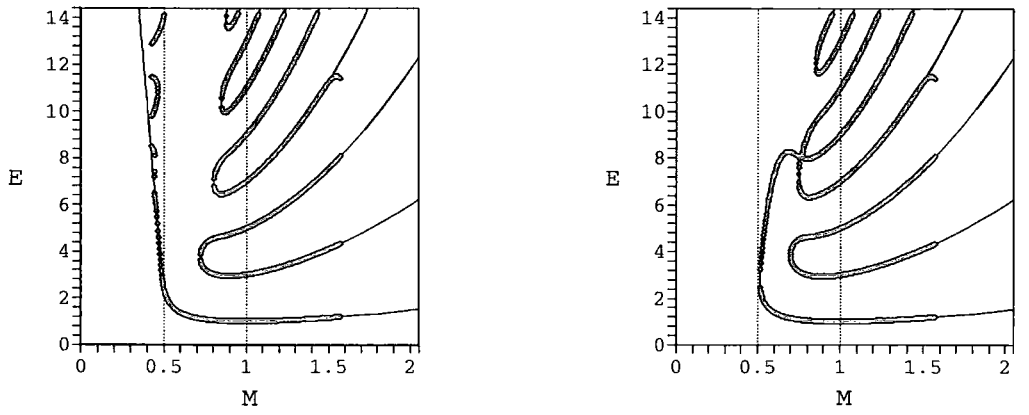

$l = 0.001$ $l = -0.001$

Figure 4.11: Comparison of perturbative data against numerical, truncation level is thirty.

three-by-three truncation.

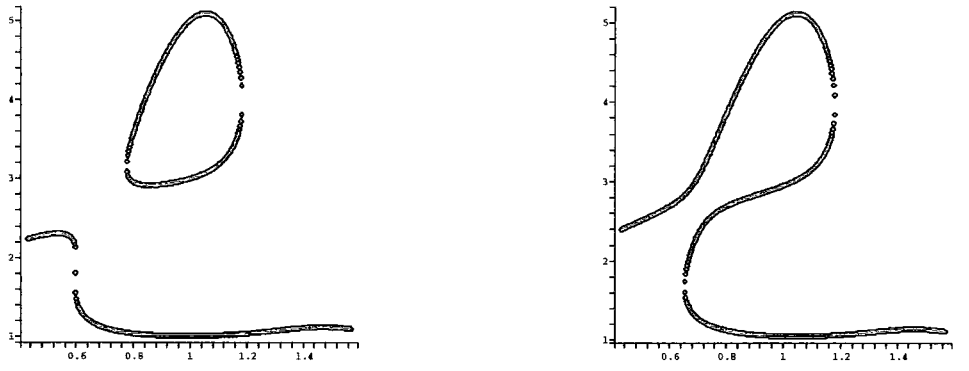

$l = 0$ $l = -0.025$

Figure 4.12: Truncation To Three Energy Levels

Figure 4.12 shows us the three-by-three truncation, for $l = 0$ and $l = -0.025$. This is good. There is a clear choice made as to the direction of pairing-off, between the energy levels. In the $l = 0$ case we see the second and third energy levels pair off, while the lowest stays free. In the $l = -0.025$ case we see the opposite situation. The first and second levels pair-off and the third energy level is free. Although quantitatively, this level of truncation does not give good results, qualitatively we

get the required result. The only behaviour we don't see is the pairing off of the third energy level, when $l = -0.025$. However, as there is no fourth energy level to pair off with, we can hardly expect to see this phenomenon.

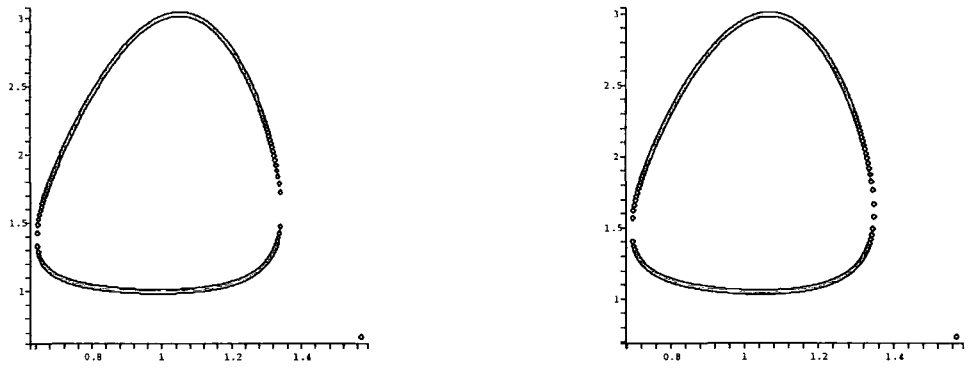

$l = 0$ $l = -0.025$

Figure 4.13: Truncation To Two Energy Levels

The next obvious step is to look at the two-by-two truncation. Fig 4.13 shows us this. The truncation is too extreme in this situation. There is no qualitative match at all; both values of l show pairing off. From this we can see, that truncating to the lowest two energy levels gives us no information, either qualitatively, or quantitatively.

4.5.2 Truncating The Matrix From Above And Below

We have been studying the matrix truncated from above, leaving the lowest energy levels. This is the area which is computationally less intensive and in which we have numerical data to compare our result with. Using this method we have had some success. However at the two-by-two truncation level, we see no sign of the changing pairing off we expect.

A slightly different approach we could take, is truncating both above and below. We hope in this case to truncate to a two-by-two case further up the energy scale and see some change in the connectivity between, say, the eighth and ninth energy levels, compared with the ninth and tenth. Figure 4.14 shows this situation for

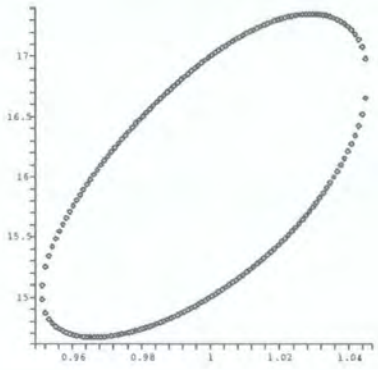

levels 8 and 9

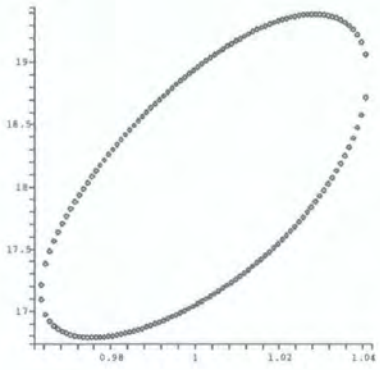

levels 9 and 10

Figure 4.14: Two-by-two truncation for $l = 0$

$l = 0$.

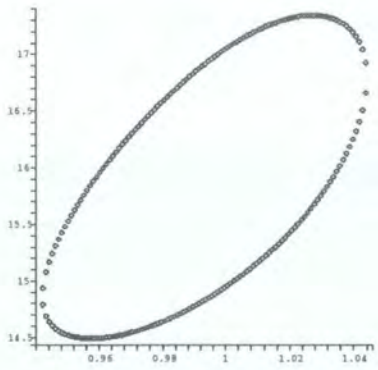

levels 8 and 9

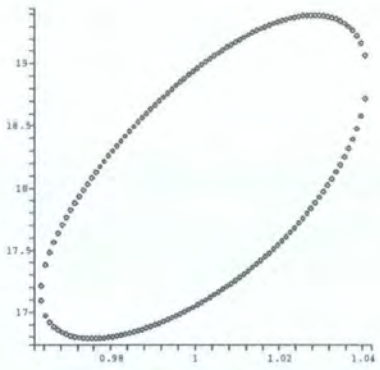

levels 9 and 10

Figure 4.15: Two-by-two truncation for $l = -0.025$

As we can see there is no significant difference between the two pictures. Perhaps we will obtain better results for non-zero values of l. Figures 4.15 and 4.16 show this. As we can see, for none of these values of l, do we have anything that suggests the change in connectivity we know to happen.

Perhaps the two-by-two truncation is too extreme, we could look at the three-by-three truncation high up the energy scale. Figure 4.17, shows the result we get when we truncate to the thirty-first, thirty-second and thirty-third energy levels, for

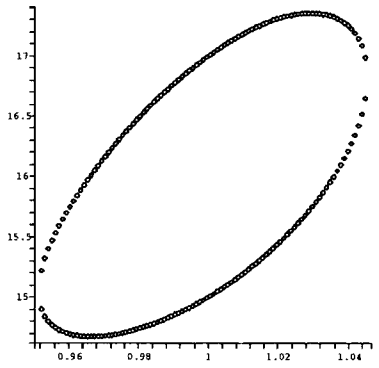

levels 8 and 9

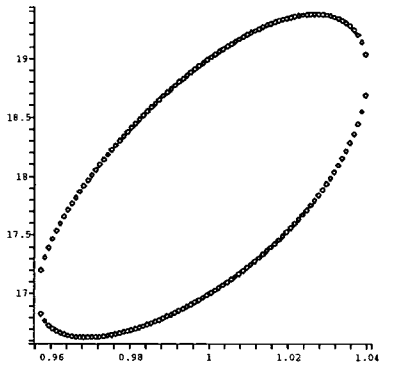

levels 9 and 10

Figure 4.16: Two-by-two truncation for $l = 0.001$

two different values of l. Unfortunately there is no appreciable difference between the two pictures. Let us try the five-by-five truncation. Figure 4.18 shows us the matrix truncated to the thirtieth to thirty-fourth energy levels, for $l = -0.025$ and $l = 0.001$. Again we see no sign of the change in connectivity we see. It seems that the truncation errors destroy any useful information.

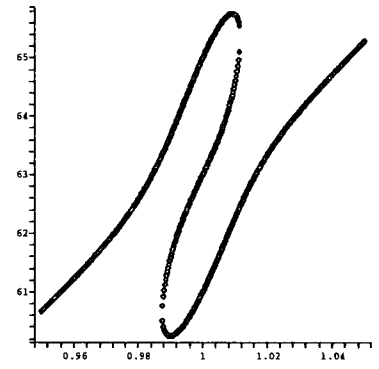

l=0.001

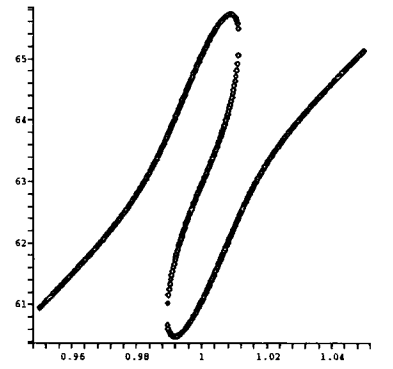

l=-0.025

Figure 4.17: Three-by-Three Truncation For Two Values Of l

However, we are still looking relatively low down the energy scale. As we ascend the energy scale, the pairing off of energy levels happens closer and closer to $M = 1$. This is also where the perturbation method is most valid. We could, then, consider

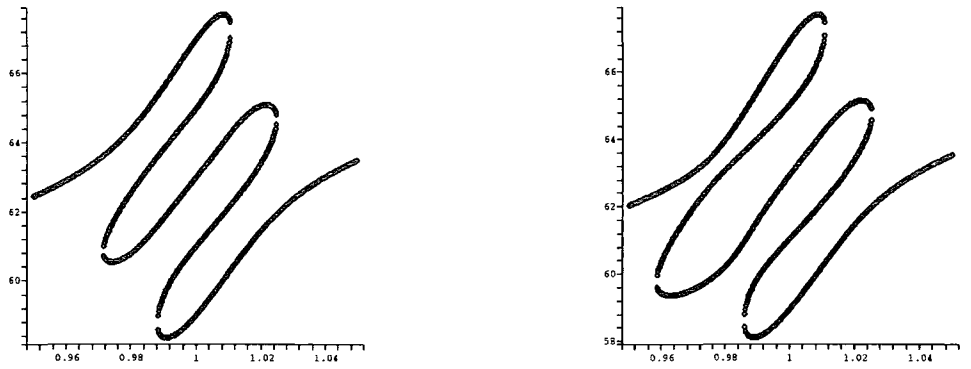

l=0.001 l=-0.025

Figure 4.18: Five-by-Five Truncation For Two Values Of l

the studying a two-by-two truncation for asymptotically large energies. Bender et al have attempted this, we will look at this idea next.

4.6 Asymptotic Two-By-Two Truncation

As previously mentioned Bender, Boettcher and Messinger [7] have considered our problem for $l = 0$. They approximated the Hamiltonian for small $\epsilon = 2(M-1)$ as

$$\mathcal{H}_{1+\epsilon/2} = p^2 + x^2 + \epsilon x^2 \left[\ln|x| + \frac{i\pi}{2}\mathrm{sgn(x)}\right] + O(\epsilon^2). \tag{4.122}$$

They represented the wave functions using the Hermite polynomials

$$\psi_n(x) = \frac{\pi^{-1/4}}{\sqrt{2^n n!}} e^{-x^2/2} H_n(x) \tag{4.123}$$

By letting ϵ tend to zero, and truncating to the two dimensional subspace spanned by $|2n>$ and $|2n-1>$, they arrived at the matrix

$$\mathcal{H}_{\text{trunc}} \approx \begin{pmatrix} a(2n-1) - E & ib(2n) \\ ib(2n) & a(2n) - E \end{pmatrix} \tag{4.124}$$

where

$$a(n) = 2n + 1 + \frac{\epsilon n}{2}\ln(n) \quad , \quad b(n) = \frac{4}{3}\epsilon n \ . \tag{4.125}$$

From this they were able to deduce that the eigenvalues would pair off for

$$\epsilon = -\frac{3}{8n} \tag{4.126}$$

Diagonalising the matrix, we can graph the function for energy levels eight and nine against our numerical result (figure 4.6a).

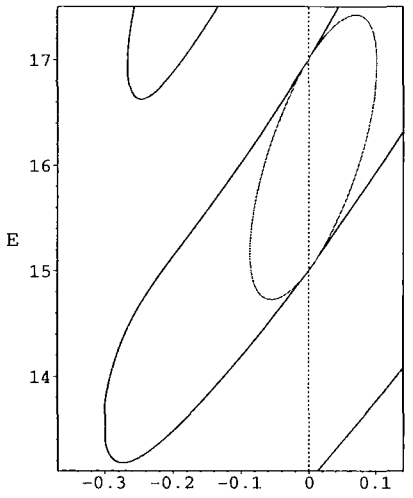

Figure 4.6a: Truncation to levels 8 and 9, compared with numerical data

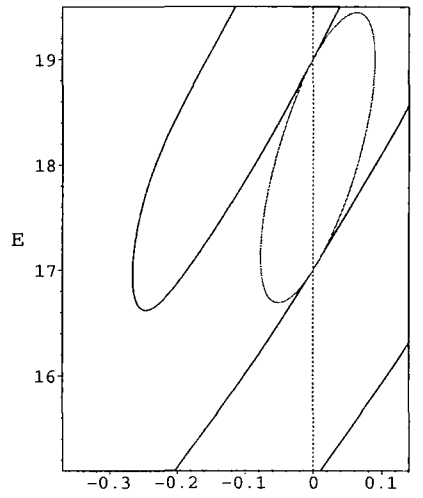

Figure 4.6b: Truncation to levels 9 and 10, compared with numerical data

We can see that there is, at least for $\epsilon < 0$, a qualitative agreement with our expectations. In their paper [7], Bender et al, studied only the region $\epsilon < 0$ and deduced that this qualitative agreement was significant.

However, we get the pairing off appearing for $\epsilon > 0$ as well as $\epsilon < 0$. Also, as we have seen, this level of agreement can be gained without asymptotic. Further, without checking against two energy levels which we expect to not pair off, this result is not significant.

As it turns out, using this method we also predict for the $(|2n>, |2n+1>)$ subspace a pairing off at $\epsilon = \frac{3}{8n}$. Let us see the graph (figure 4.6b). We do not get a match either qualitatively or quantitatively. In fact the result is not substantially different from our non-asymptotic, two-by-two truncation.

We see then that the two-by-two truncation, even in this limit, is not sensitive enough to discern the connectivity of eigenvalue merging. Some progress has

been made in calculating the matrix elements for a three-by-three case with angular momentum. However, the calculation of the asymptotic of the hypergeometric functions is very delicate. Some results we shall obtain in chapter 6, also lead us to believe this may not be the correct limit.

This takes us into some ideas for further study. The calculation of the asymptotic with l, even if this is not the relevant limit, would be of mathematical interest. Another idea would be to attempt to solve the problem of connectivity of merging levels, by using a different limit. Finally, it would be interesting to see how far away from $M = 1$, one could continue to obtain a good approximation for the energy levels by increasing the truncation size. We have seen this improving with larger truncations, could we do this indefinitely, or is there a limit after which the perturbative method breaks down for any size of truncation. One obvious point for the technique to break down is at $M = 2$. After this point the stokes sectors have moved below the real axis and our integration contour should no longer be relevant.

We have spent some time studying the perturbative approach. We have, for large truncations, succeeded in accurately creating the behaviour of the low lying energy levels. However, for smaller truncations, we do not find any meaningful results. Indeed, an analytic understanding of the interesting phenomena exhibited by this Hamiltonian seems elusive. We need to consider different methods, it is to this we turn next.

Chapter 5

Functional Equations

5.1 Introduction

Having considered the problem we are interested in from a perturbative frame work, in the next two chapters we will take a different approach. Using some results from the ODE/IM correspondence, [18], [14], we will be attempting to understand analytically the merging of eigenvalues when $M < 1$.

In this chapter we will be reviewing some earlier work by Dorey and Tateo and will obtain an analogue of the well-known T-Q relation, from the theory of integrable models. From this we will be able to construct a proof of the reality of the eigenvalues of our Hamiltonian for $M > 1$. This, as well as being a result of interest in its own right, will form the mathematical basis of the technique used in chapter 6.

5.2 The T-Q Equation

Recall the problem (2.2.2):

$$\left(-\frac{d^2}{dx^2} + x^{2M} + \frac{l(l+1)}{x^2} \right) y(x) = Ey(x) \tag{5.1}$$

With the Stokes sectors defined as,

$$S_k := \left| \arg(x) - \frac{2\pi k}{2M+2} \right| < \frac{\pi}{2M+2} \tag{5.2}$$

we are interested in the solution subdominant in the sectors S_{-1} and S_1. The problem is considered on the complex plane, with a branch cut running from zero to infinity along the negative real axis.

A solution $y \equiv y(x, E, l)$, is entire on the cut plane. There is a unique solution to the differential equation that approaches the decaying WKB approximation as $x \to +\infty$ along the real axis (Appendix C.2).

Some examples, for varying values of M are

$$M > 1: \quad y(x, E, l) \sim \frac{1}{\sqrt{2i}} x^{-M/2} \exp\left(-\frac{1}{M+1} x^{M+1}\right) \tag{5.3}$$

$$M = 1: \quad y(x, E, l) \sim \frac{1}{\sqrt{2i}} x^{-1/2+E/2} \exp\left(-\frac{1}{2} x^2\right) \tag{5.4}$$

$$1 > M > \tfrac{1}{3}: \quad y(x, E, l) \sim \frac{1}{\sqrt{2i}} x^{-M/2} \exp\left(-\frac{1}{M+1} x^{M+1} + \frac{E}{2-2M} x^{1-M}\right) \tag{5.5}$$

We also define another solution $\psi(x, E, l)$, in terms of the related radial problem, as the solution that tends to zero at the origin. For $l > -\frac{1}{2}$, as $x \to 0$

$$\psi(x, E, l) \sim x^{l+1} + O(x^{l+3}) \tag{5.6}$$

If we have a solution to the differential equation (5.1) that adheres to both these boundary conditions, we have a wavefunction to the (hermitian) radial problem.

We have a solution subdominant in the sector S_0, from this we can generate solutions subdominant in any of the other sectors. Consider the function $\hat{y}(x) = y(ax, E, l)$, this function solves the equation

$$\left(-\frac{d^2}{dx^2} + a^{2M+2} x^{2M} - a^2 E + \frac{l(l+1)}{x^2}\right) \hat{y}(x) = 0 \tag{5.7}$$

Therefore if $a^{2M+2} = 1$, $y(ax, a^{-2}E, l)$ is another solution to our original equation (5.1). If we set $a^{-1} \equiv \omega = \exp(i\pi/(M+1))$, we achieve this. We define

$$y_k \equiv y_k(x, E, l) = \omega^{k/2} y(\omega^{-k} x, \omega^{2k} E, l) \tag{5.8}$$

which define a set of solutions to our equation. y_k is subdominant in S_k and dominant in $S_{k\pm1}$. Because any y_k and y_{k+1} are linearly independent they form a spanning set, $\{y_k, y_{k+1}\}$, of the space of solutions to the differential equation. Any of the solutions can then be expanded in terms of these two solutions. In particular we can write

$$y_{-1}(x, E, l) = C(E, l) y_0(x, E, l) + \tilde{C}(E, l) y_1 \tag{5.9}$$

The C and $\tilde{C}$ are known as the Stokes multipliers for y_{-1} with respect to y_0 and y_1 respectively.

To proceed further we must take a brief detour to consider Wronskians. The Wronskian $W[f,g]$ of two functions f and g is defined as

$$W[f,g] = fg' - f'g \tag{5.10}$$

From the above it is clear that $W[f,g] = -W[g,f]$. The Wronskian of two solutions to a second order ordinary differential equation with no single derivative term, is independent of x. It is zero if and only if, the solutions are linearly dependent, (C.1).

As we know y_0 and y_1 are linearly independent, we can obtain expressions for C and $\tilde{C}$ in terms of Wronskians. If, for brevity, we write $W[y_j, y_k] \equiv W_{j,k}$ and take the Wronskian of (5.9) with y_0

$$W_{-1,0} = \tilde{C}(E,l)W_{1,0} \tag{5.11}$$

so

$$\tilde{C}(E,l) = -\frac{W_{-1,0}}{W_{0,1}} \tag{5.12}$$

Taking the Wronskian of (5.9) with y_1 we obtain

$$C(E,l) = \frac{W_{-1,1}}{W_{0,1}} \tag{5.13}$$

The Wronskians are entire functions of E and l. We know that $W_{0,1}$ is non-zero as y_0 and y_1 are linearly independent, so both of the above expressions are entire functions of E and l.

The expression for $\tilde{C}$ can be simplified. To do this we need to consider

$$\begin{aligned}
&W_{j+1,k+1}(E,l) = \\
&\omega^{\frac{j+k}{2}+1}\big(y(\omega^{-j-1}x, \omega^{2j+2}E, l)y'(\omega^{-k-1}x, \omega^{2k+2}E, l) \\
&-y'(\omega^{-j-1}x, \omega^{2j+2}E, l)y(\omega^{-k-1}x, \omega^{2k+2}E, l)\big) \\
&= y_j(\omega^{-1}x, \omega^2 E, l)y_k'(\omega^{-1}x, \omega^2 E, l) \\
&-y_j'(\omega^{-1}x, \omega^2 E, l)y_k(\omega^{-1}x, \omega^2 E, l) \\
&= W_{j,k}(\omega^2 E, l)
\end{aligned} \tag{5.14}$$

as the Wronskian is independent of x. This allows us to say

$$\tilde{C}(E,l) = -\frac{W_{0,1}(\omega^{-2}E)}{W_{0,1}(E)} \tag{5.15}$$

For $1 > M > \frac{1}{3}$ and $M > 1$ $W_{0,1} = 1$. This is found by considering the asymptotic expressions for y, which is perfectly valid as the Wronskians are independent of x. For these values of M then,

$$\tilde{C} = -1 \tag{5.16}$$

$$C(E) = W_{-1,1} \tag{5.17}$$

At $M = 1$ we return to the well understood harmonic oscillator. As $y_{-1}(x,E,l) = y_1(x^*,E^*,l^*)$, it follows that for real values of E and l, $C(E,l)$ is real.

We then arrive at the relation

$$C(E,l)y_0(x,E,l) = y_{-1}(x,E,l) + y_1(x,E,l) \tag{5.18}$$

We must now consider $\psi(x)$ the solution to the ODE that decays for $x \to 0$. This is

$$\psi(x,E,l) \sim x^{l+1} + O(x^{l+3}) \tag{5.19}$$

Similarly to to our treatment of y, the solution that decays for large x, above we can consider

$$\psi_k(x,E,l) = \omega^{k/2}\psi(\omega^{-1}x, \omega^2 E, l) \tag{5.20}$$

These solutions also solve our problem. By considering the limit as $x \to 0$ we can conclude that

$$\psi_k(x,E,l) = \omega^{-k(l+1/2)}\psi(x,E,l) \tag{5.21}$$

This conclusion can be made as the solution, ψ, which decays as $x \to 0$ is unique up to a constant. Therefore if we can find a relation between two decaying solutions, it must be valid for all x. The relation

$$W[y_{j+1}, \psi_{k+1}](E,l) = W[y_j, \psi_k](\omega^2 E, l) \tag{5.22}$$

continues to hold. This allows us to state

$$\begin{aligned} W[y_k, \psi](E,l) &= \omega^{k(l+1/2)} W[y_k, \psi_k](E,l) \\ &= \omega^{k(l+1/2)} W[y, \psi](\omega^{2k}E, l) \end{aligned} \tag{5.23}$$

We write $W[y,\psi](E,l) = Q(E,l)$, $C(E,l) = T(E,l)$ and take Wronskians of both sides of (5.18).

$$T(E,l)Q(E,l) = \omega^{-(l+1/2)}Q(\omega^{-2}E,l) + \omega^{(l+1/2)}Q(\omega^{2}E,l) \tag{5.24}$$

which is identical to Baxter's T-Q relation [3].

Let us think about the meaning of this equation. We have $T(E,l) = W[y_{-1},y_1]$, that is the Wronskian of the solutions subdominant in sectors S_{-1} and S_1. We know that this Wronskian is zero if and only if these two solutions are linearly dependent. In other words if for our given values of E and l, we have a solution which decays in both sectors. But if we have a solution to the ODE (5.1), subdominant in sectors S_{-1} and S_1, we have a solution to our problem 2.2.2. Therefore the values of E for which $T(E,l) = 0$ are the energy eigenvalues we are looking for. As this is the rotated problem, the eigenvalues of the fundamental statement are the $-E$.

We also need to consider $Q(E,l) = W[y,\psi](E,l)$. This is the Wronskian of two solutions, one subdominant in sector S_0 and one which decays as $x \to 0$. This is zero if and only if these two solutions are linearly dependent. That is if we have a solution to the radial problem. The values of E for which $Q(E,l) = 0$ are then the energy eigenvalues for the radial problem.

Let us recap briefly. We have two problems based on the differential equation

$$\left(-\frac{d^2}{dx^2} + x^{2M} + \frac{l(l+1)}{x^2}\right)y(x) = Ey(x) \tag{5.25}$$

In one, the transverse problem, we demand the solutions decay in the sectors S_1 and S_1. These are the sectors which contain the positive and negative imaginary axes, for $M \sim 1$. The function $T(E,l)$ is zero when the value of E is an eigenvalue of the transverse problem. We call these values of E $\{-e_j\}$. This problem is non-hermitian and $\mathcal{PT}$ symmetric. It is equivalent to the fundamental definition of the problem which is the focus of this thesis (2.2.1). The energy eigenvalues of our fundamental definition are the $\{e_j\}$.

The other problem, the radial problem, has boundary conditions demanding $y \to 0$ at the origin and as $x \to \infty$ along the positive real axis. The function $Q(E,l)$ is zero when the value of E is an eigenvalue of the radial problem. We will call these values of E $\{E_i\}$. This problem is hermitian.

5.3 Proof Of Reality Of Energy Spectrum For $M > 1$

From the T-Q equation we have derived, it is possible to prove the reality of the energy spectrum of our $\mathcal{PT}$-symmetric Hamiltonian for values of M larger than 1.

In order to make the proof two results must be established. Namely that:

$$\ln Q(E,l) \sim \frac{a_0}{2}(-E)^{\frac{M+1}{2M}} \qquad |E| \to \infty \quad |\arg(-E)| < \pi \tag{5.26}$$

and therefore the order of $Q(E,l)$ is $\frac{M+1}{2M}$. We must also establish that:

$$Q(0,l) = \frac{1}{\sqrt{\pi}}\Gamma(1+\frac{2l+1}{2M+2})(2M+2)^{\frac{2l+1}{2M+2}+\frac{1}{2}}. \tag{5.27}$$

We will outline the proofs of these statements in the following two subsections. The results established will also be used in chapter 6. The proof of reality of the eigenvalues, which rests upon these assumptions, will be carried out in 5.3.3.

5.3.1 The Order Of Q.

We wish to show that for $M > 1$, Q has the large E asymptotic [18]

$$\ln Q(E,l) \sim \frac{a_0}{2}(-E)^{\mu} \qquad |E| \to \infty \quad |\arg(-E)| < \pi \tag{5.28}$$

where $\mu = \frac{M+1}{2M}$ and

$$\begin{aligned} a_0 &= 2\int_0^\infty [(t^{2M}+1)^{\frac{1}{2}} - t^M]dt \\ &= -\frac{1}{\sqrt{\pi}}\Gamma(-\tfrac{1}{2}-\tfrac{1}{2M})\Gamma(\tfrac{1}{2}+\tfrac{1}{2M}) \end{aligned} \tag{5.29}$$

We first note that $Q(E,l) = W[y(x,E,l),\psi(x,E,l)]$, can be evaluated as

$$Q(E,l) = \lim_{x\to 0}\left((2l+1)x^l y(x,E,l)\right). \tag{5.30}$$

Starting from our equation (2.2.2):

$$\left(-\frac{d^2}{dx^2} + x^{2M} + \frac{l(l+1)}{x^2} - E\right)y = 0. \tag{5.31}$$

We cannot use the WKB approximation directly upon this potential, due to the singularity at the origin. We perform the Langer transform, [29]: $x = e^z$, $y(x) = e^{z/2}\phi(z)$ and write $\lambda = l + 1/2$:

$$\left(-\frac{d^2}{dz^2} + e^{(2M+2)z} - e^{2z}E + \lambda^2 \right)\phi(z) = 0 \tag{5.32}$$

The, correctly normalised WKB approximation for ϕ, that is subdominant as $x \to \infty$ is:

$$\phi(z, -E, \lambda) \sim \frac{1}{R(z,-E,\lambda)^{1/4}}$$
$$\times \exp\left(\int_z^\infty (\sqrt{R(u, -E, \lambda)} - e^{(M+1)u})du - \frac{1}{M+1}e^{(M+1)z} \right). \tag{5.33}$$

where $R(u, -E, \lambda) = e^{(2M+2)z} - e^{2z}E + \lambda^2$. This approximation is now valid for all z, so long as $\arg(-E) \neq \pi$, for a discussion see [32].

We are interested in the limit as $z \to -\infty$. In this limit we get:

$$\phi(z, -E, \lambda) \sim \lambda^{-1/2} \exp\left(-\lambda z + (-E)^{(M+1)/2M} \int_0^\infty (\sqrt{t^{2M}+1} - t^M)dt \right) \tag{5.34}$$

Reversing the transformation, we get:

$$y(x) \sim (l + 1/2)^{-1/2} x^{-l} \exp\left((-E)^{(M+1)/2M} \int_0^\infty (\sqrt{t^{2M}+1} - t^M)dt \right) \tag{5.35}$$

Putting this back into (5.30):

$$Q(E, l) = \frac{1}{2}(l + 1/2)^{1/2} \exp\left((-E)^{(M+1)/2M} \int_0^\infty (\sqrt{t^{2M}+1} - t^M)dt \right). \tag{5.36}$$

Therefore

$$\ln Q(E, l) \sim \frac{a_0}{2}(-E)^{(M+1)/2M}. \tag{5.37}$$

Hence, the order of $Q(E, l) = \frac{M+1}{2M}$.

5.3.2 The Value Of $Q(0, l)$.

We will demonstrate that the claim [15]:

$$Q(0, l) = \frac{1}{\sqrt{\pi}}\Gamma(1 + \frac{2l+1}{2M+2})(2M+2)^{\frac{2l+1}{2M+2}+\frac{1}{2}}, \tag{5.38}$$

is indeed correct. This discussion is taken from [18].

At $M = 1$, the equation becomes the well understood harmonic oscillator with angular momentum. The equation can be solved exactly:

$$y(x, E, l) = x^{l+1} e^{-x^2/2} U(\frac{1}{2}(l + \frac{3}{2}) - \frac{E}{4}, l + \frac{3}{2}, x^2) \tag{5.39}$$

where $U(a, b, z) = \frac{\pi}{\sin(\pi b)} \left(\frac{{}_1F_1(a,b,z)}{\Gamma(1+a-b)\Gamma(b)} - z^{1-b} \frac{{}_1F_1(1+a-b,2-b,z)}{\Gamma(a)\Gamma(2-b)} \right)$. This is the solution to the differential equation, not the Schrödinger equation. It solves for general E and is not necessarily a wavefunction.

At $E = 0$ we can use the relation $U(a, 2a, x^2) = \frac{1}{\sqrt{\pi}} x^{1-2a} e^{x^2/2} K_{a-1/2}(x^2/2)$. Where K_a is a Bessel function of the second kind. Thus:

$$y(x, 0, l)|_{M=1} = \frac{1}{\pi} x^{1/2} K_{l/2+1/4}(x^2/2). \tag{5.40}$$

For $\nu > 0$ and $z \to 0$, $K_\nu(z) \sim \frac{1}{2}\Gamma(\nu)(z/2)^{-\nu}$ [1]. So for $l > \frac{1}{2}$:

$$y(x, 0, l)|_{M=1} \sim \frac{1}{\pi} 2^{l-1/2} \Gamma(\frac{l}{2} + \frac{1}{4}) x^{-l} \qquad \text{as} \quad x \to 0. \tag{5.41}$$

Then using 5.30, we can write $Q(E, l)|_{M=1} = \frac{1}{\pi} 2^{l+3/2} \Gamma(1 + \frac{l}{2} + \frac{1}{4})$.

The general M case can be recovered by using the fact that at $E = 0$ a variable change relates a solution at arbitrary M and l to a solution at $M = 1$, but with l replaced by $l' = l'(l, M)$. The normalisation at large x must be agreement with the WKB solution: $y \sim x^{-M/2} \exp(-\frac{1}{M+1} x^{M+1})$. The relevant transformation is then:

$$y(x, 0, l)|_M = (\frac{2}{M+1})^{1/4} x^{-(M+1)/4} y((\frac{2}{M+1})^{1/2} x^{(M+1)/2}, 0, \frac{2l+1}{M+1} - \frac{1}{2})|_{M=1} \tag{5.42}$$

Repeating the steps used above for $M = 1$, the result quoted can be recovered:

$$Q(0, l) = \frac{1}{\sqrt{\pi}} \Gamma(1 + \frac{2l+1}{2M+2}) (2M+2)^{\frac{2l+1}{2M+2} + \frac{1}{2}}, \tag{5.43}$$

5.3.3 Reality Of Eigenvalues

This proof is taken from [15]. In the T-Q equation, we set $E = -e_j$, where the $\{-e_j\}$ are the zeros of $T(E, l)$ and hence the negated eigenvalues of our $\mathcal{PT}$-symmetric Hamiltonian. We obtain:

$$-\omega^{-2l-1} = \frac{Q(-\omega^2 e_j, l)}{Q(-\omega^{-2} e_j, l)} \tag{5.44}$$

In 5.3.1 we calculated the order $Q(E,l)$ is $\frac{M+1}{2M}$, so for $M > 1$, the order of Q is less than 1. In this case, Hadamard's factorisation theorem (see appendix C.3) states, if $Q(0,l) \neq 0$, we can write $Q(E,l)$ as an infinite product over it's zeros. We know from 5.3.2 that this constraint holds and so:

$$Q(E,l) = Q(0,l)\prod_{n=0}^{\infty}\left(1-\frac{E}{E_n}\right). \tag{5.45}$$

We put this into (5.44):

$$-\omega^{-2l-1} = \prod_{n=0}^{\infty}\left(\frac{E_n+\omega^2 e_j}{E_n+\omega^{-2}e_j}\right) \tag{5.46}$$

We write $e_j = |e_j|e^{i\delta_j}$. Taking the modulus^2 of both sides:

$$1 = \prod_{n=0}^{\infty}\left(\frac{|E_n|^2+|e_j|^2+2\cos(\frac{2\pi}{M+1}+\delta_j)}{|E_n|^2+|e_j|^2+2\cos(\frac{2\pi}{M+1}-\delta_j)}\right) \tag{5.47}$$

The only difference between the numerator and the denominator, is the cos function, which is independent of n. All of the terms are simultaneously greater than, less than or equal to one. Therefore for the product to be equal to one, each of the terms must be individually equal to one. i.e. $\cos(\frac{2\pi}{M+1}+\delta_j) = \cos(\frac{2\pi}{M+1}-\delta_j)$, or:

$$\sin(\frac{2\pi}{M+1})\sin(\delta) = 0. \tag{5.48}$$

As $M > 1$, this equation can only be satisfied when:

$$\delta_j = n\pi \tag{5.49}$$

Hence, the eigenvalues $\{e_j\}$ of the $\mathcal{PT}$-symmetric potential, 2.2.1, are real.

5.3.4 Positivity Of The Spectrum

At $M = 1$, we have the harmonic oscillator for which the eigenvalues are known to be $2n + 1 - (-1)^n 2l$, $n = 0, 1, ...$ These are all real. They are all positive if $-\frac{3}{2} < l < \frac{1}{2}$.

By substituting $E = 0$ into (5.24) and using the knowledge that $Q(0,l) \neq 0$, we can calculate:

$$T(0,l) = 2\cos\left(\pi\frac{2l+1}{2M+2}\right). \tag{5.50}$$

We know that for $M > 1$ the $\{e_j\}$ are confined to the real axis, so that as we vary M for an eigenvalue to be negative it must pass through the point $E = 0$ as we increase M. For this to be true we would have $T(0, l) = 0$. We can see that for this to be the case we need $M + 1 = |2l + 1|$. Hence the $\{e_j\}$ are real and positive, for $M > 1$ and $M + 1 > |2l + 1|$.

In this chapter, we have reviewed some earlier work originally performed by Dorey and Tateo. We have seen, from our differential equation it is possible to derive the T-Q equation of integrable model theory. From this equation we have then seen a proof that the eigenvalues of 2.2.1 are real and positive. In the next chapter we will build upon these results to eventually gain an analytic understanding of the eigenvalue merging.

Chapter 6

Integral Equation and Second Determination

6.1 Introduction

So far we have studied our problem using a number of techniques. We have studied the problem at a classical level, we have attempted a perturbative understanding of the problem and we have seen a correspondence with the T-Q equations of integrable models. From the last of these we have been able to extract a reality proof for our spectrum.

What we would really like, though, is an understanding of the change in connectivity between energy levels in the broken $\mathcal{PT}$ region. In this chapter, by building on the T-Q equation of the previous chapter, this is what we shall do.

6.2 The Integral Equation

We start from the T-Q equation (5.24) derived in the last chapter:

$$T(E,l)Q(E,l) = \omega^{-(l+1/2)}Q(\omega^{-2}E,l) + \omega^{(l+1/2)}Q(\omega^{2}E,l) \tag{6.1}$$

From this we will obtain an integral equation which allows us to find the energy levels of the radial problem.

6.2.1 Some Properties Of The Functions $T(E,l)$ and $Q(E,l)$

To continue further with our discussion, we will need to understand some properties of our functions. The properties we are interested in are:

1. The Functions T and Q are entire functions of E
2. For l real and greater than $-\frac{1}{2}$, the zeros of Q all lie on the positive real E axis.
3. For $M > 1$ and $M + 1 - |2l + 1| > 0$ the zeros of $T(E,l)$ all lie on the negative real E axis. Also for $\frac{1}{2} < M < 1$ the zeros of T lie away from the positive real E axis. In fact the zeros are all in the region $|\arg(E)| > \frac{2\pi}{3}$.
4. For $M > 1$, Q has the large E asymptotic

$$\ln Q(E,l) \sim \frac{a_0}{2}(-E)^{\mu} \qquad |E| \to \infty \quad |\arg(-E)| < \pi \tag{6.2}$$

where $\mu = \frac{M+1}{2M}$ and

$$\begin{aligned} a_0 &= 2\int_0^{\infty}[(t^{2M}+1)^{\frac{1}{2}} - t^M]dt \\ &= -\frac{1}{\sqrt{\pi}}\Gamma(-\tfrac{1}{2} - \tfrac{1}{2M})\Gamma(\tfrac{1}{2} + \tfrac{1}{2M}) \end{aligned} \tag{6.3}$$

5.

$$Q(0,l) = \frac{1}{\sqrt{\pi}}\Gamma(1 + \frac{2l+1}{2M+2})(2M+2)^{\frac{2l+1}{2M+2}+\frac{1}{2}} \tag{6.4}$$

The first of these properties follows directly from the fact that Q is a Wronskian of two functions entire in E. The others are a little more subtle.

The first part of property two is also easily seen to hold. Remember, that $Q(E,l)$ is a Wronskian of two eigenfunctions of an hermitian problem. A zero of $Q(E,l)$ signifies that there is a eigenfunction of the problem at that value of E. As the problem is hermitian, we know that this value of E must be real.

For $l \geq 0$, the potential is everywhere positive, thus we can state the energies also, must be positive (see A.3). This leaves us only the region $l < 0$. To see that in

this case the energy levels are also positive we make the Langer transformation [29]: $x = e^z$, $y(x) = e^{z/2}\phi(z)$. We also write $\lambda = l + 1/2$. Our transformed equation is:

$$\left(-\frac{d^2}{dz^2} + e^{(2M+2)z} + \lambda^2 \right)\phi(z) = e^{2z}E\phi(z). \tag{6.5}$$

We now have a potential everywhere positive. Thus $e^{2z}E > 0$ and as z is real, $E > 0$.

Properties four and five have both been shown to be true in chapter 5.

We need only now consider the third property. The claim for $M > 1$ was also proved in the previous chapter. It is only the result for $M < 1$ we have left to consider.

Property 3

In [35] a proof was given that the eigenvalues of a particular $\mathcal{PT}$-symmetric Hamiltonian lie within a certain wedge on the complex plane. The problem under consideration was:

$$-u''(x) + [P(x^2) - (ix)^{2n+1}]u(x) = \lambda u(x) \tag{6.6}$$

with $u(\pm\infty) = 0$ and where $P(x)$ is a polynomial of degree at most $n \geq 1$, with all non-negative real coefficients (possibly $P \equiv 0$). It was shown that $\Re e(\lambda) > 0$ and that $|\arg(\lambda)| \leq \pi/(2n+3)$.

We hope to extend this proof to non-integer powers of (ix) and to add an angular momentum term. The equation we shall consider is:

$$-u''(x) + x^{2M}u(x) + l(l+1)u(x)x^{-2} = \lambda u(x) \tag{6.7}$$

for $1/2 < M < 1$. We consider the eigenvalue problem along an integration contour that starts at infinity in the Stokes sector containing the negative imaginary axis, ends at infinity in the Stokes sector containing the positive imaginary axis and avoids the singularity at the origin. We take the solution that decays in both these sectors.

The rays that define the relevant Stokes sectors are $-\pi/(2M+2)$ and $-3\pi/(2M+2)$ for the sector containing the negative imaginary axis and $\pi/(2M+2)$ and $3\pi/(2M+2)$ for the sector containing the positive imaginary axis. Our integration contour is a deformation of the straight line through the origin at angle θ to the positive imaginary axis $|\theta| < \frac{M\pi}{2M+2}$. We take the deformation to be a semi-circular anti-clockwise path a distance $|a|$ from the origin.

We make the substitution $x = ze^{i\theta+i\pi/2}$, $v(z) = u(ze^{i\theta+i\pi/2})$. Where z is a complex variable.

$$-v''(z) - e^{i(2M+2)\theta+iM\pi}z^{2M}v(z) + l(l+1)v(z)z^{-2} + \lambda e^{i2\theta}v(z) = 0 \tag{6.8}$$

We multiply by $e^{-i(2M+2)\theta}v^*(z)$ and integrate the first term by parts.

$$\begin{aligned} &e^{-i(2M+2)\theta}\int_C |v'(z)|^2dz - e^{iM\pi}\int_C z^{2M}|v(z)|^2dz \\ &+l(l+1)e^{-i(2M+2)\theta}\int_C z^{-2}|v(z)|^2dz + \lambda e^{-i2M\theta}\int_C |v(z)|^2dz = 0 \end{aligned} \tag{6.9}$$

where C is the contour.

The contour splits naturally into three sections. We shall label them C_1, C_2 and C_3. C_1 runs from infinity in the lower Stokes' sector, C_2 is the semi-circular arc and C_3 is another straight line out to infinity in the upper Stokes' sector. We will make the following transformations. On C_1 and C_3 we set $z = r$ with $r = -\infty.. - |a|$ on C_1 and $r = |a|..\infty$ on C_3. On C_2 we set $z = |a|e^{i\phi}$, with $\phi = -\pi..0$. We know that close to the origin the wavefunction $u(x)$ goes like either x^{l+1} or x^{-l}, we note then that close to the origin $|v(z)|$ and $|v'(z)|$ are independent of the angular coordinate of z i.e for $|a| \ll 1$: $|v(|a|e^{i\phi})| \equiv w(|a|)$ and $|v'(|a|e^{i\phi})| \equiv W(|a|)$ are constant.

Before we get into the details it is instructive to get an overview of the argument. We will calculate the real part of our equation [6.9]. We would like this to be of the form $A + \Re e(\lambda e^{-i2M\theta})B = 0$, where A and B are real positive constants. The term involving $l(l+1)$ will make this difficult, however by a good choice of θ we will be able to make this possible. This will then lead us to be able to state:

$$\alpha\cos\left(\frac{M\pi}{2M+2}\right) \pm \beta\sin\left(\frac{M\pi}{2M+2}\right) < 0 \tag{6.10}$$

where $\lambda = \alpha + i\beta$. This will allow us to restrict the value of λ.

For the sake of clarity, we will study the terms one by one, starting with the first term. The first term can be written:

$$\begin{aligned} &e^{-i(2M+2)\theta}\int_C |v'(z)|^2dz \\ &= e^{-i(2M+2)\theta}\int_{C_3} |v'(z)|^2dz + e^{-i(2M+2)\theta}\int_{C_2} |v'(z)|^2dz + e^{-i(2M+2)\theta}\int_{C_1} |v'(z)|^2dz \end{aligned} \tag{6.11}$$

We apply the transformation:

$$e^{-i(2M+2)\theta}\int_{|a|}^{\infty}|v'(r)|^2dr$$

$$+ie^{-i(2M+2)\theta}|a|\int_{-\pi}^{0}W(|a|)^2e^{i\phi}d\phi+e^{-i(2M+2)\theta}\int_{-\infty}^{-|a|}|v'(r)|^2dr \tag{6.12}$$

For $|a|\ll 1$, $W(|a|)$ is constant and we can do the ϕ integration.

We take the real part, the result is

$$\Re e\left(e^{-i(2M+2)\theta}\int_C|v'(z)|^2dz\right) \tag{6.13}$$

$$=\cos((2M+2)\theta)\left(\int_{|a|}^{\infty}|v'(r)|^2dr+\int_{-\infty}^{-|a|}|v'(r)|^2dr+2|a||W(|a|)|^2\right) \tag{6.14}$$

Each of the terms in the bracket is positive, so the sign is dependent on $cos((2M+2)\theta)$.

We now examine the second term:

$$-e^{iM\pi}\int_C z^{2M}|v(z)|^2dz=-e^{iM\pi}\int_{|a|}^{\infty}r^{2M}|v(r)|^2dr$$

$$-ie^{iM\pi}|a|^{2M+1}\int_{-\pi}^{0}|w(|a|)|^2e^{i(2M+1)\phi}d\phi-e^{iM\pi}\int_{-\infty}^{-|a|}r^{2M}|v(r)|^2dr \tag{6.15}$$

In the last term we set $r=e^{-i\pi}\rho$, in the second we do the integration.

We get:

$$\Re e\left(-e^{iM\pi}\int_C z^{2M}|v(z)|^2dz\right)$$

$$=-\cos(M\pi)\left(\int_{|a|}^{\infty}r^{2M}|v(r)|^2dr+\int_{|a|}^{\infty}\rho^{2M}|v(e^{-i\pi}\rho)|^2d\rho+2\frac{|a|^{2M+1}w(|a|)^2}{2M+1})\right)$$

Notice that this is positive for $\frac{1}{2}<M<\frac{3}{2}$.

The next term to consider is

$$l(l+1)e^{-i(2M+2)\theta}\int_C z^{-2}|v(z)|^2dz \tag{6.16}$$

We make our transformation and obtain:

$$l(l+1)e^{-i(2M+2)\theta}\int_{|a|}^{\infty}r^{-2}|v(r)|^2dr$$

$$+il(l+1)e^{-i(2M+2)\theta}|a|^{-1}\int_{-\pi}^{0}e^{-i\phi}w(|a|)^2d\phi$$

$$+l(l+1)e^{-i(2M+2)\theta}\int_{-\infty}^{-|a|} r^{-2}|v(r)|^2dr \tag{6.17}$$

we do the ϕ integration and take the real part:

$$\Re e\Big(l(l+1)e^{-i(2M+2)\theta}\int_C z^{-2}|v(z)|^2dz\Big)$$

$$= l(l+1)\cos((2M+2)\theta))\Big(\int_{|a|}^{\infty} r^{-2}|v(r)|^2dr + \int_{-\infty}^{-|a|} r^{-2}|v(r)|^2dr - 2|a|^{-1}w(|a|)^2\Big)$$

Notice there is a minus sign inside the bracket, making it difficult to say what the sign of the bracket is. Notice also that even if we could state the sign of the bracket, the fact that $l(l+1)$ can have either sign would mean that in some cases this term would have a different sign to the v' term.

We treat the last term in a similar manner:

$$\Re e\Big(\lambda e^{-i2M\theta}\int_C |v(z)|^2dz\Big)$$

$$= \Re e(\lambda e^{-i2M\theta})\Big(\int_{|a|}^{\infty}|v(r)|^2dr + 2|a||w(|a|)|^2 + \int_{-\infty}^{-|a|}|v(r)|^2dr\Big) \tag{6.18}$$

This is, then, the final term. The part in brackets on the right hand side is real and positive.

Putting all the terms together, the real part of our equation [6.9] becomes:

$$\cos((2M+2)\theta)\Big(\int_{|a|}^{\infty}|v'(r)|^2dr + \int_{-\infty}^{-|a|}|v'(r)|^2dr + 2|W(|a|)|^2\Big)$$

$$-\cos(M\pi)\Big(\int_{|a|}^{\infty} r^{2M}|v(r)|^2dr + \int_{|a|}^{\infty}\rho^{2M}|v(e^{-1\pi}\rho)|^2dr + 2\frac{|a|^{2M+1}w(|a|)^2}{2M+1})\Big)$$

$$+l(l+1)\cos((2M+2)\theta))\Big(\int_{|a|}^{\infty} r^{-2}|v(r)|^2dr + \int_{-\infty}^{-|a|} r^{-2}|v(r)|^2dr - 2|a|^{-1}w(|a|)^2\Big)$$

$$+\Re e\Big(\lambda e^{-i2M\theta}\Big)\Big(\int_{|a|}^{\infty}|v(r)|^2dr + 2|a||w(|a|)|^2 + \int_{-\infty}^{-|a|}|v(r)|^2dr\Big) = 0 \tag{6.19}$$

We have then an equation relating the real part of our integrals. We would like to have it in the form: $A + \Re e(\lambda e^{-i2M\theta})B = 0$, where A and B are real positive constants. This is stopped from being true by the relative minus sign in the $l(l+1)$ term and also by the possible relative minus sign between the $l(l+1)$ term and the v' term. This can be solved by setting $\cos((2M+2)\theta) = 0$. We set $\theta = \pm\frac{\pi}{2(2M+2)}$.

Recall that to stay within the correct Stokes' sector we must have: $|\theta| < \frac{M\pi}{2M+2}$, thus our choice of θ is valid for $1/2 < M < 1$. Our equation is now greatly simplified:

$$-\cos(M\pi)\left(\int_{|a|}^{\infty} r^{2M}|v(r)|^2dr + \int_{|a|}^{\infty} r^{2M}|v(-r)|^2dr + 2\frac{|a|^{2M+1}w(|a|)^2}{2M+1})\right)$$

$$+\Re e(\lambda e^{\mp i\frac{M\pi}{(2M+2)}})\left(\int_{|a|}^{\infty}|v(r)|^2dr + \int_{-\infty}^{-|a|}|v(r)|^2dr + 2|a|w(|a|)^2\right) = 0 \qquad (6.20)$$

As $1/2 < M < 1$, $-\cos(M\pi)$ is positive and our equation is of the form required. If we write $\lambda = \alpha + i\beta$ this allows us to state:

$$\Re e(\lambda e^{\mp i\frac{M\pi}{(2M+2)}}) = \alpha\cos\left(\frac{M\pi}{2M+2}\right) \pm \beta\sin\left(\frac{M\pi}{2M+2}\right) < 0 \qquad (6.21)$$

Which is the inequality we claimed to be able to derive.

For $1/2 < M < 1$, $\frac{\pi}{6} < \frac{M\pi}{(2M+2)} < \frac{\pi}{4}$, so both the sin and cos functions are positive. Therefore

$$\alpha < 0 \qquad (6.22)$$

We can further restrict λ. We know

$$\tan(\frac{M\pi}{(2M+2)}) < \frac{|\alpha|}{|\beta|} \qquad (6.23)$$

and using $\tan(\phi) = \cot(\frac{\pi}{2} - \phi)$

$$\tan(\frac{\pi}{2} - \frac{M\pi}{(2M+2)}) > \frac{|\beta|}{|\alpha|} \qquad (6.24)$$

if we call $a = \arg(|\alpha| + i|\beta|)$ we can say

$$\frac{\pi}{2} - \frac{M\pi}{(2M+2)} > a \qquad (6.25)$$

However $|\arg(\lambda)| = \pi - a$ and we can say

$$|\arg(\lambda)| > \frac{2M+1}{2M+2}\pi \qquad (6.26)$$

So for $1/2 < M < 1$:

$$|\arg(\lambda)| > \frac{2\pi}{3} \qquad (6.27)$$

6.2.2 The Integral Equation

We have the T-Q equation:

$$T(E,l)Q(E,l) = \omega^{-(l+1/2)}Q(\omega^{-2}E,l) + \omega^{(l+1/2)}Q(\omega^{2}E,l) \tag{6.28}$$

Dividing by $\omega^{-(l+1/2)}Q(\omega^{-2}E,l)$ and setting

$$a(E) = \omega^{2l+1}\frac{Q(\omega^{2}E,l)}{Q(\omega^{-2}E,l)} \tag{6.29}$$

we can write:

$$a(E_k) + 1 = 0, \tag{6.30}$$

where the E_k are the zeros of $Q(E,l)$. It is also true that $a(-e_j)+1=0$, when $-e_j$ are the zeros of $T(E,l)$.

We at first take $M > 1$, later we will continue our equation, in M, to to allow us to discuss the eigenvalues for $M < 1$. For $M > 1$ the order of $Q(E,l)$ is less than one, we can use the Hadamard representation for this function (C.3).

$$Q(E,l) = Q(0,l)\prod_{k=1}^{\infty}\left(1-\frac{E}{E_k}\right) \tag{6.31}$$

We can then write:

$$\ln a(E) = \frac{i\pi(2l+1)}{M+1} + \sum_{k=1}^{\infty} F(E/E_k) \tag{6.32}$$

where

$$F(E) = \ln\frac{1-\omega^{2}E}{1-\omega^{-2}E} \tag{6.33}$$

Note that the logarithmic derivative $\partial_E \ln(1+a(E))$ has a simple pole at each eigenvalue E_k, with residue one. These are the only poles of this function on the positive real axis. This, combined with the fact that $F(E)$ is holomorphic in an area surrounding the positive real axis, allows us to write $\ln(a)$ as a contour integral.

$$\ln a(E) = \frac{i\pi(2l+1)}{M+1} + \int_C \frac{dE'}{2\pi i}F(E/E')\partial_{E'}\ln(1+a(E')) \tag{6.34}$$

The contour must encircle the points in an anti-clockwise direction. Care must also be taken to ensure we do not catch any other poles of $\partial_E \ln(1+a(E))$. For this

reason, we choose our contour to come from $+\infty$ to zero, just above the real axis, circle around the origin and go back out to $+\infty$, just below the real axis.

We make the variable change $E^{(M+1)/2M} = re^{\theta}$. Abusing the notation slightly we shall write $a(\theta) \equiv a(E(\theta))$. This allows us to state:

$$\begin{aligned} \ln a(\theta) = & \frac{i\pi(2l+1)}{M+1} \\ & - \int_{-\infty}^{\infty} \frac{d\theta'}{2\pi i} F(e^{2M(\theta-\theta'-i\epsilon)/(M+1)} \partial_{\theta'} \ln(1+a(\theta'+i\epsilon)) \\ & + \int_{-\infty}^{\infty} \frac{d\theta'}{2\pi i} F(e^{2M(\theta-\theta'+i\epsilon)/(M+1)} \partial_{\theta'} \ln(1+a(\theta'-i\epsilon)) \end{aligned} \tag{6.35}$$

We integrate by parts and use the fact that $a^*(\theta) = a^{-1}(\theta^*)$ to obtain:

$$\begin{aligned} \ln a(\theta) = & \frac{i\pi(2l+1)}{M+1} \\ & + \int_{-\infty}^{\infty} d\theta' R(\theta-\theta') \ln(1+a(\theta')) \\ & -2i \int_{-\infty}^{\infty} d\theta' R(\theta-\theta') \Im m \ln(1+a(\theta'-i\epsilon)) \end{aligned} \tag{6.36}$$

Where

$$R(\theta) = \frac{i}{2\pi} \partial_{\theta} F(e^{2M\theta/(M+1)}) \tag{6.37}$$

Now we notice that the integrals are the convolution of two functions and take the Fourier transform of both sides.

$$\begin{aligned} F[ln(a)](k) = & \frac{i\pi(2l+1)}{M+1} \frac{\delta(k)}{1-2\pi F[R]} \\ & -4i\pi \frac{F[R] F[\Im m \ln(1+a(\theta'-i\epsilon))]}{1-2\pi F[R]} \end{aligned} \tag{6.38}$$

We are only going to need to calculate the Fourier transform of $R(\theta)$. This can be done using the following two formula:

$$i\partial_{\theta} \ln \frac{\sinh(h\theta + i\pi\tau)}{\sinh(h\theta - i\pi\tau)} = \frac{2h \sin(2\pi\tau)}{\cosh(2h\theta) - \cos(2\pi\tau)} \tag{6.39}$$

and

$$\int \frac{d\theta}{2\pi} e^{-ik\theta} \frac{2h \sin(2\pi\tau)}{\cosh(2h\theta) - \cos(2\pi\tau)} = \frac{\sinh((1-2\tau)\frac{\pi k}{2h})}{\sinh(\frac{\pi k}{2h})} \tag{6.40}$$

So

$$F[R] = \frac{1}{2\pi} \frac{\sinh(\frac{\pi}{2M}(M-1))}{\sinh(\frac{\pi}{2M}(M+1))} \tag{6.41}$$

We can then write:

$$F[ln(a)](k) = \frac{i\pi(2l+1)}{M+1}\frac{\delta(k)\sinh(\frac{\pi k}{2M}(M+1))}{\sinh(\frac{\pi k}{2M}(M+1)) - \sinh(\frac{\pi k}{2M}(M-1))}$$
$$-2i\frac{\sinh(\frac{\pi k}{2M}(M-1)}{\sinh(\frac{\pi k}{2M}(M+1)) - \sinh(\frac{\pi k}{2M}(M-1))}$$
$$\times F[\Im m \ln(1+a(\theta' - i\epsilon))] \tag{6.42}$$

We take the inverse Fourier transform:

$$\ln(a(\theta)) = i\pi(l+\frac{1}{2}) - imre^{\theta} + \int_{C_1} d\theta' \varphi(\theta-\theta')\ln(1+a(\theta'))$$
$$-\int_{C_2} d\theta' \varphi(\theta-\theta')\ln(1+a^{-1}(\theta')) \tag{6.43}$$

Where

$$\varphi(\theta) = \int_{-\infty}^{\infty} e^{ik\theta}\frac{\sinh(\frac{\pi}{2}\frac{1-M}{M}k)}{2\cosh(\frac{\pi}{2}k)\sinh(\frac{\pi}{2M}k)}\frac{dk}{2\pi} \tag{6.44}$$

This function is recognisable as the Sine-Gordon S-matrix, [4], [41].

The contours C_1 and C_2, run from $-\infty$ to ∞ just below and just above the real axis, respectively. The term proportional to e^{θ} comes from a zero mode from a pole in $\frac{1}{1-R}$ and

$$m = \pi^{1/2}\Gamma(1+\frac{1}{2M})/\Gamma(\frac{3}{2}+\frac{1}{2M}) \tag{6.45}$$

The value of r is arbitrary, but we take

$$r = (2M+2)\Gamma\left(\frac{M}{M+1}\right)^{(M+1)/M} \tag{6.46}$$

to match with the conventions of [4], [18].

Finally we set $f(\theta) = \ln(a(\theta))$, to obtain:

$$f(\theta) = i\pi(l+\frac{1}{2}) - ib_0e^{\theta} + \int_{C_1} d\theta' \varphi(\theta-\theta')\ln(1+e^{f(\theta')})$$
$$-\int_{C_2} d\theta' \varphi(\theta-\theta')\ln(1+e^{-f(\theta')}) \tag{6.47}$$

This non-linear integral equation allows us to find the zeros of $Q(E,l)$, that is the energy levels of the radial problem, with high accuracy. We search along the real θ axis for values of θ where the 'counting function' $f(\theta) = i\pi(2n+1)$. The real θ axis gives us the values of E that are real and positive. We know that all the zeros

of $Q(E,l)$ lie on the positive real E axis. We also know all the zeros of $T(E,l)$ lie away from the positive real E axis. We can then be confident, that along the real θ axis, we have an energy level of the radial problem if and only if $f(\theta) = i\pi(2n+1)$ and that we will not miss any of the energy levels.

If we are to understand the change in connectivity of the energy levels, we need to find the zeros of $T(E,l)$, that is the energy levels of the transverse problem. The zeros of $T(E,l)$ are still those values of θ where $f(\theta) = i\pi(2n+1)$, but away from the real θ axis. We know the zeros of $T(E,l)$ are on or near the negative E axis. As we are interested in the real eigenvalues, the line we should be looking along in the complex-θ plane is $\Im m\theta = \pi(M+1)/2M$.

We cannot naively look along this line because of the poles in $\varphi(\theta)$. We must instead take the 'second determination' of the NLIE. In the next section, we shall see how this is done.

6.3 Second Determination

We wish to be able to find those values of θ, such that $f(\theta) = i\pi(2n+1)$ along the line $\Im m\theta = \pi(M+1)/2M$. The poles in the kernel $\varphi(\theta)$ closest to the real θ axis are at $\theta = \pm i\pi$ and $\pm i\pi/M$. Therefore outside the strip $|\Im m(\theta)| < \min(\pi, \pi/M)$, we will pick up some residue terms in our expression. For $M > 1$, $1 > \frac{M+1}{2M} > \frac{1}{M}$, while for $M < 1$, $\frac{1}{M} > \frac{M+1}{2M} > 1$. Thus we will only need to cross one of the poles in each case.

For $M > 1$ as we increase $\Im m(\theta)$, the pole at $\theta = -i\pi/M$ crosses first C_1 and then C_2. We assume the contours are infinitesimally close to the real axis, so we do not need to consider cases when the pole has crossed only C_1. The residue of $\varphi(\theta)$ at the pole is $\frac{1}{2\pi i}$. This makes the residue we must add:

$$-\ln(1+e^{f(\theta-i\pi/M)}) + \ln(1+e^{-f(\theta-i\pi/M)}) = -f(\theta - i\pi/M) \tag{6.48}$$

If we write

$$\varphi_{II}(\theta) = \varphi(\theta) - \varphi(\theta - i\pi/M) = \frac{2i\cos(\frac{\pi}{2M})\sinh(\theta - \frac{i\pi}{2M})}{\pi(\cosh(2\theta - \frac{i\pi}{M}) - \cos(\frac{\pi}{M}))}, \tag{6.49}$$

we are lead to:

$$f(\theta) = -i(1-e^{-i\pi/M})mre^{\theta} + \int_{C_1} d\theta' \varphi_{II}(\theta-\theta')\ln(1+e^{f(\theta')}) - \int_{C_2} d\theta' \varphi_{II}(\theta-\theta')\ln(1+e^{-f(\theta')}). \quad (6.50)$$

This revised NLIE is valid in the strip $\pi/M < \theta < \pi$, which contains the region we are interested in.

Next we must consider $M < 1$. In this case the pole of $\varphi(\theta)$ is at $-i\pi$ and the residue is $\frac{-1}{2\pi i}$. This makes the extra term $+f(\theta - i\pi)$. If in this case we write:

$$\varphi_{II}(\theta) = \varphi(\theta) + \varphi(\theta - i\pi) = \frac{M\sin(\pi M)}{\pi(\cosh(2M\theta - i\pi M) - \cos(\pi M))} \quad (6.51)$$

our NLIE for $M < 1$ is:

$$f(\theta) = 2\pi i(l+\tfrac{1}{2}) + \int_{C_1} d\theta' \varphi_{II}(\theta-\theta')\ln(1+e^{f(\theta')}) - \int_{C_2} d\theta' \varphi_{II}(\theta-\theta')\ln(1+e^{-f(\theta')}) \quad (6.52)$$

This holds for $\pi < \theta < \pi/M$.

We define

$$\gamma := \theta - i\pi(M+1)/2M \quad (6.53)$$

and

$$g(\gamma) := f(\gamma + i\pi(M+1)/2M) \quad (6.54)$$

Abusing the notation slightly again, we shall sometimes write g as a function of E, $g(E) = f(-E)$.

$$E = (re^{\gamma})^{2M/(M+1)} \quad (6.55)$$

If we write

$$\psi(\gamma) = \varphi_{II}(i\pi(M+)/2M + \gamma) \quad (6.56)$$

we can write an expression for $g(\gamma)$ on the strip $|\Im m\gamma| < \frac{\pi}{2}\left|\frac{M-1}{M}\right|$.

For $M > 1$:

$$g(\gamma) = 2i\sin(\tfrac{\pi}{2M})mre^{\gamma} + \int_{C_1} d\theta' \psi(\gamma-\theta')\ln(1+e^{f(\theta')}) - \int_{C_2} d\theta' \psi(\gamma-\theta')\ln(1+e^{-f(\theta')}) \quad (6.57)$$

For $M < 1$:

$$\begin{aligned} g(\gamma) = \; & 2\pi i(l+\tfrac{1}{2}) + \int_{C_1} d\theta' \psi(\gamma-\theta') \ln(1+e^{f(\theta')}) \\ & - \int_{C_2} d\theta' \psi(\gamma-\theta') \ln(1+e^{-f(\theta')}) \end{aligned} \tag{6.58}$$

This gives us the function $g(\gamma)$ in terms of the function $f(\theta)$ along the contours C_1 and C_2, where the first determination holds. By searching along the real γ axis and searching for points where $g(\gamma) = i\pi(2n+1)$, we are able to locate the zeros of $T(E,l)$.

However, we are attempting an analytical understanding of the pairing off phenomena. For this we will need to consider the large-E asymptotic of our function.

6.4 Asymptotic Of The Non-Linear Integral Equation

6.4.1 Leading Asymptotic

We are attempting to extract the large E, that is large γ, asymptotic for the non-linear integral equation $g(\gamma)$. The kernel function $\psi(\gamma)$ is peaked around $\gamma = 0$. For this reason the dominant contribution from the integrals comes when $\Re e\gamma \approx \Re e\theta'$. For large θ' the leading approximation of $f(\theta')$ is found by dropping the integrals, giving us $f(\theta') \sim i\pi(l+1) - imre^{\theta'}$. From this it follows that for large θ', $\ln(1+e^{f(\theta')}) \to 0$ on C_1 and $\ln(1+e^{-f(\theta')}) \to 0$ on C_2. We can therefore find the leading large-γ asymptotic by dropping the integrals in (6.57), (6.58). They are:

$$M > 1: \qquad g(\gamma) \sim 2i\sin(\tfrac{\pi}{2M}) m E^{\frac{M+1}{2M}} \tag{6.59}$$

$$M < 1: \qquad g(\gamma) \sim 2i\pi(l+\tfrac{1}{2}) \tag{6.60}$$

For $M = 1$, we must take a little more time to consider what is going on. The T-Q equation in this case is 'renormalised' to $T(E)Q(E) = \omega^{-l-1/2+E/2}Q(\omega^{-2}E) + \omega^{l+1/2-E/2}Q(\omega^2 E)$. This has a knock on effect on the the function $a(E)$, which becomes $a(E) = \omega^{2l+1-E}Q(\omega^2 E)/Q(\omega^{-2}E)$. But for $M = 1$, we have $\omega = i$, so the Q terms cancel and we are left with $f(\theta) = \frac{i\pi}{2}(2l+1-E)$. So:

$$M = 1: \qquad g(\gamma) = \frac{i\pi}{2}(2l+1-E) \tag{6.61}$$

From the $M = 1$ case we can immediately recover the energy levels of this case, by setting $\gamma = i\pi(2n+1)$. We remember that E is the *negated* value of the energy of the transverse problem and that the system is symmetric under $l \to -l-1$, to obtain:

$$E_m = 2m - (-1)^m 2l + 1 \tag{6.62}$$

For $M > 1$ we can similarly recover the WKB result:

$$E_n = \left(\frac{\sqrt{\pi}\Gamma(\frac{3}{2} + \frac{1}{2M})(n+\frac{1}{2})}{\sin(\frac{\pi}{2M})\Gamma(1+\frac{1}{2M})} \right)^{2M/(M+1)} \tag{6.63}$$

For $M < 1$ though, the leading $g(\gamma)$ approximation is a constant and we can gain no insight into the energy levels. From this we can see the break down in the WKB approximation, for $M < 1$, is caused by the difference in the second determination.

We can see then, that our approximation was too harsh and we have failed to capture a lot of the behaviour. It is also not clear from our approximation how the function $g(\gamma)$ moves smoothly from the $M > 1$ region to $M < 1$. We know that for $M < 1$, the energy levels are radically altered by varying l, whereas for $M \geq 1$ they are relatively stable. One way of viewing our problem is that we are trying to understand this change. Although from this leading approximation which can see there is a large difference between the regimes, we cannot yet see how this happens smoothly, nor why it effects the connectivity of the eigenvalues.

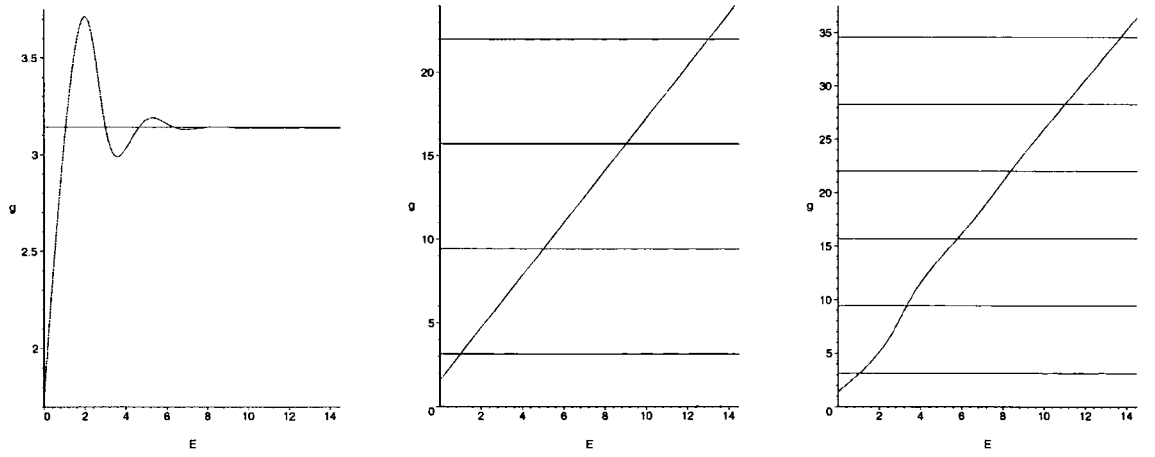

6.4.1a: $M = 0.8$ 6.4.1b: $M = 1$ 6.4.1c: $M = 1.2$

Figure 6.4.1: $\Im m\, g(E)$ from the nonlinear integral equation. In all three cases, $l = -0.001$. The horizontal lines show the 'quantisation levels' $g = (2n+1)\pi i$.

Figure (6.4.1) shows us a numerical plot of $\Im m\, g(E)$ in the various regimes. We can see that for $M < 1$, the behaviour is significantly changed. There is, even for the real energy levels, no obvious way to allocate unique WKB, Bohr-Sommerfeld numbers to the energy levels. We clearly need to take a more detailed look at the asymptotic.

6.4.2 A Better Approximation

To obtain a better approximation, we can use the steepest descent treatment on $g(\gamma)$. We expand the kernels $\psi(\gamma - \theta')$ for large $\gamma - \theta'$. To take maximum effect of the fact the the functions $\ln(1 + e^{f(\theta')})$ and $\ln(1 + e^{-f(\theta')})$ decay as $\Re e\theta' \to 0$ along the relevant contours, we shift the contours to the value of $\Im m\theta'$ where this happens the fastest. As, for large θ', $f(\theta') \sim i\pi(l + \frac{1}{2}) - imre^{\theta}$, this means shifting C_1 down so that $\Im m\theta' = -\pi/2$ and C_2 up so that $\Im m\theta' = \pi/2$. In doing so we cross the poles in the kernel function at $\gamma = \pm\frac{i\pi}{2}\frac{|M-1|}{M}$, picking up residue terms. These residue terms are 'beyond all orders' and as we will see, very important to our understanding of the phenomena we are attempting to understand. There is one other subtly we must be careful about. Namely that as $f(\theta')$ is only defined on the strip $|\Im m(\theta')| < \min(\pi, \pi/M)$, we cannot shift the contours outside this strip. For $M < 2$ we will not be doing this, so we restrict our interest to $M < 2$.

The expansion of the kernel function is:

$$M > 1: \qquad \psi(\gamma) = \textstyle\sum_{n=1}^{\infty}(-1)^{n+1}\frac{2}{\pi}\cos(\frac{\pi}{2M}(2n-1))e^{-(2n+1)\gamma} \tag{6.64}$$

$$M < 1: \qquad \psi(\gamma) = \textstyle\sum_{n=1}^{\infty}(-1)^{n}\frac{2M}{\pi}\sin(\pi M n)e^{-2Mn\gamma} \tag{6.65}$$

If we call $\tilde{C}_1$ and $\tilde{C}_2$ the contours along $\Im m(\theta') = -\pi/2$ and $\Im m(\theta') = \pi/2$ respectively, we can, for $1 < M < 2$, write:

$$\begin{aligned} g(\gamma) = \; & 2i\sin(\tfrac{\pi}{2M})mre^{\gamma} + \textstyle\int_{\tilde{C}_1} d\theta'\psi(\gamma-\theta')\ln(1+e^{f(\theta')}) \\ & - \textstyle\int_{\tilde{C}_2} d\theta'\psi(\gamma-\theta')\ln(1+f^{-f(\theta')}) \\ & + \ln(1+e^{f(\gamma-\frac{i\pi}{2}\frac{|M-1|}{M})}) - \ln(1+e^{-f(\gamma+\frac{i\pi}{2}\frac{|M-1|}{M})}) \end{aligned} \tag{6.66}$$

We do the expansion and write g as a function of E.

$$g(E) \sim 2i\sin(\tfrac{\pi}{2M})mE^{\frac{M+1}{2M}}$$
$$+i\sum_{n=1}^{\infty}(-1)^{n+1}\tfrac{2b_n}{\pi}\cos(\tfrac{\pi}{2M}(2n-1))E^{-\frac{M+1}{2M}(2n+1)} - g_{\text{nonpert}}(E) \tag{6.67}$$

Where

$$ib_n = \int_{C_1} d\theta'(re^{\theta})^{2n-1}\ln(1+e^{f(\theta')}) - \int_{C_2} d\theta'(re^{\theta})^{2n-1}\ln(1+e^{-f(\theta')}) \tag{6.68}$$

and

$$g_{\text{nonpert}}(E) = \ln\left(\frac{1+e^{-f(\gamma+\frac{i\pi}{2}\frac{|M-1|}{M})}}{1+e^{f(\gamma-\frac{i\pi}{2}\frac{|M-1|}{M})}}\right) \tag{6.69}$$

The contours in b_n are the unshifted ones as we can, after the expansion, shift the contours back without encountering any poles.

For $\frac{1}{2} < M < 1$ the result is:

$$g(E) \sim 2i\pi(l+\tfrac{1}{2})$$
$$+i\sum_{n=1}^{\infty}(-1)^{n}\tfrac{2Mc_n}{\pi}\sin(\pi Mn)E^{-(M+1)n} + g_{\text{nonpert}}(E) \tag{6.70}$$

with

$$ic_n = \int_{C_1} d\theta'(re^{\theta})^{2Mn}\ln(1+e^{f(\theta')}) - \int_{C_2} d\theta'(re^{\theta})^{2Mn}\ln(1+e^{-f(\theta')}) \tag{6.71}$$

and g_{nonpert} is as before. Note, that although the non-perturbative term is the same, it contributes with opposite sign. Note also, that the definition of g_{nonpert} contains modulus signs, so the numerator is always evaluated above the real axis and the denominator is always evaluated below.

From the ODE/IM correspondence we have closed form expressions for both b_1 and c_1. They are:

$$b_1 = \pi^{3/2}\frac{\Gamma(\frac{1}{2}+\frac{1}{2M})}{\Gamma(\frac{1}{2M})}((l+\frac{1}{2})^2 - M - 1) \tag{6.72}$$

$$c_1 = -\frac{2^{2M+1}\pi}{M}\frac{\cos(\pi M)\Gamma(M+1)\Gamma(-2M-1)\Gamma(M+l+\frac{3}{2})}{\Gamma(-M)\Gamma(M+l\frac{1}{2})} \tag{6.73}$$

Let us now consider the term g_{nonpert}. As $f(\gamma-\frac{i\pi}{2}\frac{|M-1|}{M}) = -f^*(\gamma+\frac{i\pi}{2}\frac{|M-1|}{M})$, we can write:

$$g_{\text{nonpert}}(E) = 2i\arg\left(1+e^{-f(\gamma+\frac{i\pi}{2}\frac{|M-1|}{M})}\right) \tag{6.74}$$

Using the leading expansion for $f(\theta)$, we obtain:

$$g_{\text{nonpert}}(E) \sim$$
$$2i \arg\left(1 + e^{-i\pi(l+\frac{1}{2})+im\cos\frac{\pi|M-1|}{2M}E^{\frac{M+1}{2M}}} e^{-m\sin\frac{\pi|M-1|}{2M}E^{\frac{M+1}{2M}}}\right) \tag{6.75}$$

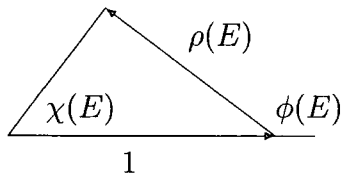

Figure 6.2: The trigonometry of $g_{\text{nonpert}}(E)$.

We can understand this relation using trigonometry. $g_{\text{nonpert}}(E)$ is approximately $2i\chi(E)$ where $\chi(E)$ is the angle shown in figure (6.2). The angle $\phi(E)$ and the length $\rho(E)$ are given by:

$$\phi(E) = -\pi(l+\tfrac{1}{2}) + m\cos\tfrac{\pi|M-1|}{2M}E^{\frac{M+1}{2M}} \tag{6.76}$$
$$\rho(E) = e^{-m\sin\frac{\pi|M-1|}{2M}E^{\frac{M+1}{2M}}} \tag{6.77}$$

Now, if $M \neq 1$, $\rho(E)$ is always less than 1 and for increasing E, $1+\rho e^{i\phi}$ traces a diminishing spiral about the point 1. For $M < 1$ this captures the behaviour of $g_{\text{nonpert}}(E)$.

From here it is also clear why $g_{\text{nonpert}}(E)$ is not a perturbative term. In (6.67) and (6.70), the expansion parameters are, respectively, $\varepsilon := E^{-\frac{M+1}{2M}}$ and $\eta := E^{-(M+1)}$. In terms of these parameters, then, our function $\rho(E)$ is either $\exp(-m\sin(\frac{|M-1|}{M})/\varepsilon)$ or $\exp(-m\sin(\frac{|M-1|}{M})/\eta^{\frac{1}{2M}})$, which are clearly not terms that come from the perturbative expansion.

Alternatively, if we leave E finite and look at $M \approx 1$, then $\rho(E) \approx 1$ and $\chi(E) \approx \phi(E)/2$, so:

$$g_{\text{nonpert}}(E) \approx -i\pi(l+\frac{1}{2}) + im\cos\frac{\pi|M-1|}{2M}E^{\frac{M+1}{2M}} \tag{6.78}$$

which is exactly the behaviour that smooths transition between the regimes.

In figure (6.3) we can see our approximation compared with the numerical results. We take in each of them the leading approximation and then add, a) the first perturbative term, b) the leading approximation to $g_{\text{nonpert}}(E)$ and c) both. We can

see, that even this low down the energy scale, our approximation is very good. The extra crosses in the graph showing both terms, comes from a perturbative error. We see now why it is important to have both the perturbative term and the non-perturbative term. The perturbative term, for $M < 1$ only picks up the lowest energy level, while the non-perturbative term governs the pairing off the higher energy levels.

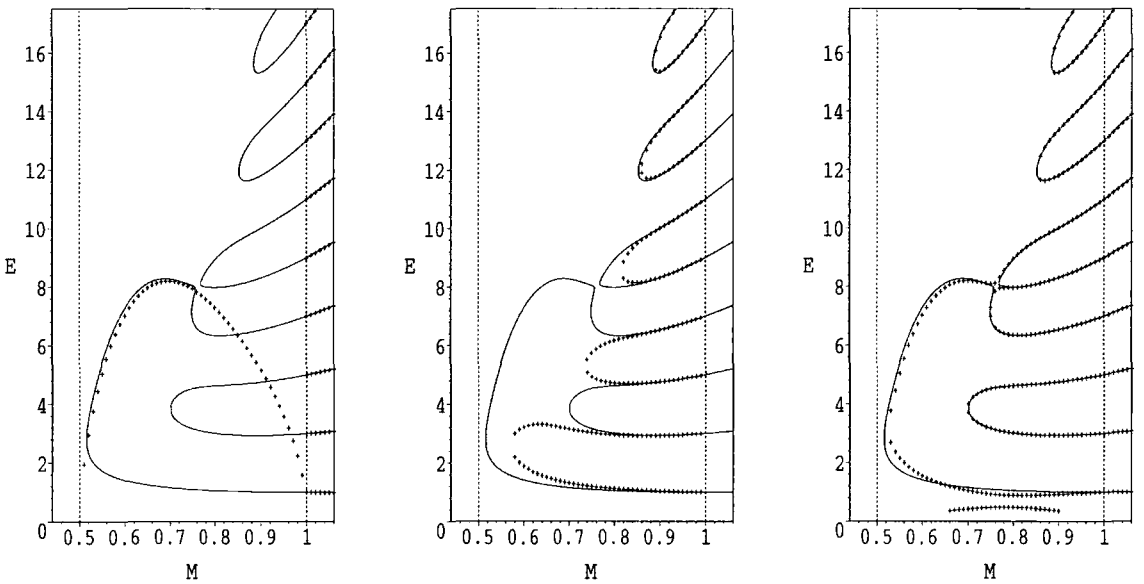

6.3a: Perturbative term

6.3b: Nonperturbative term

6.3c: Both terms

Figure 6.3: Different approximation schemes for the energy levels (small crosses) compared with the exact levels (continuous lines), for $l = -0.001$.

Most sensitive to the approximation, is the area just where the change in connectivity is taking place. Figure (6.4) takes a closer look at this. We can see there is a slight error. It is not surprising that this is where the error is worse, the recombination of the levels makes the locations of the eigenvalues particularly sensitive to errors in the value of $g(E)$.

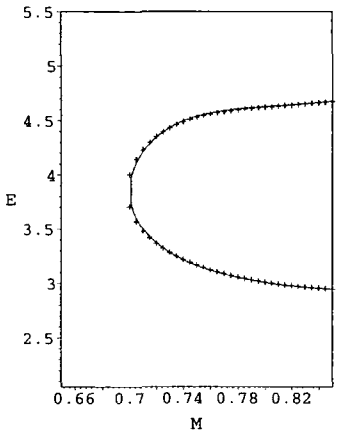

6.4a: First merging

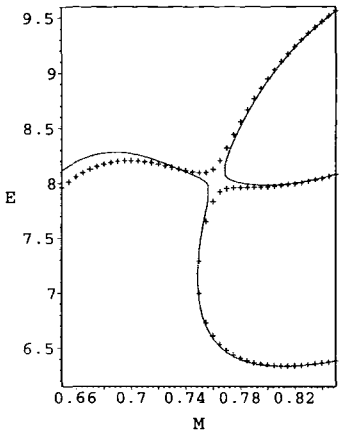

6.4b: Second merging

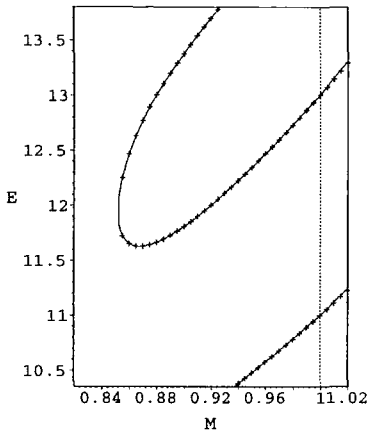

6.4c: Third merging

Figure 6.4: The perturbative-plus-nonperturbative approximation for $l = -0.001$ (small crosses) compared with the exact levels (continuous lines) near the first three level mergings shown on figure 6.3c.

Explicitly the crosses are those points at which $g_{\text{approx}}(E) = i\pi(2n+1)$, where

$$M > 1: \quad g_{\text{approx}}(E) = 2im\sin(\frac{\pi}{2M})E^{\frac{M+1}{2M}} + \frac{i\pi^{3/2}(6(l+\frac{1}{2})^2+M+1)}{3\Gamma(\frac{\pi}{2M})\Gamma(\frac{1}{2}-\frac{1}{2M})}E^{-\frac{M+1}{2M}} - g_{\text{nonpert}}(E) \tag{6.79}$$

$$M < 1: \quad g_{\text{approx}}(E) = 2i\pi(l+\frac{1}{2}) + \frac{i\pi^{3/2}\Gamma(M+\frac{3}{2}+l)}{\Gamma(M+\frac{3}{2})\Gamma(-M)\Gamma(-M+\frac{1}{2}+l)}E^{-(M+1)} + g_{\text{nonpert}}(E) \tag{6.80}$$

with $g_{\text{nonpert}}(E)$ given by the leading approximation, (6.75), and m by (6.45). We can use the above expressions to gain some understanding of the change in connectivity of the level merging, high up the energy scale.

6.5 An Analytic Understanding Of The Level Merging

As we will wish to study the level merging high up the energy scale, we must also look close to $M = 1$, as this is where we expect the eigenvalues to pair off. To do this set $\epsilon = 2M - 2$ and consider ϵ small and negative, with E fixed and large. We work from (6.80) and wish to obtain the quantisation condition in this limit. For this we

will need to calculate the limiting from of the second term in equation (6.80):

$$I = \frac{i\pi^{3/2}\Gamma(M+\frac{3}{2}+l)}{\Gamma(M+\frac{3}{2})\Gamma(-M)\Gamma(-M+\frac{1}{2}+l)}E^{-(M+1)}. \tag{6.81}$$

Now $\Gamma(x+\epsilon) \approx \Gamma(x) + \epsilon\Gamma(x)\psi(x)$ where $\psi(x) = \Gamma'(x)/\Gamma(x)$ is the digamma function, [1], which is finite for $x > 0$ and has poles for x a non-positive integer. This means some care must be taken with the denominator gamma function $\Gamma(-M+\frac{1}{2}+l)$. We have:

$$\Gamma(-\frac{\epsilon}{2}-\frac{1}{2}+l) = \Gamma(l-\frac{1}{2})\Big(1-\frac{\epsilon}{2}\psi(l-\frac{1}{2})\Big) \tag{6.82}$$

In this expression, both the gamma and digamma function on the right hand side, diverge for $l \to \pm\frac{1}{2}$. As we are interested in the area $l \sim 0$ we will only consider this region. We are in fact considering a reciprocal gamma function, so as $l \to \pm\frac{1}{2}$, the term we are considering tends to zero. This term is subleading order, when $l \neq= 0$, thus the fact that it becomes small quicker for non-zero values of l is not important. There is one other problematical gamma function, we shall treat this in a different way:

$$\frac{1}{\Gamma(-1-\epsilon/2)} = \frac{-1-\epsilon/2}{\Gamma(-\epsilon/2)} \approx (1+\epsilon/2)\frac{\epsilon}{2} \tag{6.83}$$

Where we have used the series expansion from [1]. We can now write down the first order approximation for I:

$$I \approx \frac{i\pi^{3/2}\Gamma(\frac{5}{2}+l)}{\Gamma(\frac{5}{2})\Gamma(l-\frac{1}{2})}E^{-2}\frac{\epsilon}{2} \tag{6.84}$$

Now using $\Gamma(z+1) = z\Gamma(z)$ and $\Gamma(3/2) = \pi^{1/2}/2$ we can write:

$$I \approx -i\pi\frac{2}{3}\Big(\frac{3}{2}+l\Big)\Big(l^2-\frac{1}{4}\Big)|\epsilon|E^{-2} \tag{6.85}$$

Our quantisation condition then becomes:

$$g_{\text{approx}}(E) = i\pi(2k+1) = i\pi 2(l+\tfrac{1}{2}) \quad -i\pi\frac{2}{3}\Big(\frac{3}{2}+l\Big)\Big(l^2-\frac{1}{4}\Big)|\epsilon|E^{-2} \\ +g_{\text{nonpert}} \tag{6.86}$$

for $k \in \mathbb{Z}$. Rearranging we obtain:

$$\chi(E) = \pi k - \pi l + \frac{\pi}{3}\Big(\frac{3}{2}+l\Big)\Big(l^2-\frac{1}{4}\Big)|\epsilon|E^{-2} \tag{6.87}$$

where $\chi(E) = \frac{1}{2i} g_{\text{nonpert}}$, is the angle shown in figure 6.2.

In the same approximation, we have:

$$\rho(E) = e^{-\frac{\pi^2}{8}|\epsilon|E} \tag{6.88}$$

$$\phi(E) = -\pi(l + \frac{1}{2}) + \frac{\pi}{2}E + \frac{\pi}{8}|\epsilon|E\ln(E). \tag{6.89}$$

As $\chi(E)$ is always between $-\frac{\pi}{2}$ and $\frac{\pi}{2}$, for small l, all the solutions of (6.87) occur when $k = 0$. When l is non-zero and E is large we may drop the last term and the condition reduces to $\chi(E) = -\pi l$. Figure 6.5 shows us this situation. Given that $|\epsilon|$ is small we can see that, as we increase E, $\phi(E)$ behaves as a fast mode, and $\rho(E)$ as a slow mode. The point $1 + \rho e^{i\phi}$, traces a circle of roughly constant radius, this radius slowly decreasing as E increases. Eigenvalues occur when this point crosses the ray from the origin with argument $-\pi l$. These rays are shown on the diagram by the dashed lines.

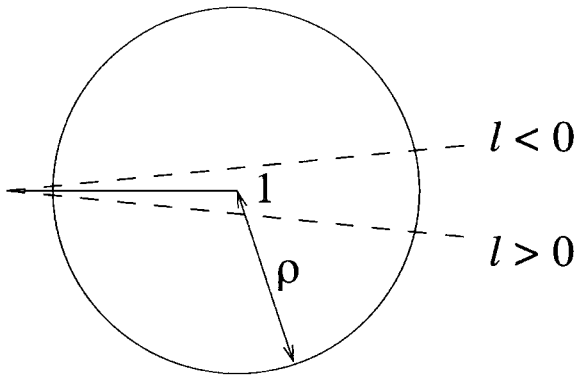

Figure 6.5: The approximate quantisation condition for $l \neq 0$.

When ρ is small enough, the point $1 + \rho e^{i\phi}$, will no longer intersect the rays, for real ϕ. This shows us the eigenvalues have become complex. The critical value of ρ is $|\sin(\pi l)|$. Thus the merging of the energy levels happens asymptotically as:

$$E = -\frac{8\ln|\sin(\pi l)|}{\pi^2|\epsilon|}. \tag{6.90}$$

Figures 6.6 and 6.7 shows how the prediction compares to the actual results, low down the scale.

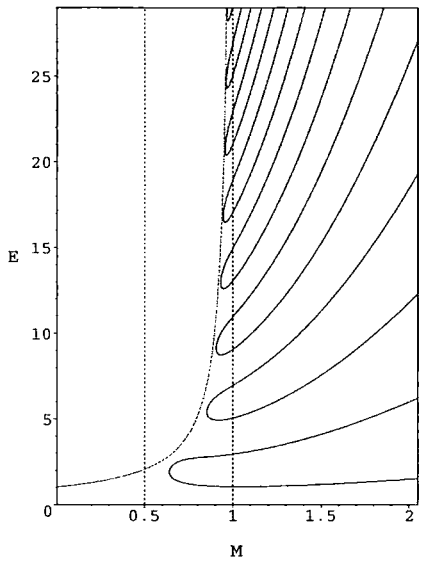

$l = -0.025$

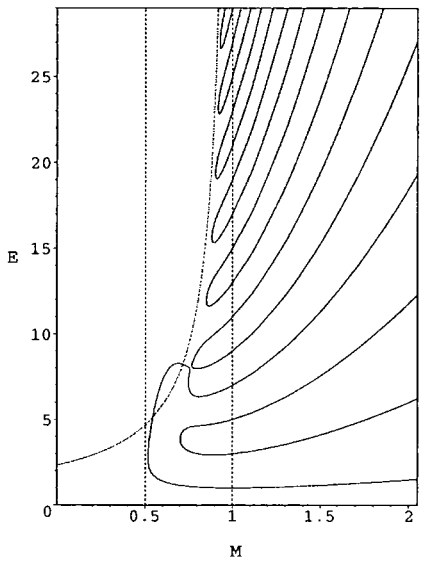

$l = -0.001$

Figure 6.6: The Energy Levels With The Predicted Value Of M For Merging To Occur

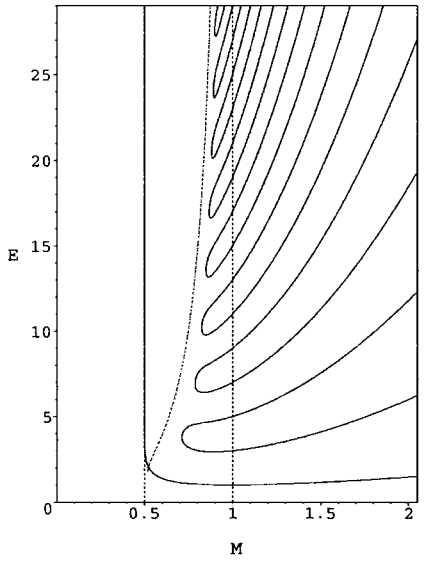

$l = 0$

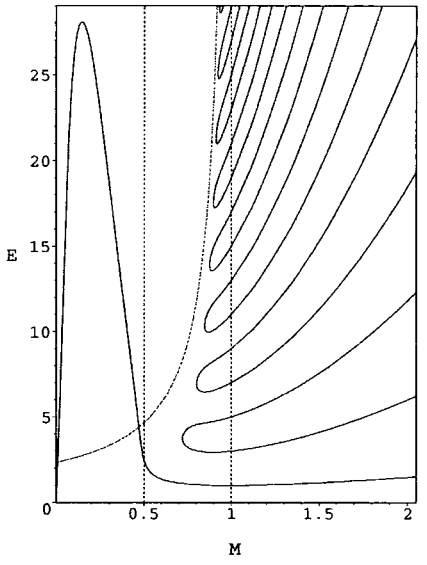

$l = 0.001$

Figure 6.7: The Energy Levels With The Predicted Value Of M For Merging To Occur

By considering the fast mode, ϕ, we can also predict which eigenvalues pair off high up the energy spectrum. If E is kept approximately fixed and we increase $|\epsilon|$,

that is decrease M, ρ decreases, while ϕ remains unchanged. We can see then that it is the eigenvalues associated with neighbouring crossings of the ray $\arg(z) = -\pi l$, which merge. If we now increase E, from zero, the angle ϕ starts from $-\frac{\pi}{2} - \pi l$, that is below the real axis. Hence, when $l < 0$, our point crosses the real axis, before crossing our ray, *twice* before coming back below the real axis. It is then the first and second, third and fourth, etc. energy levels that pair off. A fact we have already seen numerically and can now see analytically.

We should emphasise here that we have not predicted that the first and second eigenvalues pair off. We have predicted that far up the energy scale, it is the $(2n-1)$'th and $2n$'th eigenvalues that pair off. The approximation we have taken is only valid for large E. We consider the first eigenvalue only to allow us to understand the connectivity of the pairing off high up the energy scale. We have used the leading order plus non-perturbative approximation, which does in fact predict the first and second eigenvalues pair off for $l < 0$. This can be seen graphically in figure 6.3b. However we can also see from this figure, that for low E the first perturbative term must also be taken into account to give the proper behaviour. This is in fact what we expect. For large E the connectivity of eigenvalue merging is dependent only upon the sign of l, whereas further down the situation is more complicated. Having understood this important point, we will return to considering the mergings, now for $l > 0$.

When $l > 0$ our ray is below the real axis and our point crosses it *once* before crossing the real axis. Therefore, in this case the first eigenvalue does not pair off. This time it is the $2n$'th and $(2n+1)$'th which merge to become complex. This is again in agreement with our earlier results. It only remains now to treat the case $l = 0$.

The case $l = 0$ contains some subtleties not present in the l non-zero cases. This comes from the fact we can no longer ignore the final term in (6.87), as the $-\pi l$ term is now zero. Our quantisation condition becomes:

$$\chi(E) = -\frac{\pi}{8}|\epsilon|E^{-2}. \tag{6.91}$$

It is this term on the right hand side that now acts like our $-\pi l$ term in the non-zero l cases. We can see that our ray will be below the real axis and therefore as

in the $l > 0$ case it is the $2n$'th and $(2n+1)$'th eigenvalues that merge. This is as predicted numerically. To estimate where this pairing off occurs, we note that the critical value of ρ is now $\sin(\frac{\pi}{8}|\epsilon|E^{-2}) \approx \frac{\pi}{8}|\epsilon|E^{-2}$. We need then to solve the equation:

$$e^{-\frac{\pi^2}{8}|\epsilon|E} = \frac{\pi}{8}|\epsilon|E^{-2} \tag{6.92}$$

We can solve this equation, by making use of the Lambert W function, [12]. The Lambert W function $W(x)$, is defined to be the function that solves:

$$W(x)e^{W(x)} = x. \tag{6.93}$$

The Lambert W function is multi-valued, so some care will need to be taken in choosing the correct branch. Before we consider this, let us rearrange our equation, (6.92), into a form that explicitly matches (6.93). To do this, we take the square root of both sides and multiply by $-\frac{\pi^2}{16}|\epsilon|E$:

$$-\frac{\pi^2}{16}|\epsilon|Ee^{-\frac{\pi^2}{16}|\epsilon|E} = -\frac{\pi^{\frac{5}{2}}|\epsilon|^{\frac{3}{2}}}{32\sqrt{2}} \tag{6.94}$$

which is of the same form as (6.93), as required. We can then say that:

$$E = -\frac{16}{\pi^2|\epsilon|}W\left(-\frac{\pi^{\frac{5}{2}}|\epsilon|^{\frac{3}{2}}}{32\sqrt{2}}\right) \tag{6.95}$$

where we have yet to specify which particular branch we are using. Notice that the argument of W is small and negative. If $-e^{-1} \leq x \leq 0$, there are two possible real values for $W(x)$, these are shown in figure 6.8. The branch which satisfies $-1 \leq W(x)$, is denoted by $W_0(x)$, or sometimes just $W(x)$ when no confusion can arise. This known as the principal branch. The branch for which $W(x) \leq -1$, is denoted by $W_{-1}(x)$. As the factor in (6.95) in negative and we want E to be large for small $|\epsilon|$, we want the branch W_{-1}. So therefore:

$$E = -\frac{16}{\pi^2|\epsilon|}W_{-1}\left(-\frac{\pi^{\frac{5}{2}}|\epsilon|^{\frac{3}{2}}}{32\sqrt{2}}\right) \tag{6.96}$$

In [12] we are given an asymptotic expansion for $W_{-1}(x)$ as $x \to 0^-$.

$$W_{-1}(x) \approx \ln(-x) - \ln(-\ln(-x)) \tag{6.97}$$

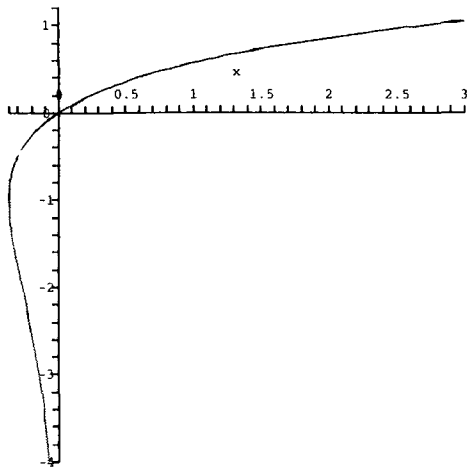

Figure 6.8: The two real branches the Lambert W function, $W(x)$. $W_0(x)$ is shown in red, $W_{-1}(x)$ in green.

This allow us to write down a final approximation for E when $l = 0$ and $|\epsilon|$ is small.

$$E \approx \frac{16}{\pi^2|\epsilon|}\left(\ln\left(\frac{32\sqrt{2}}{\pi^{\frac{5}{2}}|\epsilon|^{\frac{3}{2}}}\right) + \ln\ln\left(\frac{32\sqrt{2}}{\pi^{\frac{5}{2}}|\epsilon|^{\frac{3}{2}}}\right)\right) \tag{6.98}$$

This result corrects the result in [7] that was discussed in chapter 4. We can see now why the truncation method in the limit used there was not precise enough to capture the asymptotic behaviour.

We have in this chapter, succeeded in gaining an analytic understanding of the eigenvalue merging using results from the ODE/IM correspondence. In doing so we have discovered that the behaviour at high energy levels is determined in large part by a non-perturbative term. It was this "beyond all orders" term that smoothed the transition between the regions on either side of the line $M = 1$. It is also this term that governs the asymptotic connectivity of eigenvalue merging as well as where the merging occurs for large E. The merging was found to happen asymptotically as:

$$E = -\frac{8\ln|\sin(\pi l)|}{\pi^2|\epsilon|}. \tag{6.99}$$

for $l \neq 0$ and as:

$$E \approx \frac{16}{\pi^2|\epsilon|}\left(\ln\left(\frac{32\sqrt{2}}{\pi^{\frac{5}{2}}|\epsilon|^{\frac{3}{2}}}\right) + \ln\ln\left(\frac{32\sqrt{2}}{\pi^{\frac{5}{2}}|\epsilon|^{\frac{3}{2}}}\right)\right) \tag{6.100}$$

for $l = 0$. As had been thought, the case $l = 0$ was a borderline, particularly sensitive case.

Chapter 7

Conclusion

We have over the course of this thesis, taken a in depth study of the Schrödinger equation:

$$\left(-\frac{d^2}{dx^2} - (ix)^{2M} + \frac{l(l+1)}{x^2} \right) \psi(x) = E\psi(x), \tag{7.1}$$

viewing it as a continuation of the harmonic oscillator. We have been particularly interested in the transition between the broken and unbroken $\mathcal{PT}$-symmetry regions that occurs at $M = 1$. This seemingly simple extension of a well understood problem, opened up to give a rich mathematical structure.

We studied our problem first at the classical level. We were able to see that there was a classical analogue of the phase transition seen in the quantum case. The trajectories that particles in the classical potential traversed, were seen the be closed and periodic for $M \geq 1$, whereas for $M < 1$, paths did not close and instead spiralled out to infinity. We found examples of broken and unbroken $\mathcal{PT}$-symmetry in both regimes. This was different to that found in earlier work, where the interpretation was of broken $\mathcal{PT}$-symmetry of the trajectories being responsible for the phase transition.

Perturbative methods were applied in the quantum case. The method was seen to be effective for calculating the eigenvalues when the truncation size was taken large enough. This is a general technique and could be applied to other potentials. The weakness of the perturbative technique, was that an analytic understanding proved elusive. To gain accurate results, it was necessary to make the truncation

size of the matrix large. Even when taking asymptotic of the matrix this continued to be the case. To be able to understand the eigenvalue merging we had to use a different approach.

The solution came from a consideration of the ODE/IM correspondence. From our Hamiltonian it was possible to obtain a functional relation involving the eigenvalues of our potential and another, related problem. From this an integral equation was derived. The final analytic solution was found by taking the high energy asymptotic of this integral equation. In taking these asymptotics, we had to include a "beyond all orders" term to get the correct result. It was this that moved us smoothly between the two regimes.

Some further study that leads on naturally from this thesis is based on the generality of the techniques used. The perturbative method has been shown to be an effective one for studying $\mathcal{PT}$-symmetric Hamiltonians and could be applied in other situations. It would be interesting to explore how far away from the unperturbed problem at $M = 1$ the method could be used. Another possible avenue to explore is the technique's applicability to related eigenvalue problems in the other Stokes sectors. The ODE/IM correspondence is also a general technique that could be applied other problems. It is possible to derive expressions relating the T functions in the T-Q equation with their counterparts in other Stokes sectors [18].

In the classical domain, probably the most interesting area for further study is the possibility of discovering closed trajectories for particles with imaginary energy in the case $\epsilon < 0$. This would add weight to the idea that closed trajectories in the classical case are related to solutions to the Schrödinger equation. Any trajectories found for imaginary E would, by necessity, not be $\mathcal{PT}$-symmetric, nor have $\mathcal{PT}$-symmetric partners, as when the energy is imaginary the $\mathcal{PT}$-symmetry of the complex plane is broken.

The study of PT-symmetric quantum mechanics involves some interesting mathematics, we hope the subject continues to expand and further advances are made.

Appendix A

Hermitian Quantum Mechanics

A.1 Hermiticity

In conventional hermitian quantum mechanics, the Hamiltonian of a system is taken to be hermitian. This condition imposed on the Hamiltonian ensures the energy spectrum will be entirely real.

For an operator, $\hat{f}$, we define the complex conjugate so that if we have

$$\hat{f}\psi = \phi \tag{A.1}$$

the complex conjugate, $\hat{f}^*$, acts like

$$\hat{f}^*\psi^* = \phi^* \tag{A.2}$$

The transpose of an operator $\widetilde{\hat{f}}$ is defined so that

$$\int \psi \widetilde{\hat{f}} \phi = \int \phi \hat{f} \psi \tag{A.3}$$

The hermitian conjugate, $\hat{f}^\dagger$, of an operator, $\hat{f}$, is defined to be the operator obtained by transposing and taking the complex conjugate of $\hat{f}$.

$$\hat{f}^\dagger = \widetilde{\hat{f}}^* \tag{A.4}$$

An operator is said to be hermitian if it is equal to its hermitian conjugate

$$\hat{f}^\dagger = \hat{f} \tag{A.5}$$

A.2 Reality Of Eigenvalues Of Hermitian Operators

If we demand that an operator is hermitian we can guarantee that the operators eigenvalues will be real. We call the eigenvalues of $\hat{f}$ to be f and the eigenstates ψ. We then have

$$\hat{f}\psi = f\psi \tag{A.6}$$

and

$$\int \psi^* \hat{f} \psi = f \tag{A.7}$$

We can take the transpose of the equation (A.3)

$$\int \psi \tilde{\hat{f}} \psi^* = f \tag{A.8}$$

If we complex conjugate the expression we obtain

$$\int \psi^* \tilde{\hat{f}}^* \psi = \int \psi^* \hat{f}^\dagger \psi = f^* \tag{A.9}$$

Now, we have constrained $\hat{f}$ to be hermitian so this equation can be written as

$$\int \psi^* \hat{f} \psi = f^* \tag{A.10}$$

the left hand side of which is the same as (A.7). We therefore have

$$f = f^* \tag{A.11}$$

i.e. the eigenvalues are real.

It is for this reason that the operators of observables in conventional quantum mechanics are hermitian. In particular the Hamiltonian is always hermitian, ensuring the energy spectrum is real.

A.3 Everywhere Positive Potentials

If we have the Schrödinger equation:

$$-\psi''(x) + V(x)\psi(x) = E\psi(x) \tag{A.12}$$

with $V(x) > 0$, for all $x \in \mathbb{R}$, the energy spectrum is completely positive; $E > 0$.

To see this we multiply both sides of (A.12) by $\psi^*(x)$ and integrate.

$$-\int \psi^*(x)\psi''(x)dx + \int V(x)|\psi(x)|^2 dx = E\int |\psi(x)|^2 dx \tag{A.13}$$

The first term can be integrated by parts:

$$\int |\psi'(x)|^2 dx + \int V(x)|\psi(x)|^2 dx = E\int |\psi(x)|^2 dx \tag{A.14}$$

There is no boundrary term as $\psi(x) \to 0$ as $|x| \to \infty$.

Now, as $V(x)$, $|\psi'(x)|^2$ and $|\psi(x)|^2$ are all non-negative over the entire real line, each of the integrals is positive. Therefore, the left hand side of our equation is strictly positive. Hence:

$$E\int |\psi(x)|^2 dx > 0 \tag{A.15}$$

and as the integral is positive, $E > 0$.

Appendix B

Maple Programmes

B.1 Maple Programme For Classical Trajectories

This Maple worksheet calculates the trajectory of a particle in our potential. The output is an ordered list of the positions of the particle.

```
with(linalg):
Digits:=30;
```

The value of epsilon

```
epsilon:=0;
```

```
dx:=(r,theta)->evalf(dt*sqrt(E+r^(2+epsilon)*
exp(I*(Pi/2+theta+2*Pi*Rmn)*(2+epsilon))
-l*(l+1)*r^(-2)*exp(-2*I*(theta+2*Pi*Rmn))));
```

```
d2x:=(r,theta)->evalf(dt^2*(1/2)*(I*(2+epsilon)
*r^(1+epsilon)*exp(I*(Pi/2+theta+2*Pi*Rmn)*(1+epsilon))
+2*l*(l+1)*r^(-3)*exp(-3*I*(theta+2*Pi*Rmn))));
```

The Riemann sheet which we start on must be specified. This is only important if epsilon is non-integer. It should be noted that although the branch cut is on the positive imaginary axis, Maple thinks it is on the negative real axis. The programme takes this into account, but when defining the intial sheet some care must be taken.

```
Rmn:=0;
```

The value of l.

```
l:=0;
```

The value of E.

```
E:=1;
```

The number of steps to be taken.

```
num:=10000;
```

The intial position.

```
x[0]:=0.5;
```

The step size.

```
dt:=0.001;

r[new]:=evalf(abs(x[0]));
theta[new]:=evalf(argument(x[0]));
dattable:=array(1..num+2);
dattable[1]:=num+2;
for i from 1 to num do
 if (i mod (num/10)=0) then print(i); fi: gc():
 v[new]:=evalf(dx(r[new],theta[new])):
 a[new]:=evalf(d2x(r[new],theta[new])):
 if i <> 1 then  if abs(v[new]-v[old])>abs(v[new]+v[old])
  then  v[new]:=-v[new]:
  dt:=-dt:print(i): print(change): fi:  fi:
 x[i]:=evalf(r[new]*exp(I*theta[new]))+v[new]+(1/2)*a[new]:
 if Re(x[i])<0 then if (Im(x[i-1])<0 and Im(x[i])>0)
  then Rmn:=Rmn-1: print(i): print("going down"):
  print(Rmn): fi: fi:
```

```
 if Re(x[i])<0 then if (Im(x[i-1])>0 and Im(x[i])<0)
  then Rmn:=Rmn+1: print(i): print("going up"):
  print(Rmn): fi: fi:
 r[old]:=r[new]: r[new]:=evalf(abs(x[i])):
 theta[old]:=theta[new]:
 theta[new]:=evalf(argument(x[i])):  v[old]:=v[new]:
od:


for j from 2 to num+2 do dattable[j]:=x[j-2]; od:


save dattable, 'dattableep010':
```

The above code does the calculation and then saves the output as dattableep010, in this case.

B.2 Maple Program For Perturbative Calculation

This program calculates the matrix and solves for its eigenvalues. It does this for a range of values of M. The out put is a matrix, which in each row has as the first entry the value of M. The other entries in each row are the corresponding eigenvalues.

```
with(linalg):
with(plots):
with(plottools):
interface(quiet=true);
Digits:=50;
```

The truncation level

```
nlev:=20;
```

The maximum value of M.

```
Mmax:=1+4/7;
err:=0.00000000001;
```

The number of different values of M.

```
num:=100;
```

The value of l

```
l:=0;
Hmn:=Matrix(nlev,nlev);
E0:=Matrix(nlev,nlev);
DM1:=Matrix(nlev,nlev);
AA:=Matrix(nlev,nlev);
datmat:=Matrix(num,nlev+1);
Aplus:=(s,t,M,lo)->evalf((cos(M*Pi)-sin(M*Pi)*tan(lo*Pi))
*pochhammer(lo+3/2,t)*pochhammer(-M,s)
*GAMMA(lo+3/2+M)*(1/(sqrt(s!*t!*GAMMA(lo+s+3/2)*GAMMA(lo+t+3/2)))
*hypergeom([-t,lo+3/2+M,1+M],[lo+3/2,1+M-s],1)));

Aneg:=(s,t,M,lo)->evalf((cos(M*Pi)+sin(M*Pi)*tan(lo*Pi))
*pochhammer(-lo+1/2,t)*pochhammer(-M,s)
*GAMMA(-lo+1/2+M)*(1/(sqrt(s!*t!*GAMMA(-lo+s+1/2)*GAMMA(-lo+t+1/2)))
*hypergeom([-t,-lo+1/2+M,1+M],[-lo+1/2,1+M-s],1)));
AplusM1:=(s,t,lo)->evalf(pochhammer(-1,s-t)*(-1)^(t)
*sqrt(GAMMA*(t+lo+(3/2))/(GAMMA(s+1)
*GAMMA(t+1)*GAMMA*(s+lo+(3/2))))*
(((5/2)+lo)*pochhammer(-s,t)-2*pochhammer(-s-1,t)));
AnegM1:=(s,t,lo)->evalf(pochhammer(-1,s-t)*(-1)^(t)
*sqrt(GAMMA*(t-lo+(1/2))/(GAMMA(s+1)
*GAMMA(t+1)*GAMMA*(s-lo+(1/2))))*
(((3/2)-lo)*pochhammer(-s,t)-2*pochhammer(-s-1,t)));
```

```
Bplus:=(s,t,M,lo)->evalf(I*sin(M*Pi)*(1/cos(l*Pi))
*sqrt(1/((s!*t!)*GAMMA(s+lo+3/2)
*GAMMA(t-lo+1/2)))*pochhammer((1/2)-lo,t)*GAMMA(M+1)
*pochhammer(lo+(1/2)-M,s)
*hypergeom([-t,M+1,(1/2)-lo+M],[(1/2)-lo,(1/2)-lo+M-s],1));

for i from 1 to (nlev) do E0[i,i]:=2*(i-1)-(-1)^(i-1)*2*l+1; od:

for i from 1 to nlev do a:=(i-1) mod 2; if a=1 then
DM1[i,i]:=AplusM1((i-2)/2,(i-2)/2,l);
if (i+2)<nlev+1 then DM1[i+2,i]:=AplusM1(i/2,(i-2)/2,l);
DM1[i,i+2]:=DM1[i+2,i] fi;
else DM1[i,i]:=AnegM1((i-1)/2,(i-1)/2,l); if (i+2)<nlev+1
then DM1[i+2,i]:=AnegM1((i+1)/2,(i-1)/2,l);
DM1[i,i+2]:=DM1[i+2,i] fi; fi; od:

for k from 1 to num do if (k mod (num/10))=0 then print(k);
gc(); fi;
M:=Mmax+(1/num)*(1/(num-1))-(k-1)*(8/7)*(1/(num-1));
for j from 1 to nlev do b:=(j-1) mod 2: if b=0 then
AA[j,j]:=-Aneg((j-1)/2,(j-1)/2,M,l);
else AA[j,j]:=-Aplus((j-2)/2,(j-2)/2,M,l); fi;
for i from (j+1) to nlev do
a:=(i-1) mod 2:
if a=0 then if b=0 then AA[i,j]:=-Aneg((i-1)/2,(j-1)/2,M,l); else
AA[i,j]:=-Bplus((j-2)/2,(i-1)/2,M,l); fi; else if b=1 then
AA[i,j]:=-Aplus((i-2)/2,(j-2)/2,M,l);
else AA[i,j]:=-Bplus((i-2)/2,(j-1)/2,M,l);  fi; fi;
AA[j,i]:=AA[i,j];     od: od:
AA;
```

```
Hmn:=E0+DM1+AA;
E:=([eigenvals(Hmn)]);



sorted:=false;
Imcount:=nlev;
resorted:=true;

while (sorted=false) do sorted:=true:
for j from 1 to (nlev-1) do
if Re(E[j])>Re(E[j+1]) then temp:=E[j]: E[j]:=E[j+1]:
E[j+1]:=temp: sorted:=false: fi; od; od;
if Imcount>1 then if abs(Im(E[Imcount])+Im(E[Imcount-1]))<err then
if abs(Re(E[Imcount])-Re(E[Imcount-1]))<err then I
mcount:=Imcount-2; fi; fi; fi;
if Imcount<3 then resorted:=false fi; while (resorted=false) do
resorted:=true: for j from 1 to
(nlev-1) do if abs(Im(E[j]))>err then if abs(Im(E[j+1]))<err then
temp:=E[j]: E[j]:=E[j+1]: E[j+1]:=temp:
resorted:=false: fi; fi; od; od;



datmat[k,1]:=M;
for y from 2 to nlev+1 do datmat[k,y]:=E[y-1]  od; od:

save datmat, 'mapleperturbationoutput';
```

The out put is saved as 'mapleperturbationoutput'

Appendix C

Some Miscellaneous Results

C.1 Wronskians

The Wronskian of two solution to a second order differential equation is defined as:

$$W[f,g] = fg' - f'g. \tag{C.1}$$

We take our differential equation to have no first derivative term, i.e. we have:

$$f'' + P(x)f = 0 \tag{C.2}$$

$$g'' + P(x)g = 0 \tag{C.3}$$

We first show that the Wronskian of these two solutions is independent of x. We take the derivative of (C.1):

$$W'[f,g] = fg'' - f''g. \tag{C.4}$$

Then using (C.2), we have:

$$W'[f,g] = f(g'' + P(x)g), \tag{C.5}$$

which from (C.3) is identically zero. The derivative of the Wronskian is zero, hence the Wronskian is independent of x.

The other result to obtain is that the Wronskian is zero if and only if the solutions are linearly dependent. The fact that if the solutions are linearly dependent

the Wronskian is zero follows trivially from (C.1). If the Wronskian is zero a rearrangement of (C.1) leads us to:

$$\frac{f'}{f} = \frac{g'}{g} \tag{C.6}$$

Integrating gives us:

$$\ln(f) = \ln(Cg) \tag{C.7}$$

$$\Rightarrow \quad f = Cg \tag{C.8}$$

for some constant C. Therefore the solutions are linearly dependent.

C.2 The WKB Approximation

The WKB approximation, for large E, of the Hamiltonian:

$$\left(-\frac{d^2}{dx^2} + V(x)\right)\psi(x) = E\psi(x), \tag{C.9}$$

is given by

$$\psi_{\pm}^{WKB}(x) = \frac{1}{\sqrt{p(x)}} \exp\left(\pm \int dx' p(x')\right) + . \tag{C.10}$$

Here we have written $p(x) = \sqrt{V(x) - E}$. The sign must be chosen so as to give the correct, subdominant, behaviour as $|x| \to \infty$.

The leading order WKB phase-integral quantization condition is:

$$\pi(n + \frac{1}{2}) = \int_{x_-}^{x_+} dx \sqrt{E - V(x)}, \tag{C.11}$$

where the $x_\pm$ are the turning points, $p^2(x) = 0$.

For the potential $V(x) = x^2(ix)^{2+\epsilon}$, used in [7], we can use this to approximate the energy for $\epsilon > 0$. The $x_\pm$ are the turning points that analytically continue off the real axis as M moves away from the harmonic oscillator point, $M = 1$. As we are now working in the complex plane, we must take care to ensure that the integral follow a path on which the integral is real. For $\epsilon > 0$ this path is entirely in the lower half plane. For $\epsilon < 0$, the path crosses the branch cut on the imaginary axis and hence we cannot perform the WKB approximation. For $\epsilon > 0$ we obtain:

$$E_n \sim \left(\frac{\Gamma\left(\frac{8+3\epsilon}{4+2\epsilon}\right)\sqrt{\pi}(n + \frac{1}{2})}{\sin\left(\frac{\pi}{2+\epsilon}\right)\Gamma\left(\frac{3+\epsilon}{2+\epsilon}\right)}\right)^{\frac{4+2\epsilon}{4+\epsilon}}. \tag{C.12}$$

C.3 Hadamard's Factorization Theorem.

This section is from [38]. The order of an integrable function, $f(z)$, is defined to be the lower bound of numbers A, for which as $|z| = r \to \infty$,

$$f(z) = O(e^{r^A}) \tag{C.13}$$

Thus if $f(z)$ is of order ρ,

$$f(z) = O(e^{r^{\rho+\epsilon}}) \tag{C.14}$$

for every positive value of ϵ, but no negative value.

The primary factors of an integrable equation are the functions:

$$E(u,0) = 1-u, \quad E(u,p) = (1-u)e^{u+\frac{u^2}{2}+..+\frac{u^p}{p}} \qquad (p = 1,2,...). \tag{C.15}$$

For an integrable equation of finite order, with zeros z_n, there is an integer $p \leq \rho$, that is independent of n such that:

$$\prod_{n=1}^{\infty} E\left(\frac{z}{z_n}, p\right) \tag{C.16}$$

converges for all values of z. This is known as the canonical product.

Having defined the order of an integrable function and the canonical product, we can now state Hadamard's Theorem: If $f(z)$ is an integral function of order ρ, with zeros z_n and $f(0) \neq 0$ then:

$$f(z) = e^{Q(z)}P(z), \tag{C.17}$$

where $P(z)$ is the canonical product and $Q(z)$ is a polynomial of degree not greater than ρ.

Consider in the case $\rho < 1$. The only allowed primary factors are the $E(u,0)$ and $Q(z)$ must be constant. And so,

$$f(z) = e^{Q}\prod_{n=1}^{\infty}\left(1-\frac{z}{z_n}\right). \tag{C.18}$$

A consideration of $f(0) \neq 0$, tells us $Q = \ln f(0)$. Hence:

$$f(z) = f(0)\prod_{n=1}^{\infty}\left(1-\frac{z}{z_n}\right). \tag{C.19}$$

Bibliography

[1] Abramowitz M. and Stegun I.A. eds *Handbook of Mathematical Functions* (National Bureau of Standards 1964)

[2] Bagchi B. and Roychoudhury R. 'A new $\mathcal{PT}$ symmetric complex Hamiltonian with a real spectra' 2000 *J Phys. A* **33**, L1-L3 247 `quant-ph/9911104`

[3] Baxter, R.J. *Exactly Solved Models In Statistical Mechanics* Academic Press 1982

[4] Bazhanov V.V., Lukyanov S.L. and Zamolodchikov A.B. 'Integrable Structure of Conformal Field Theory II. Q-operator and DDV equation' 1997 *Commun. Math. Phys.* **190** 247 `hep-th/9604044`

[5] Bender C.M. and Boettcher S. 'Quasi-exactly solvable quartic potential' 1998 *J.Phys. A* **31** L273-L277 `physics/9801007`

[6] Bender C.M. and Boettcher S. 'Real Spectra in Non-Hermitian Hamiltonians Having PT Symmetry' 1998 *Phys. Rev. Lett.* **80** 4243 `physics/9712001`

[7] Bender C.M., Boettcher S. and Meisinger P.N. 'PT-Symmetric Quantum Mechanics' `quant-ph/9809072`

[8] Bender C.M., Brody D.C and Jones H.F. 'Must a Hamiltonian be Hermitian?' 2003 *Am.J.Phys.* **71** 1095-1102 `hep-th/0303005`

[9] Bender C.M., Brody D.C and Jones H.F. 'Complex Extension of Quantum Mechanics' 2002 *Phys.Rev.Lett* **89** 270401 `quant-ph/0208076`

[10] Bender C.M. and Orszag S.A. *Advanced Mathematical Methods For Scientists And Engineers* McGraw-Hill 1978.

[11] Berry M.V. and Mount K.E. 'Semiclassical aproximations in wave mechanics' 1972 *Rep. Prog. Phys.* **35** 315-397

[12] Corless R.M., Gonnet G.H., Hare D.E.G., Jeffrey D.J. and Knuth D.E. 'On the Lambert W function', Adv. Comp. Math. **5** (1996) 329-359.

[13] Destri C. and de Vega H.J. Ńew thermodynamic Bethe ansatz equations without strings' 1992 *Phys. Rev. Lett* **69** 2313

[14] Dorey P., Dunning C., Millican-Slater A. and Tateo R. 'Differential equations and the Bethe ansatz' *Proceedings of ICMP 2003* `hep-th/0309054`

[15] Dorey P., Dunning C. and Tateo R. 'Spectral equivalences, Bethe Ansatz equations, and reality properties in PT-symmetric quantum mechanics' 2001 *J.Phys. A* **34** 5679-5704 `hep-th/0103051`

[16] Dorey P., Millican-Slater A. and Tateo R. 'Beyond the WKB approximation in $\mathcal{PT}$-symmetric quantum mechanics' 2005 *J.Phys.A* **38** 1305-1332

[17] Dorey P. and Tateo R. Ánharmonic oscillators, the thermodynamic Bethe Ansatz, and nonlinear integral equations' 1999 *J.Phys.* **A32** L419-L425 `hep-th/9812211`

[18] Dorey P. and Tateo R. 'On the relation between Stokes multipliers and the T-Q systems of conformal field theory' 1999 *Nucl. Phys. B* **563** 573 [Erratum-ibid. B **603** (2001) 581] `hep-th/9906219`

[19] Flugge S. *Practical Quantum Mechanics, Vol. 1* 1971 New York, Springer

[20] Galindo A. and Pascual P. *Quantum Mechanics II* Springer-Verlag 1989.

[21] Hall R. L., Saad N. and von Keviczky A.B. 'Spiked harmonic oscillators' 2002 *J. Math. Phys.* **43** 94-112 `math-ph/0109014`

[22] Hatano N. and Nelson D.R. *Phys. Rev. Lett* **77**, 570 (1996).

[23] Hatano N. and Nelson D.R. *Phys. Rev. B* **56**, 8651 (1997).

[24] Hollowood T.J. *Nucl. Phys. B* **386**, 166 (1992).

[25] Khare A. and Sukhatme U. 'New Solvable and Quasu Exactly Solvable Periodic Potentials.' 1999 *Jour. Math. Phys.* **40** 5473 quant-ph/042106

[26] Khare A. and Sukhatme U. 'Analytically Solvable $\mathcal{PT}$-Invariant Periodic Potentials.' 2004 *Phys.Lett.A* **324** 406-414 quant-ph/042106

[27] Krajewska A., Ushveridze A. and Walczak Z. Ánti-Isospectral Transformations In Quantum Mechanics' 1997 *Mod.Phys.Lett.* **A12** 1225

[28] Landau L.D. and Lifshitz E.M. *Quantum Mechanics* Pergamon Press 1958.

[29] Langer R. E. 'On the connection formulas and the solutions of the wave equation' Phys. Rev. 51 (1937) 669-676.

[30] Mostafazadeh A. 'Pseudo-Hermiticity versus PT Symmetry: The necessary condition for the reality of the spectrum of a non-Hermitian Hamiltonian' 2002 *J. Math. Phys.* **43** 205-214 math-ph/0107001

[31] Nelson D.R. and Shnerb N.M. *Phys. Rev. E* **58**,1383 (1998).

[32] Olver F. W. J. *Asymptotics and special functions* (Academic Press, New York and London, 1974).

[33] Rainville, E.D. *Bull. Amer. Math. Soc.* **51**, 714-723.

[34] Shin K.C. 2002 *Commun.Math.Phys.* **229** 543-564 math-ph/0201013

[35] Shin K.C. 2001 *J. Math. Phys.* **42(6)** 2513-2530 math-ph/0007006

[36] Slater, L.J. *Generalized Hypergeometric Functions* CUP 1966

[37] Teshbach H., Porter C.E. and Weisskopf V.F. *Phys. Rev.***96**, 448 (1954).

[38] Titchmarsh E. C. *The Theory Of Functions* Oxford : Clarendon Press, 1932.

[39] Voros A 'Airy function (exact WKB results for potentials of odd degree)' 1999 *J. Phys, A: Math. Gen.* **32** 1301

[40] Yudell L. L. *Mathematical Functions and their Approximations* Academic Press

[41] Zamolodchikov A.B. and Zamolochikov Al.b. 'Factorised S-matrices in two dimensions as the exact solutions of certain relativistic quantum field theory models.' 1979 *Ann. Phys.* **120**, 253-291.

[42] Znojil M. '$\mathcal{PT}$-symmetric harmonic oscillators' 1999 *Phys. Lett. A* **259** 573 quant-ph/9905020